Golder Associates
CONSULTING ENGINEERS

LARGE SCALE LABORATORY SIMULATION of HYDRAULIC FRACTURE PROPAGATION IN OIL SANDS

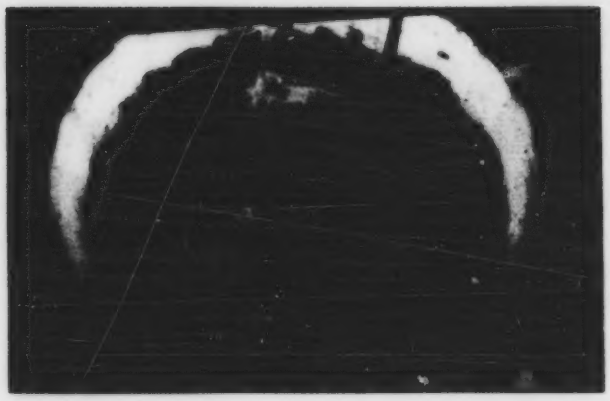

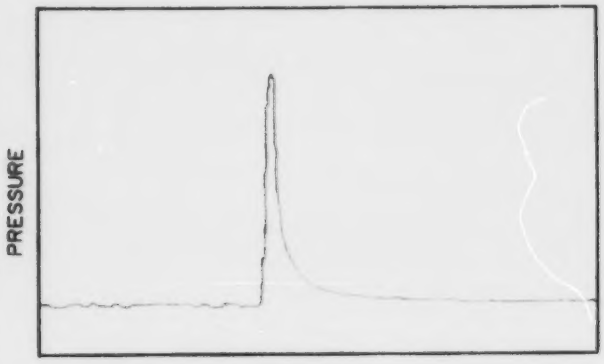

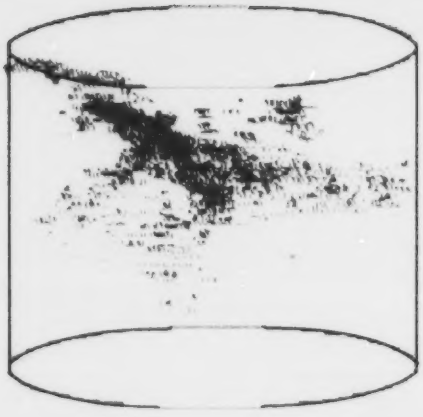

JOINT INDUSTRY PROJECT

April, 1991

902-2013

92-00202/

TITLE:
LABORATORY SIMULATION AND CONSTITUTIVE BEHAVIOUR FOR HYDRAULIC FRACTURE PROPAGATION IN OIL SANDS

Part of Energy, Mines and Resources Cost-Shared Energy Conversion Program and Part of the Program of the Federal Panel on Energy Research & Development (PERD)

CONTRACT SERIAL NO. 23440-9-9263-01-SQ

CONTRACT REQ'N NO. 23440-9-9263

CONTRACTOR: GOLDER ASSOC.

Final Report
(Phase 1)

Work on the project was conducted under the auspices of the Canada Centre for Mineral and Energy Technology, Energy, Mines and Resources Canada.

SSC FILE No.: 06SQ.23440-9-9263
CONTRACT FILE No.: 23440-9-9263/01-SQ
CANMET SCIENTIFIC AUTHORITY: Dr. A.E.D. GEORGE

Distribution:
5 copies - Canada Centre for Mineral and Energy Technology (CANMET)
Ottawa, Ontario
2 copies - Esso Resources Canada Ltd.
Calgary, Alberta
2 copies - Shell Canada Ltd.
Calgary, Alberta
2 copies - Mobil Oil Canada
Calgary, Alberta
2 copies - Alberta Oil Sands Technology and Research Authority (AOSTRA)
Calgary, Alberta
2 copies - Golder Associates Ltd.
Calgary, Alberta

July, 1991

902-2013

135pp

MICROMEDIA

TABLE OF CONTENTS

1.0 INTRODUCTION 1
1.1 Background 1
1.2 Mechanisms of Failure During Fluid Injection 2
1.3 Objectives 3
1.4 Project Funding 4

2.0 Materials Used 5
2.1 Selection of Test Sand 6
2.1.1 Grain Size Analyses 6
2.1.2 Permeability Tests 7
2.2 Selection of Pore Fluid 7
2.2.1 Viscosity Measurements 7
2.2.2 Permeability Tests 9
2.3 Saturation and B Tests 9
2.4 Injection and Diffusion Tests 10

3.0 EQUIPMENT AND PROCEDURES 12
3.2 Sample Preparation 14
3.3 Test Procedures 17
3.4 Sample Excavation and Sampling 19

4.0 FRACTURE TESTS 21
4.1 Fracture Test No. 1 22
4.2 Fracture Test No. 2 24
4.3 Fracture Test No. 3 24
4.4 Fracture Test No. 4 25
4.5 Fracture Test No. 5 27
4.6 Fracture Test No. 6 28
4.7 Fracture Test No. 7 32
4.8 Fracture Test No. 8 34

5.0 ASSOCIATED TESTS 36
5.1 Stress-Deformation and Strength Tests 36
5.2 Density Measurements 37

6.0 DISCUSSION 38

7.0 CONCLUSIONS AND RECOMMENDATIONS 40

TABLE OF CONTENTS

LIST OF TABLES

4.1 - Summary of Hydraulic Fracture Test Program

LIST OF FIGURES

1.1 - Shear Failure Due to Fluid Injection
2.1 - Drained Triaxial Test on McMurray Formation Oil Sands at In Situ Stresses
2.2 - Typical Drained Triaxial Test on Dense Quartzitic Sand at 350 kPa
2.3 - Grain Size Distribution Lane Mtn Sand
2.4 - SIL Sand
2.5 - Viscosity of Viscous Pore Fluids
2.6 - Permeability Test on Glycerine Impregnated Sand
2.7 - Predicted Injection Rate for Glycerine Impregnated Sand
2.8 - Saturation Tests on Glycerine Impregnated Lane Mtn 125 Sand
2.9 - Injection/Diffusion Test
3.1 - Large Triaxial Stress Chamber
3.2 - Pressure Control Board
3.3 - Cross Section of Injection Well at Mid-Height of Sample
3.4 - Constant Flow Pump
3.5 - Piezometer Detail
3.6 - Photograph of Piezometer
3.7 - Injection Well Detail
3.8 - Extensometer Detail
3.9 - Internal Deformation Measuring Devices
3.10- Photograph of Large Triaxial Chamber
3.11- Pluviation of Sand Into Stress Chamber
3.12- Instrumentation Detail for Fracture Simulations
3.13- Lower Drainage Boundary (to minimize friction)
3.14- Delineation of Fluorescent Dye during Excavation for Digitizing Process
4.1 - Location of Fluorescent Dye after Injection - Test 1
4.2 - Response of LVDT Extensometers and Fluid Injection Record - Test 1
4.3 - Response of Strain Gauge Foil Extensometers - Test 1
4.4a- Response of Piezometers Test 1
4.4b- Response of Piezometers Test 1
4.5 - Location of Fluorescent Dye after Injection - Test 3
4.6 - Response of LVDT Extensometers and Fluid Injection Record - Test 3
4.7 - Response of Strain Gauge Foil Extensometers - Test 3
4.8a- Response of Piezometers Test 3
4.8b- Response of Piezometers Test 3

TABLE OF CONTENTS

4.9 - Location of Fluorescent Dye after Injection - Test 4
4.10- Response of LVDT Extensometers and Fluid Injection Record - Test 4
4.11- Response of Strain Gauge Foil Extensometers - Test 4
4.12- Injection Curves - Fracture - Test 4
4.13- Drained Loading - Test 5
4.14- B Test - Test 5
4.15- Location of Fluorescent Dye after Injection - Test 5
4.16- Response of LVDT Extensometers and Fluid Injection Record - Test 5
4.17- Response of Piezometers - Test 5
4.18- Permeability Test - Test 6
4.19- Injection Test No. 1 - Test 6
4.20- Injection Test No. 2 - Test 6
4.21- Drained Loading and B Test - Test 6
4.22- Location of Fluorescent Dye after Inspection - Test 6
4.23- Injection Pressure Curves - Test 6
4.24- Response of Piezometers - Test 6
4.25- Response of LVDT Extensometers and Fluid Injection Record - Test 6
4.26- Injection Test - Test 7
4.27- Location of Fluorescent Dye after Injection - Test 7
4.28- Response of LVDT Extensometers and Fluid Injection Record - Test 7
4.29- Response of Piezometers - Test 7
4.30- Injection Pressure Curves - Test 7
4.31- Injection Pressure - Time Curves - Test 7
4.32- Drained Loading and Injection Test - Test 8
4.33- Location of Fluorescent Dye after Injection - Test 8
4.34- Response of LVDT Extensometers and Fluid Injection Record - Test 8
4.35- Response of Piezometers - Test 8
4.36- Injection Pressure Curves - Test 8
5.1 - Shear Strength of Samples taken from Large Scale Fracture Tests
5.2 - Bulk Density of Samples taken from Large Scale Fracture Tests
5.3 - Porosity of Samples taken from Large Scale Fracture Tests
6.1 - Summary of Large Scale Fracture Tests
6.2 - Summary of Injection Pressure-time Curves

EXECUTIVE SUMMARY

The bitumen contained within the oil sands reservoirs of Alberta is highly viscous and will not flow readily at formation temperatures. Bitumen production from deeply buried oil sands formations requires mobilizing the bitumen by in situ stimulation techniques. The most common method for reducing the viscosity of the bitumen so it can be pumped to the surface involves injecting pressurized steam into the reservoir. The flow of the steam into the reservoir is inhibited by the low permeability of the oil sands formation. In order to achieve economic injection rates the formation must fracture or fail.

The mechanics of hydraulic fracture in oil sands reservoirs is complicated by highly non-linear and inelastic geotechnical behaviour exhibited by unconsolidated clastic sediments. A significant obstacle to the development and use of fracture models has been the lack of reliable verification data. Verification data is normally inferred from in situ tests. However, the boundary conditions in field tests are not well defined because the in situ stress field is unknown and the geology may be complex. Spatial variations in mechanical, physical and thermal properties of the geological strata may occur over the length of a fracture. Due to these uncertainties, field results alone are not adequate to evaluate the fracture model. This report documents the initial phase of a joint industry laboratory testing project carried out to enhance the mathematical formulations of models by providing data to calibrate and verify the models currently employed for fracture analysis.

A series of laboratory high rate injection simulations on homogeneous sand impregnated with a highly viscous fluid were carried out in a large triaxial stress chamber. The main advantage of these large scale laboratory tests is that the boundary conditions on the sample are known and fracture parameters to be used in the fracture model are measured directly for the test specimen. In addition, after the test the sample can be dissected and the fracture propagation traced. The design of the testing was to study the propagation of leak off dominated fractures. The program included propagation of 6 horizontal fractures (i.e. the initial minor principal stress is vertical) in which the fracture location is dictated by the radial symmetry of the test apparatus. A seventh test was carried out with the initial minor principal stress horizontal so that the effect of varying the initial stress conditions could be investigated. Constant pressure (below the minimum effective confining stress applied to the sample) injectivity tests, permeability tests as well as drained/undrained loading tests were carried out prior to the fracture tests. Small scale laboratory testing was also carried out to provide constitutive parameters for stress-strain behaviour and flow characteristics for the materials tested in the large chamber.

The results of the testing have demonstrated that the mode of failure of the sand and how the fluid is transported through the sample depend on both the injection rate and the applied stress field. The data appear to support two distinct failure mechanisms during injection; tensile parting and shear. Tensile parting appears to dominate at the higher injection rates. In contrast shear failure appears to occur at all injection rates. This report provides recommendations regarding future testing to delineate these effects.

Sommaire exécutif

Le bitume contenu dans les dépôts de sable bitumineux de l'Alberta est hautement visqueux et ne s'écoulera pas de lui-même à la température ambiante des formations. La production de bitume de formations profondes de sable bitumineux requert une mise en circulation du bitume par des techniques de stimulation in situ. La méthode la plus commune pour réduire la viscosité du bitume, de façon à ce qu'il puisse être pompé vers la surface, implique l'injection de vapeur à haute pression dans le dépôt. L'écoulement de la vapeur dans le réservoir est contré par la faible perméabilité de la formation de sable bitumineux. De façon à obtenir des taux d'injection qui soient économiques, la formation doit être fracturée.

Le processus de fracturation hydraulique dans les dépôts de sable bitumineux est rendu plus complexe par le comportement géotechnique hautement non-linéaire et inélastique propre aux sédiments détritiques non consolidés. Un obstacle de taille au developpement et à l'usage de modèles de fracturation fut le manque de données fiables pour opérer leur vérification. Les données de vérification sont généralement déduites des essais in situ. Cependant les conditions limites des essais de chantier ne sont pas très bien définies puisque le champ de contraintes en place demeure inconnu et que la géologie du site peut être complexe. Des variations spatiales dans les propriétés mécaniques, physiques et thermales des horizons stratigraphiques peuvent se produire le long d'une fracture donnée.

Suite à ces incertitudes, les résultats de chantier à eux seuls ne sont pas adéquats pour évaluer un modèle de fracturation. Le présent rapport fournit les résultats de la phase initiale d'un projet conjoint, réalisé par l'industrie et un laboratoire d'essai, destiné à supporter les formulations mathématiques de modèles, en fournissant des données permettant de calibrer et de vérifier les modèles actuellement utilisés dans le cas de la fracturation hydraulique.

Une série de simulations en laboratoire, impliquant des taux d'injection élevés dans un sable homogène, imprégné d'un fluide à haute viscosité, furent réalisés dans une enceinte triaxiale de grandes dimensions. L'avantage principal de ces essais de laboratoire à grande échelle tient au fait que les conditions limites de l'échantillon sont connues et que les paramètres de fracturation à utiliser dans le modèle sont mesurés directement sur l'échantillon analysé. De plus, à la fin de l'essai, l'échantillon peut être disséqué et le tracé

des fractures peut être établi. Le but de ce type d'essai visait à étudier une propagation dominée pour des fractures à grand débit. Le programme d'essai incluait la propagation de six fractures horizontales (i.e. la contrainte principale mineure initiale est verticale) dans laquelle la localisation des fractures est dictée par la symétrie radiale de l'équipement utilisé. Un septième essai fut réalisé avec une contrainte principale mineure initiale dans le plan horizontal, de sorte que l'effet d'une variation des conditions de contraintes initiales puisse être investiquée. Des essais d'injection à pression constante (sous le niveau de la contrainte de confinement effective minimum appliquée à l'échantillon), des essais de perméabilité, de même que des essais de chargement drainés et non drainés furent réalisés avant les essais de fracturation. Des essais de laboratoire à plus petite échelle furent également effectués de façon à fournir des valeurs aux paramètres constitutifs pour l'analyse du comportement contrainte-déformation et les caractéristiques d'écoulement des matériaux utilisés dans l'enceinte triaxiale.

Les résultats des essais ont démontré que le mode de rupture du sable et la façon dont le fluide est transporté aux travers l'échantillon dépendent à la fois du taux d'injection et du champ de contraintes appliquées. Les données semblent supporter la thèse de deux mécanismes de rupture lors de l'injection, soit par tension et par cisaillement. La rupture par tension semble dominer aux taux d'injection élevés. Au contraire, la rupture par cisaillement semble se produire pour tous les taux d'injection. Le présent rapport fournit des recommandations à propos de futurs essais destinés à évaluer ces effets.

1.0 INTRODUCTION

Development of satisfactory numerical models for fracture formation and propagation in the oil sands of Alberta is considered to be an important requirement for the future of the oil industry in Alberta. This report describes the first phase of a project to gain a better understanding of the fundamental mechanisms of fracturing of unconsolidated sand formations. The project is based on carrying out hydraulic fracturing in a large scale triaxial stress chamber. A laboratory test of this nature allows the major factors controlling the fracture process to be measured or controlled. It is also possible to trace fracture propagation by careful examination of the specimen after the test. Therefore such tests provide the information required to develop new mathematical and numerical models, and to validate existing models. Field data for the same purpose is subject to much larger uncertainties with regard to most of the measurements made.

1.1 Background

To fracture an oil sands reservoir, injection fluid is forced rapidly into the oil sands matrix causing individual sand grains to slide relative to each other to accommodate the induced mechanical and/or thermal strain. These structural changes to the oil sands matrix are generally highly non-linear and inelastic. The associated volume change significantly alters the in situ stress field in the fracture zone and therefore controls the initiation, propagation and orientation of fractures. As a result, the mechanics of hydraulic fracturing in unconsolidated sediments is complex and consideration must be given to the mechanical behaviour of oil sands.

The reliability of fracture models to predict fracture propagation in situ depends on an adequate mathematical representation of the physical processes involved. Limitations of a particular model employed for the mechanics of fracture are obscured by the uncertainty in the material parameters and reservoir characteristics

as inferred from field tests and the inability to observe and accurately track fracture propagation in situ.

The current project focuses on large scale laboratory tests. These tests are supplemented by conventional small scale testing to determine material properties and behaviour. As known boundary conditions are imposed in the large laboratory tests and material and fracture parameters are measured directly from the test sample, the physics of fracture growth in unconsolidated sands may be addressed directly to enable realistic modelling and evaluation of existing models.

1.2 Mechanisms of Failure During Fluid Injection

The manner in which unconsolidated clastic sediments fail during fluid injection in situ is controlled almost entirely by the amount of injected fluid that is lost through the interconnected pores between the mineral grains. The amount of formation flow or "leak off" depends on such factors as the rate (and pressure) of injection, the relative viscosities of the injected fluid and resident pore fluid, and the permeability of the reservoir strata. When the amount of fluid leak off during injection is small, the injected fluid acts like a wedge which is driven into and parts the formation. The formation undergoes tensile failure. This failure mechanism is common when fluid is injected into low permeability, cemented reservoirs.

When fluid is injected into a reservoir where fluid leak off is high, pore fluid pressures peripheral to the well increase as flow into the formation occurs. The principal effective stresses (σ_1', σ_2', and σ_3') within this zone of excess pore fluid pressure decrease proportionally. This process results in a decrease in the available shearing resistance of the formation strata. The increase in excess pore fluid pressure may be sufficient to cause shear failure. Figure 1.1 illustrates the mechanism by which unconsolidated sands fail by shearing during fluid injection in

a high leak off environment. The initial Mohr-Coulomb effective stress circle is driven to the left by the pore pressure increase, until the stress circle becomes tangent to the failure envelope (assuming total stress increases less rapidly than the pore pressure).

Oil sands reservoirs in Alberta are commonly fractured using water or steam. The relatively low viscosity of these fluids may lead to formation leak off even at high injection rates. Therefore, portions of the reservoir may shear even as tensile partings are initiated and propagated. Because the leak off phenomenon in oil sands which contains two separate liquid phases (bitumen and water) is difficult, if not impossible to model analytically, the present program has focused on large scale laboratory simulations on samples where the resident and injected fluids are the same. The rate of leak off is therefore dependent on the rate of fluid injection and the absolute permeability. The injection rate can therefore be manipulated to study both failure mechanisms.

1.3 Objectives

The major objective of the study was to provide a better understanding of the mechanisms of hydraulic fracture formation process in a large triaxial stress chamber. The purposes of the Phase 1 study described in this report was to provide a preliminary indication of the mechanism of hydraulic fracturing under conditions high leakoff. In order to keep the testing and analysis simple, a single fluid was used for pore saturation and injection. In addition, the minor principal stress was generally vertical so that predominantly horizontal fractures were anticipated.

While there are many different mathematical models for hydraulic fracturing, all these models are based on particular assumptions regarding the mechanisms of fracture generation, propagation and leakoff. For example, these models make assumptions regarding fracture geometries and patterns, fracture fluid storage and

leakoff, pressure distribution in the fracture, changes in formation confirming stress caused by leakoff, and so forth. The purpose of this study was to examine the mechanisms and the assumptions that are appropriate for such models, rather than the models themselves. Of particular interest to this study is whether the failure mechanisms that occurs in the sand matrix during fracturing is best described by shear or tensile failure of the sand. It was also recognized before the study that the rate of fluid injection may have a significant influence on the failure mechanisms. Tests were therefore carried out at conditions of very high leakoff, as this best represents field conditions.

The ultimate goal of this work is to provide the basis for developing a framework to evaluate, verify and refine analytical models for fracturing of uncemented sands.

1.4 Project Funding

The project documented in this report has been jointly funded by the following companies and government agencies:

- Canada Centre for Mineral and Energy Technology (CANMET)
- Alberta Oil Sands Technology and Research Authority (AOSTRA)
- Mobil Oil Canada
- Shell Canada Ltd
- Esso Resources Canada Ltd.
- Golder Associates Ltd.

2.0 Materials Used

The large scale laboratory simulations of hydraulic fracture which have been carried out, consist of injection of a dyed fluid into a large sand sample saturated with a similar undyed, fluid. The sand, pore and injection fluid and tracer used in the large scale laboratory simulations of hydraulic fracture had to satisfy the following criteria:

1. Sand. The basic mechanical behaviour of the sand used in the laboratory tests had to be very similar to in situ oil sands at stresses associated with hydraulic fracture; an uncemented, granular media of appropriate absolute permeability.

2. Fluids. The resident and injection fluid must be of sufficient viscosity to enable the amount of fluid leak off during injection to be controlled by the injection rate. The fluids must also have good mineral grain wetting characteristics to allow full saturation of the test samples. The selection of an injection and pore fluid depends on its mobility in the test sand and injection rates practical to the laboratory.

3. Tracer. The tracer which is mixed with the injection fluid must enable accurate mapping of the fracture and the zone of leak off. The tracer must be easily visible during excavation, must not alter the viscosity of the injection fluid, and must not diffuse into the resident pore fluid over the time required to excavate the sample after the test.

2.1 Selection of Test Sand

Figure 2.1 shows the stress strain curve and volumetric strain curve for an undisturbed oil sands sample tested at in situ stresses. Oil sands exhibit high dilatancy and post-peak softening behaviour during triaxial compression under the low effective confining stresses such as those associated with hydraulic fracture. Figure 2.2 shows the response of a dense sample of quartzitic sand to triaxial compression. The strong dilatancy is clearly evident. Both sands show very similar behaviour even though the stress level of the in situ sample is very much higher. It is therefore is appropriate to use a quartz sand to investigate the fundamental fracture mechanisms in the field.

2.1.1 Grain Size Analyses

Sieve analyses were carried out on 6 samples of quartz sand obtained from commercial outlets in the Calgary area. Each sand had a uniform grain size distribution with the diameter of the particles at 50 percent finer by weight on the grain size distribution curve as follows:

Sand	D_{50} (mm)
Lane Mtn. 125	0.07
Lane Mtn. 70	0.18
Lane Mtn 20/30	0.52
Sil - 1	0.21
Sil - 3	0.29
Sil - 8	0.69

The complete grain size distribution curves for each type of sand are given in Figures 2.3 to 2.4.

2.1.2 Permeability Tests

The permeability of these sands to water was also determined to provide a data base for selecting the sand for the large scale fracture tests. The permeability of each of the uniformly graded quartz sands is as follows:

- Lane Mountain 125 $k = 4.56 \times 10^{-3}$ cm/s or 4.7 darcys
- Lane Mountain 70 $k = 1.48 \times 10^{-2}$ cm/s or 15.3 darcys
- Lane Mountain 20/30 $k = 3.00 \times 10^{-1}$ cm/s or 310.5 darcys
- Sil - 1 $k = 1.37 \times 10^{-2}$ cm/s or 14.2 darcys
- Sil - 3 $k = 5.00 \times 10^{-2}$ cm/s or 51.8 darcys
- Sil - 8 $k = 2.40 \times 10^{-1}$ cm/s or 248.4 darcys

Calculations based on poroelastic theory were carried out to give a general indication of the effect of fluid and sand properties on the injection rate required to propagate a radial fracture in the triaxial stress chamber. Details of the formulations are given in Appendix I. On the basis of the these calculations, Lane Mountain 125 sand was chosen for the fracture tests.

2.1.3 Specific Gravity

The specific gravity of Lane Mountain 125 sand grains was determined in the laboratory to be 2.65.

2.2 Selection of Pore Fluid

2.2.1 Viscosity Measurements

The major characteristics affecting the selection of the permeant for the large scale fracture tests was fluid viscosity. This controls the mobility of the fluid in the sand

pack and keeps the injection rate sufficiently slow to be manageable in the laboratory. Initially petroleum oils were considered because of their availability in a wide range of viscosities. For example, the viscosity of commercial oils range from 0.02 Pa-s to approximately 6.7 Pa-s. There are, however, difficulties associated with the use of petroleum oils in the large triaxial stress chamber. First, these oils are likely to have a chemical effect on the membrane and rubber sealing systems utilized in the chamber. Secondly, it may be very difficult to wet the sand grains and achieve full saturation of the test specimen without the use of very volatile surfactants such as pentane. To avoid the above problems alternate liquids were considered. The most promising of the liquids considered were glycerine and invert liquid sugar.

Glycerine and invert liquid sugar are clear, colourless, viscous liquids which are fully soluble in water. Invert liquid sugar is treated with enzymes which prevents crystallization of the dissolved sugar. The viscosity - temperature relationships for both liquids are given in Figure 2.5. The viscosity of glycerine at 20°C is 1.49 Pa-s, the viscosity of invert liquid sugar is 1.6 Pa-s at 20°C. The viscosity of either liquid may be adjusted to any lower level through mixing with water. There is no chemical reaction between glycerine or liquid sugar and any component of the triaxial stress chamber. Both liquids are also not controlled products under WHMIS regulations and therefore can be easily handled and disposed.

Glycerine was used as the pore and injection fluid in the first 5 tests, but was replaced in Test 6 with invert liquid sugar. The change was made due to the difficulty in obtaining glycerine in western Canada. Liquid sugar is manufactured in Alberta and can be attained on a more reliable basis. The viscosity-temperature relationship of this liquid is well documented and is very close to that of glycerine. Like glycerine, liquid sugar is soluble with water in all proportions and is compatible with the membrane and sealing systems used in the chamber. The viscosity of

glycerine (1.49 Pa-s) was matched exactly by mixing the liquid sugar (1.6 Pa-s) with a small amount of water (about 5% by volume).

2.2.2 Permeability Tests

The results of a permeability test carried out on Lane Mountain 125 sand impregnated with glycerine are shown in Figure 2.6. The hydraulic conductivity at 20°C was 4.42×10^{-6} cm/s (5.39 darcys).

The predicted injection rate versus fracture pressure relationship (based on poroelastic theory) for Lane Mountain 125 sand saturated with a 1.49 Pa-s fluid is given in Figure 2.7. For a fracture pressure of 400 kPa, a minimum injection rate of about 5 ml/s is required to ensure fracture propagation. Under these conditions, the time to propagate a radial fracture 0.21 m from the injection point (one third of specimen radius) would be about 4 seconds.

2.3 Saturation and B Tests

Prior to the execution of the large scale fracture tests several small scale triaxial tests were carried out to characterize the saturation properties of the test sand with a high viscosity pore fluid. The procedure used for preparing the small scale triaxial samples was similar to that employed in the large tests. A standard 7.5 cm diameter by 15.5 cm high triaxial sample was pluviated into a mould. The mould was vibrated to obtain the densest sample possible. The sample was then evacuated to -70 kPa and heated to 60 °C. Glycerine was heated in a reservoir to 45 °C. The hot glycerine was then introduced to the bottom stone and was allowed to flow for a few days under a small hydraulic head to achieve saturation. After saturation was complete, the sample was allowed to cool. During the cooling period, the top and bottom ports of the sample were open to glycerine reservoirs.

After preparation of the sample was complete, each sample was subjected to a series of pore pressure parameter B tests. Pore pressure parameter B is the measure of the undrained pore fluid pressure response of a sample to a change in isotropic stress. The B value can be used to determine the pore fluid pressure required to fully saturate a test sample. The confining and back pressures applied to the sample were raised in equal increments and the B value was measured following each increment. Pore fluid saturation is determined when the B parameter becomes constant or close to one. For sand samples made in the laboratory, the B value is usually close to one.

Figure 2.8 shows the results of a typical small scale glycerine saturation test. The results indicate that a back pressure of at least 200 kPa is required to saturate the test sample. This pressure was used for all large scale fracture simulations performed in this study.

2.4 Injection and Diffusion Tests

In the large scale fracture tests, the injected fluid was coloured with a fluorescent dye so that the fracture could be traced when the sample was excavated. To ensure the dye would not diffuse through the sample between the time the fracture test was carried out and the sample was excavated, a series of injection and diffusion tests were performed. Several test procedures were employed:

1. The standard size triaxial samples used in the saturation tests were removed from cell and injected with fluorescent dye using a syringe. After several weeks the samples were cut open under black light and the pattern of dye was observed.

2. Sand saturated with both glycerine and liquid invert sugar were compacted into bowls. The same fluid coloured with dye was poured on top of each

sample and the bowls were stored. A bowl of each material was excavated under black light each day for 4 days. The depth of penetration of the dye was observed.

3. Sand was pluviated into a glass permeameter and saturated with liquid sugar. Liquid sugar coloured with dye was injected into the top of the sample under a 50 kPa pressure. After the dye had infiltrated the sample several cm the sample was locked off and the position of the dye front was mapped on the glass walls of the permeameter. The position of the dye front was monitored daily for 2 weeks. This test is shown in Figure 2.9.

In all of the above tests migration of the fluorescent dye in the sand samples was not observed. It was concluded from these tests that diffusion of dye in the large fracture sample would not be significant over the time required to disassemble the apparatus and excavate the sample (i.e. 2 - 5 days).

3.0 EQUIPMENT AND PROCEDURES

This section describes the equipment and test procedures used for the large scale hydraulic fracture simulations.

3.1 Test Equipment

The large scale hydraulic fracture tests were carried out in the triaxial stress chamber shown in Figure 3.1. The apparatus accommodates samples 1.4 m in diameter and up to 1 m high. Principal stresses of up to 1000 kPa can be applied independently through a circumferential (σ_h) and upper (σ_v) cavity as illustrated in the figure. The pore fluid pressure is applied to the sample through drainage ports in the base of chamber and through ports in top loading plate. A manually controlled system (Figure 3.2), fed by a pressurized air supply, is used to impose a variety of stress conditions on the test sample using 130 litre capacity air-over-water cells (one cell each for σ_h, σ_v, and pore fluid pressure) and pressure regulators. Constant stress conditions are achieved by pressure regulators. Horizontal stresses are transmitted to the sample through a latex rubber membrane, as in triaxial testing, while vertical stresses are applied through a steel plate.

The injection well is situated in the centre of the sample cavity and extends the full height of the sample. For each test the well is located and the sand sample placed around it. The well was a hollow steel pipe with an inside diameter of 25.4 mm and an outside diameter of 33.5 mm. The well is perforated at mid-sample height over an interval of 50.0 mm with 8 rows of 3.5 mm diameter holes (Figure 3.3). The perforated zone is protected against sand infiltration by a 230 mesh screen. The injection well passes through the loading plate, the upper pressure cavity and the chamber top lid and is connected with 12.7 mm copper tubing to the injection pump. The injection well is vented through the base of the chamber with 12.7 mm copper tubing.

The injection pump unit (Figure 3.4) consists of the following major components:

- an AC hydraulic power unit (hydraulic pump, electric motor, fluid tank, set relief valve and check valve);
- an 9.4 litre pressure accumulator;
- a pressure compensated temperature stabilized flow control valve with compensator stroke adjustment;
- a 6.4 cm diameter, 30.5 cm stroke hydraulic cylinder

The hydraulic power unit drives oil through the flow control valve and into the hydraulic cylinder to drive a metal piston. The piston provides an interface between the hydraulic oil and the injection fluid which is pumped into the sample through the injection well. A LVDT was attached to the piston rod of the hydraulic cylinder to measure volume of fluid pumped into the sample during a test. The injection pump unit was designed to deliver a constant flow rate (0 to 200 ml/sec) independent of load or flow resistance up to a maximum 3500 kPa. This is accomplished by the flow control valve and the pressure accumulator.

Prior to the fracture simulations the injection pump unit was tested by rapidly cycling the output pressure between 0 kPa and 3500 kPa and recording the displacement of the LVDT (i.e. flow rate). A linear relationship between displacement and time was attained. This confirmed that the flow rate was independent of flow resistance over the working range of the pump.

Instrumentation was embedded in the sample to measure pore fluid changes and deformations in the sample during the fracture tests. Internal pore fluid pressures were monitored using "subminiature" pressure transducers. These transducers have strain gauged diaphragms 7 mm in diameter. Transducer circuits are Wheatstone Bridge configurations. The pressure range of these transducers is 0 to 3500 kPa.

The pressure transducers were mounted inside copper tubes (Figures 3.5 and 3.6) to isolate the diaphragms from stress exerted by the sand grains. This ensures the transducers are measuring pore fluid pressures only. An additional subminiature pressure transducer was mounted inside the well at the point of injection (Figure 3.7). Later in the laboratory program, this transducer was mounted outside the well at the same location to negate measuring head losses as the fluid passes through the perforations and well screen. Standard size pressure transducers were used to measure the pressures in the horizontal and vertical stress cavities, pressure of the fluid entering the top of the injection well, and the pressure at the injection well vent.

Deformations at points within the sample were monitored using LVDT and strain gauge extensometers. These devices are shown in Figure 3.8 and 3.9. The strain gauge extensometer consisted of a 75 mm long, 12 mm wide strip of copper foil mounted between two 45 mm diameter anchor plates. A strain gauge was mounted on the copper foil to measure deflection of the anchor plates. The LVDT extensometer consisted of miniature LVDTs (20 mm in diameter and approximately 92 mm long) mounted between two anchor plates as shown in Figures 3.8 and 3.9. The stroke range of the LVDTs is 5 mm. The LVDTs are protected from the pore fluid and sand by protective tubing and o-ring seals.

Pore fluid pressures, vertical stress, radial stress, sample deformation, injection pressures, and injection flow rate were recorded electronically using an IBM based computer data acquisition system located adjacent to the stress chamber (Figure 3.10).

3.2 Sample Preparation

Samples were prepared by pluviation of dry sand from a hopper directly above the chamber (Figure 3.11). The hopper is exactly the same diameter as the sample and

equally high so that one complete sample can be formed without reloading. The equal diameters result in essentially one dimensional pluviation conditions. The base plate of the hopper is perforated with 5.2 mm diameter holes on 63 mm centres (approximately 400 holes). Pluviation was initiated and terminated by moving a shutter plate installed directly below the base plate of the hopper.

Prior to pluviation the injection well was installed and instrumentation for measuring sand deformation and pore fluid pressure changes were suspended at strategic points in the sample. The instrumentation was placed on three levels, two above the injection zone and one below. Details of the instrument placement is given in Figure 3.12.

A bed of uniform gravel was placed at the base of the sample cavity to provide uniform distribution of pore fluid and back pressure at the bottom drainage interface. A filter cloth was placed over the gravel to prevent migration of sand into the gravel and drainage tubing. Later in the laboratory program the drainage boundary was changed to reduce friction at the ends of the sample. The modified configuration consisted of the following (Figure 3.13):

- a layer of gravel
- metal screen
- a layer of POLYNET (geonet consisting of two sets of polyethylene strands forming a diamond shape)
- a layer of high density polyethylene (HDPE), 40 mil perforated with 6.4 mm diameter holes
- metal screen
- a layer of gravel

The friction angle between the geonet and HDPE was measured to be approximately 8 degrees.

Once the sample was deposited the top surface was levelled and the chamber was assembled. Two methods were used to saturate the sample with the viscous pore fluid:

1. An isotropic confining stress of approximately 50 kPa was applied to the sample. Heating coils on the outside of the chamber were used to preheat the sand prior to flooding (about 36 hours) and viscous pore fluid was heated to reduce its viscosity and allow it to penetrate the pore space of the sand more easily. The hot fluid was injected through the bottom drainage ports under a pressure of approximately 35 kPa. The top of the sample was subjected to a negative 70 kPa (vacuum) pressure during injection. This helps draw the fluid into the sample and reduces the amount of air in the system. This method was used for Tests 1 through 6.

2. An isotropic confining stress of 450 kPa was applied to the sample. The top of the sample was subjected to a negative 70 kPa (vacuum) pressure. The viscous pore fluid was injected at room temperature under a driving pressure of 400 kPa through the bottom drainage ports. This method was used for Tests 7 and 8.

Both methods were equally successful in providing a fully saturated sample. The first method was found to be much faster than the second method, however, it was much more labour intensive.

3.3 Test Procedures

The test procedure for carrying out a large scale hydraulic fracture test is summarized below. It is noted that supplementary tests were added to the basic procedure as the laboratory program progressed. The purpose of these tests was to provide additional information regarding the geomechanical and fluid flow characteristics of the samples prior to hydraulic fracturing. Therefore, not all tests were carried out on each sample.

After the sample was saturated and the applied stresses relaxed back to atmospheric pressure, the test procedure was as follows:

- The data acquisition system was started and initial reading of the instruments taken to provide a zero reference level.

- Vertical and horizontal confining stresses were applied in equal increments to the test sample. The sample was permitted to consolidate under these isotropic stress increments.

- A constant head permeability test was performed. A constant head was maintained across the sample and the volume of pore fluid flowing per unit time (q) was measured. The piezometers embedded in the sample were used to measure the hydraulic gradient (h/l). Permeability was calculated using Darcy's law:

  $$k = ql/Ah$$

  Permeability tests were carried out on fracture samples 6, 7, and 8.

- A sub-fracture pressure injectivity test was carried out. The injection well was pressurized rapidly to one-half the applied isotropic stress. The response of pressure transducers in the injection well and piezometers

embedded in the sample were monitored. The volumes of fluid entering the sample through the injection well and leaving the sample through the top and bottom drainage boundaries were recorded. Injectivity tests were carried out on fracture samples 6, 7, and 8.

- A drained loading test was performed. The isotropic confining stress was increased rapidly, the sample was permitted to drain freely at both ends. Piezometers in the sample were monitored in order to detect any anomalies in the stress field or pore pressure distribution in the sample. These tests were carried out on samples 4, 5, 6, 7, and 8.

- A B value test was performed. The pore pressure parameter B is ratio of the undrained pore fluid pressure response of the sample to a change in isotropic total stress. This B value is used to assess the saturation of the sample. B tests were carried out in tests 3, 4, 5, 6, 7, and 8.

- The sample was unloaded to atmospheric pressure to allow the injection well to be primed with dyed injection fluid. The well is then connected to the injection pump.

- The vertical and horizontal stresses applied to the sample were manipulated independently to attain the desired stress difference (K_o value) applied to the sample.

- The data acquisition was placed on "fast scan mode"; at this rate the system records data at a rate of 50 readings per channel per second. Fast scan mode occurs for 20 seconds after which the system reverts back to a slower scan rate (normally 3 readings per channel per second).

- The injection pump was activated to carry out the fracture test. A given volume of dyed fluid was injected at a pre-determined rate for each test.

- After injection, the sample was allowed to reach equilibrium based on readings of the internal instrumentation. After equilibrium conditions were attained, the system was depressurized slowly under undrained conditions.

After the test was completed the computer logged data was stored on permanent data discs. The data was then processed and plots of each measurement versus time were produced.

3.4 Sample Excavation and Sampling

Once the chamber lid and upper loading plate were removed the upper drainage boundary was placed under black light and checked for the presence of fluorescent dye. The drainage boundary (gravel, screens, etc.) was then carefully removed and the top of the sample was exposed. A wooden platform was then erected around the chamber and the black light unit was affixed above the chamber. The sample was then excavated in horizontal lifts, normally 2 to 4 cm in thickness, under black light using small spatulas and scoops. When the lift was completely excavated, locations of fluorescent dye were marked with black string. The black light was then turned off and under normal light, signs indicating the test number, orientation of the sample (0, 90, 180, 270 degrees), and depth of the lift as well as a meter stick were placed on the surface of the sample. A photograph of the sample surface was then taken with a camera located directly above the chamber (Figure 3.14). The procedure was then repeated for each lift until the lower drainage boundary was reached.

Thin walled tube samples were extracted from the sample at various depths. These samples were used to determine the geotechnical properties (strength-deformation, density etc) of the sand at various levels from within the fracture sample.

The photographs showing the locations of the dye were digitized. Each photograph was orientated on the grid of an electronic tablet using the angle markers placed on the sample surface. The meter stick on the surface of the sample was used to scale each photograph. The cross hairs of the input curser of the digitizer were used to target and record in cartesian coordinates the dye locations. Patches of dye on the photographs were digitized on grid points. Digitized data were then plotted in three dimensions. Areas in the sample where the dye was concentrated appear as clouds of points on the plot. The plotting program allows rotation of the three dimensional axes so that the orientation of surfaces can be observed. Hard copies of each plot showing the dye surfaces from several viewing angles were made.

4.0 FRACTURE TESTS

A total of 8 hydraulic fracture tests were carried out during this project, as summarized on Table 4.1. Initial stress conditions, injection rates are also shown. The results of these large scale fracture simulations are presented in this section.

Instrument response data is given as plots of the channel output in engineering units versus time. The instruments which are embedded in the fracture sample are identified by numbers which indicate their positions as follows:

XXX - YZ

where:

XXX is the angular position of the instrument in degrees (see Figure 2.6)

Y is the vertical position of the instrument
1 = 25 cm above injection point
2 = 10 cm above injection point
3 = 10 cm below injection point

Z is the radial position of the instrument
i = 0.5 x radius (tests 1, 2, 3 and 4)
= 0.25 x radius (tests 5, 6, 7 and 8)
o = 0.75 x radius (tests 1, 2, 3 and 4)
= 0.5 x radius (tests 5, 6, 7 and 8)

It is noted that the LVDT extensometers were placed on a horizontal plane level with the perforated zone of the injection well for tests 5, 6, 7, and 8.

As discussed in the previous section, locations of fluorescent dye are plotted as point clouds in "three dimensional" plots.

4.1 Fracture Test No. 1

Before the fracture test was carried out, the sample was subjected to a vertical confining stress of 400 kPa and a horizontal confining stress of 600 kPa. The sample was permitted to drain and to dissipate the excess pore fluid pressure which developed during the application of the external loading. The time required for the fluid drainage to occur depends on factors such as the size and geometry of the specimen, permeability of the sand to the permeant, and compressibility of the sand structure. The time needed to drain glycerine from the sample to establish the required effective stress conditions was calculated based on consolidation theory to be approximately 60 minutes. Examination of the measurements after the test, however, indicated that the amount of drainage prior to the fracture test was small. The rate of drainage may have been reduced significantly by frictional losses between the highly viscous cold glycerine and the inside surfaces of ports, tubes and valves egressing the sample cavity.

Because the rate of dissipation of excess pressure in the glycerine pore fluid was underestimated and the computer software was originally designed to measure changes in pore fluid pressure rather than absolute magnitudes, the fracture test was carried out at a horizontal to vertical effective stress ratio much greater than 2. Examination of the voltage readings of the pore pressure transducers and transducers connected to the vertical and horizontal stress cavities indicated that the vertical and horizontal effective stresses acting on the sample at the time the fracture test was carried out could not be calculated with a high degree of certainty. This is because the data acquisition was based on pressure differences and therefore the voltage measurements of the transducers were not referenced to a common datum. The data acquisition software was modified for subsequent tests to overcome the above limitations.

In this fracture test, 927 ml of glycerine, coloured with fluorescent dye, was injected into the test specimen in 9.7 seconds. This corresponds to an injection rate of 96 ml/s. Figure 4.1 shows the locations of dye found after the test. Also shown in the figure is the position of instrumentation embedded in the sample. It is noted, that the pattern of dye found in each lift was digitized by direct measurement during excavation. The digitizing grid was fairly coarse and resulted in poor delineation of the dyed surfaces found in the sample. In subsequent tests the surface of the sample was photographed and the pattern of dye was digitized electronically (refer to Section 3.4). This permitted the use of a very fine grid and greater definition of dye surfaces. The results of this test (Figure 4.1) appeared to show the development of a horizontal fracture accompanied by considerable vertical leak off.

The response of the LVDT extensometers are shown in Figure 4.2. Also shown in the figure is the fluid injection record (i.e. volume vs. time). The injection occurred between 12 and 21 seconds on the time axis.

Two of the four LVDT extensometers did not show movement during the test. The other extensometers display fluctuation in the readings between 10 and 30 seconds. During this time period the sampling rate was increased and the fluctuation in measurements likely reflects electronic "noise" as fewer readings are averaged prior to collection by the data acquisition unit.

Figure 4.3 shows voltage readings of strain gauge extensometers with time. Instrument 0-1i appears to show significant response at the onset of injection (12 seconds on time axis). This instrument was located 25 cm above the injection point in the direct path of the fracture (Figure 4.1). It is noted, however, that no other extensometer displays a response during the test.

The response of the piezometers embedded in the sample and the pressure transducer inside the well at the point of injection are shown in Figure 4.4a and

4.4b. These pressure measurements correspond to the change in pore fluid pressure above the pore pressure existing in the sample prior to injection. Instruments 90-1i and 240-3i appear to be giving erroneous readings and should be ignored.

4.2 Fracture Test No. 2

A leak between the injection well assembly and the sample was detected during priming of the injection well for Fracture Test 2. Repair of the problem would have required significant disturbance of the sand around the injection well. Although the test could have been carried out, it was concluded that disturbance of the sample would cause preferential flow paths to develop during injection and the results would be extremely difficult to interpret.

4.3 Fracture Test No. 3

In this test 907 ml of glycerine was injected into the sample in 9.7 seconds (injection rate of 93.5 ml/s). As in Test 1, the rate of pore fluid pressure dissipation was extremely slow due to the high viscosity of the cold glycerine. The stresses at the time the fracture test was carried out were as follows:

Vertical confining stress, σ_v = 460 kPa
Horizontal confining stress, σ_h = 493 kPa
Pore fluid pressure, u = 432 kPa

This corresponds to a vertical effective confining stress of 28 kPa and a horizontal effective confining stress of 61 kPa. Therefore the horizontal to vertical effective stress ratio (Ko value) prior to the fracture test was 2.2.

The locations of dye found during excavation of the specimen after the test are given in Figure 4.5. Figure 4.6 shows the response of the LVDT extensometers and the fluid injection record. The response of the strain gauge foil extensometers are

given in Figure 4.7. Extensometers did not show any significant response during the fracture test. This result is similar to that of Test 1 in this regard.

The specimen displayed a significant pore fluid pressure increase when vertical and horizontal loads were applied. Figures 4.8a and 4.8b show the response of piezometers situated in the injection well and embedded within the sample. The zero pressure corresponds to the pore fluid pressure a the start of the test. Piezometers 270-1i and 300-2i did not display any response during the test probably as a result of electrical shorts after flooding the sample with glycerine. The remaining piezometers which were embedded in the sample show a pore fluid pressure increase of about 40 kPa. This pore pressure increase could be due to:

- a total stress increase due to dilation around the fracture zone, or
- a pore pressure increase due to transmission of the increased pore pressure in the injection zone/well/fracture.

The chamber stress conditions limit the amount of total stress increase. Similarly, the injection volume is small so that pore pressures would only increase locally around the fracture.

4.4 Fracture Test No. 4

The injection rate for Test 4 was 20 ml/s, 80 ml of dyed glycerine was injected in 4 seconds. The sample was subject to a horizontal confining stress of 600 kPa, a vertical confining stress of 400 kPa, and a pore fluid pressure of 200 kPa at the time the fracture test was carried out. This corresponds to a K_o value of 2.0.

Figure 4.9 shows the pattern of dye found in the sample after injection. A cupped surface extending laterally from the injection zone to one edge of the sample and diagonally from the injection zone to the upper edge of the sample is visible. Substantial leak off from this surface is apparent.

The response of the sample and system instrumentation is given in Figures 4.10 and 4.11. In these figures the total pressures (rather than changes from initial pressures) are shown. None of the instrumentation embedded in the sample showed a significant response during injection. It is noted, however, that four of the internal piezometers and two of the LVDT extensometers were damaged during sample placement and pressurization and were not working during the test.

An expanded plot of the pressure pulse in the injection well during the fracture test is given in Figure 4.12. The peak injection pressure measured inside the well at the perforations was 1200 kPa. This value is about 300 kPa greater than that measured upstream from the injection point by the transducer at the top of the injection well. The transducer at the top of the well should read a slightly lower value due to head losses in the well. Both transducers were re-calibrated after the test and were found to be operating properly. It is apparent that the transducer at the top of the well lags the transducer at the perforations, measures a lower peak pressure, and has a linear rather than curved pressure response. Such behaviour is usually symptomatic of air in the transducer port. Instead of only compressing the fluid in the system, a small pocket of air in the vicinity of the transducer would also have to be compressed during injection, which delays deflection of the diaphragm in the transducer. In later tests, an additional transducer was installed at the bottom of the well (at the well vent) to provide addition data.

4.5 Fracture Test No. 5

In this test 20 ml of dyed glycerine was injected into the test sample in 4 seconds (5 ml/s). The K_o value for this test was 2.0 (σ_h = 600 kPa, σ_v = 400 kPa, and u = 200 kPa).

A drained loading test was carried out on this specimen prior to the fracture test. The purpose of this test was to determine whether stress abnormalities in the specimen occur during sample loading. The test was carried out by rapidly increasing the isotropic confining stress by 50 kPa and observing the response of the piezometers embedded in the specimen. The top and bottom boundaries of the sample were permitted to drain freely during the test. The results of this test is given in Figure 4.13. Each of the four internal piezometers shown in the figure display a small gradual build up pressure followed by a gradual reduction in pressure. These results do not indicate the presence of any major stress concentrations in the sample caused by external loading.

After the drained loading test, a pore pressure parameter B test was performed. The pore pressure parameter B is a measure of the undrained pore fluid pressure response of the sample to a change in isotropic stress. The greater the increase in pore pressure, the greater the sand skeleton compressibility. For most reconstituted sands the B parameter is usually close to one because the sand structure is more compressible than the pore fluid and therefore the load is taken almost entirely by the fluid. The pore pressure response is affected by the volume increase of the drainage lines which separate the test chamber from the upstream and downstream back pressure valves and by the presence of air in the sample, drainage filters or lines.

In this test the top and bottom drainage boundaries were closed and the sample was subjected to an isotropic stress increase of 45 kPa. The results of the be test are

given in Figure 4.14. The internal piezometers show an increase in pore fluid pressure of about 15 kPa. This corresponds to a B value of about 0.33. It is noted that the pore pressure generated in the sample due to the loading decays slowly with time. This may be due to compliance of the plastic tubing between the drainage boundaries of the sample and the shut in valves. This compliance would also contribute to the low B value, which is normally in the vicinity of 0.9 for a sand of similar density.

The results of Fracture Test 5 are given in Figures 4.15, 4.16 and 4.17. In contrast to the "cupped" type surface observed in Fracture Test 4, a distinct "conical feature" is visible on the fracture plot (Figure 4.15).

The peak injection pressure measured at the top of the injection well (Figure 4.17) is about 240 kPa, 160 kPa less than that required to overcome the minimum confining stress. (It is noted that the transducer outside the well at the perforations shows an initial reading prior to fracture of 500 kPa rather than the 200 kPa applied fluid pressure. This is because the transducer was not shielded against the sand and is therefore is measuring the total stress in the sand matrix.)

Based on the dye distribution in the sample and the low peak injection pressure it does not appear that a tensile parting, as observed in Test 4, was generated in this test at a low injection rate.

4.6 Fracture Test No. 6

Test 6 was carried under the same stress conditions and injection rate utilized for Test 5 (σ_h = 600 kPa, σ_v = 400 kPa, and u = 200 kPa). The purpose of the test was to determine if the results of the previous test were repeatable. In addition, permeability and sub-fracture injection tests were carried out on this sample before the fracture test.

Figure 4.18 gives the results of a permeability test carried out on Fracture Sample 6 after saturation. The permeability of the sample was measured at 1.5 darcys. The permeability measured in the standard size triaxial test sample was 5.4 darcys (Section 2). Permeability measurements were carried out in the test chamber by means of a constant head test. A steady vertical flow of fluid, under constant head, was maintained through the sample and the volume of fluid flowing per unit time was measured. The hydraulic gradient was measured between two points in the sample using the internal piezometers. The length of the sample used in the calculations is the vertical distance between the piezometers. Flow was assumed to be uniform through the cross-sectional area of the sample.

The difference in permeability between that measured in the standard size triaxial test and that measured in the large fracture chamber can be explained by the differences in sand fabric and porosity resulting from sample preparation. (Fabric refers to the distribution and orientation of grains in the sand mass and the forces between adjacent sand grains). Experience has shown that the determination of permeability of sand samples prepared in this manner vary and that only a 5 to 10 times permeability change is considered significant. It is noted that mechanical behaviour is much less variable than permeability.

The results of two separate sub-fracture injectivity tests carried out on this sample are given in Figures 4.19 and 4.20. For both tests a pressure of 200 kPa was applied instantaneously to the fluid in the injection well. In both tests the sample was subject to an isotropic confining total stress of 400 kPa. The initial condition for each test was slightly different. In the first test (Figure 4.19) the sample had an initial pore fluid pressure throughout the sample of 35 kPa, while in the second test (Figure 4.20) the initial pore fluid pressure was 0 kPa. In both tests the top and bottom drainage boundaries of the sample were vented to atmosphere.

Both injection tests would result in samples with the same pressure distribution at equilibrium. However, the rate and path of pore pressure redistribution and dissipation can be expected to vary. The response of the transducer in the injection well, the transducer outside the well at the perforations and the piezometers embedded in the sample prior to reaching equilibrium in each test were significantly different.

In Test 1 the pressure in the well increases rapidly to about 200 kPa and then slowly decays with time until it reaches an equilibrium pressure of about 150 kPa. The difference between the applied injection pressure of 200 kPa and the equilibrium pressure of 150 kPa reflects head loss in the tubes and fittings. One of the piezometers in the sample shows a pressure increase, two show a pressure decrease and one remains constant.

In Test 2 the pressure in the injection well reaches the equilibrium pressure of about 150 kPa quickly and the piezometers in the sample each show a pressure increase. This difference in sample behaviour is due to different initial conditions and boundary conditions during the two tests. In Test 1 two boundary conditions of the sample are changed simultaneously. The centre of the sample experiences an increase in pressure while the pressure at the top and bottom of the sample is decreased by opening the drainage valves to the top and bottom of the sample simultaneously. In Test 2 only the boundary condition in the well changes; excess pore pressure above atmospheric pressure in the sample were dissipated before the test was carried out.

The results of the pore pressure parameter B test and the drained loading tests are given in Figure 4.21. An isotropic stress increase of 90 kPa causes an initial increase in pore fluid pressure of about 30 kPa (B value of 0.33). This increase in pore fluid pressure dissipates slowly with time. Again, the low B value and pressure drainage may be due to compliance of the plastic tubing between the drainage

boundaries of the sample and the shut in valves. There may also have been some air trapped in the pores of the sample during the saturation process.

The response of the internal piezometers during the drained loading tests are very similar. This would tend to indicate the stress distribution in the sample is uniform. It is also noted in Figure 4.21 that when the pore fluid pressure at the boundaries are increased each internal piezometer shows an almost identical response. This also tends to indicate that the sample exists under an uniform stress field. This rapid transmission of pore pressure indicates that the sample is fully saturated.

Data from Fracture Test 6 are given in Figures 4.22 to 4.25. Several interesting observations may be derived from these test results:

1. Fluorescent dye was found almost uniformly distributed throughout the entire sample after the fracture test (Figure 4.22). This is attributed to contamination of the sample during the injectivity and permeability tests by residue dye in the injection well assembly from the previous fracture test. Propagation of dye into the sample during the fracture test itself could not be determined. However, the presence of dye throughout the sample indicates the absence of preferential flow paths

2. The peak injection pressure measured during the test was about 32 kPa above the initial pressure of 200 kPa (Figure 4.23). This result is very similar to that observed in Fracture Test 5 which was carried out under the same stress condition and injection rate. This result demonstrates repeatability of the testing procedures.

3. Two of the piezometers embedded in the sample show a pressure increase during the fracture test, 10912 to 10916 seconds (piezometers 300 - 2i and 240 - 3i, Figure 4.24). These piezometers are located in the

same quadrant of the sample, one above the injection point and one below.

4. Two of the LVDT extensometers display movement during the test (Extensometers 225 - 2i and 315 - 3i, Figure 4.25). These extensometers are located near the piezometers which also showed a response during the test.

The results attained from Test 5 and Test 6 tend to indicate that, at an injection rate of 5 ml/s, tensile parting of the sample does not occur because the peak injection pressure is far less than the minimum confining stress. This assumes that the stress fields in the sample is uniform. However, the pattern of dye in the sample (in Test 5) and its distance from the point of injection, suggests that flow was along isolated surfaces within the media and not due to uniform seepage through the pore system. It may be possible that surfaces may have resulted from shear deformations caused by the increase in pore fluid pressure during injection. More extensive analysis are required to characterize the cause of these discontinuities.

4.7 Fracture Test No. 7

In this test 40 ml of dyed invert liquid sugar was injected into the test sample in 4 seconds (10 ml/s). The K_o value for this test was 2.0, i.e.

- Horizontal total stress, (σ_h) = 600 kPa
- Vertical total stress, (σ_v) = 400 kPa
- Pore fluid pressure, (u) = 200 kPa

A permeability test carried out after the sample was saturated yielded a permeability of 4.4 darcys. This value is slightly greater than the 1.5 darcys

measured in Test 6. As discussed previously, a variation in permeability of this magnitude can be attributed to variations in sand fabric and porosity resulting from sample preparation. A permeability change of this magnitude is not considered significant.

The results of the injectivity test are given in Figure 4.26. The sample was subjected to an isotropic confining stress and allowed to drain under atmospheric pressure. A constant pressure of 200 kPa was then applied at the injection well. The results show the injection pressure outside the well screen reaches a equilibrium pressure of 150 kPa in about 1 minute. Piezometers in the specimen display a slight pressure increase in response to the injection pressure. The pore pressure parameter B measured just prior to the fracture test was about 0.3. The drained loading test did not indicate any stress abnormalities in the sample. The above test results are consistent with previous tests.

The results of Fracture Test 7 are given in Figures 4.27 to 4.31. The following observations are noted:

1. Fluorescent dye was not found more than 15 cm from the well screen. The injected dye was concentrated in the pore space near the well. It would appear that leakoff in this test occurred by seepage through the pore system rather than along stress discontinuities as observed in previous tests.

2. The instrumentation embedded in the sample did not respond during fluid injection.

3. The peak injection pressure exceeded the minimum confining stress by about 25 kPa, but only for a fraction of the injection time.

These observations indicate that a tensile parting could have been developed but did not propagate an appreciable distance from the well during the 4 second injection period.

4.8 Fracture Test No. 8

Fracture Test 8 was carried out with a Ko value of 0.5 (σ_h = 400 kPa, σ_v = 600 kPa, and u = 200 kPa). Thus, the minor principal stress was horizontal. As in Test 7, 40 ml of dyed invert liquid sugar was injected into the test sample in 4 seconds (10 ml/s).

Figure 4.32 shows the results of a drained loading test and a fluid injectivity test carried out prior to the fracture test. An isotropic confining stress is applied slowly to the sample over several minutes with the top and bottom of the sample vented to atmosphere. The pore fluid pressure in the sample (e.g. Piezometer 270-1i) increases to about 70 kPa, levels off and begins to dissipate as the confining stress becomes constant. During this drainage period, the injectivity test is initiated when, 200 kPa pressure is applied to the fluid in the well. The injection pressure increases rapidly to about 190 kPa, levels off and remains constant. Application of the injection pressure appears to result in a slight decrease in the rate of pore fluid pressure dissipation as shown by the internal piezometers.

A permeability test carried out on this sample gave 2.8 darcys. The pore pressure parameter B prior to fracture was consistent with previous tests at 0.3.

The results of Fracture Test 8 are summarized in Figures 4.33 to 4.36. The important aspects of the test results are noted as follows:

1. The pattern of dye in the sample after injection is in the form of a conical feature starting above the injection zone and extending to bottom

of the sample. A few small dyed surfaces in the sand were also found near the edge of the sample, although no direct connection between these surfaces and the main conical feature were observed. The surfaces on which the dyed fluid travelled from the main conical feature to these areas were therefore very thin with little or no leakoff from these surfaces.

2. Three of the four LVDT extensometers display movement at the onset of injection. Two piezometers also show a response during injection. The response of these internal instruments occurs in all quadrants of the sample which appears consistent with the pattern of dye observed in the sample after the test.

3. The peak injection pressure recorded during the test was approximately 320 kPa (Figure 4.36). It is noted that this pressure is 80 kPa below the minimum confining stress applied to the sample during the test.

The pattern of dye observed in this test after injection appears to be similar to that found in Test 5. In both tests the peak injection pressure was well below the minimum confining stress applied in the sample.

5.0 ASSOCIATED TESTS

This section describes standard-sized triaxial tests carried out on samples from the large scale simulations. The purpose of these tests was to characterize the geomechanical and fluid flow behaviour of the large scale fracture samples.

5.1 Stress-Deformation and Strength Tests

The shear strength data on undisturbed samples taken from several large scale fracture tests are summarized in the form of a p'-q diagram in Figure 5.1. It is noted that:

$$p' = \sigma_1' + \sigma_3' / 2$$
$$q = \sigma_1' - \sigma_3' / 2$$

The diagram is plotted in terms of p' and q because on a p'-q plot each test is represented by a single point (which corresponds to the top of the Mohr circle) instead of a series of semi-circles as in a Mohr-Coulomb diagram. It is therefore easier to evaluate test results using p'-q diagrams. The data included in Figure 5.1 were derived from cemented drained triaxial tests. A linear failure line can be drawn through the test values, corresponding to Mohr-Coulomb strength parameters $\Phi' = 38^\circ$ and $c' = 53$ kPa.

The stress-strain and volume change relationships for these tests are given in Appendix II. Each specimen displays dilatant behaviour during shear and this increase in volume during shear straining was accompanied by strain softening behaviour in the post-peak region. It is noted that this geomechanical response is consistent with the behaviour of Alberta oil sands under stress conditions associated with injection in situ (Section 2).

5.2 Density Measurements

Bulk density determinations were carried out on the thin-wall tube samples taken during the excavation of the fracture samples. A plot of bulk density versus depth is given in Figure 5.2. No apparent trend between sample bulk density and depth is evident. The overall range in bulk density of one sample (for example, fracture sample 4) is similar to that for all fracture test samples. The above results plotted in terms of porosity are given in Figure 5.3.

6.0 DISCUSSION

The data from the large scale fracture tests indicate a relationship between injection rate and peak injection pressure. Fracture tests 4, 5, 6, and 7 were carried out under identical stress conditions (σ_h = 600 kPa, σ_v = 400 kPa and u = 200 kPa), and only the injection rate was varied. Figure 6.1 is a plot of injection rate versus the difference between peak injection pressure and minimum confining stress.

For Tests 4 and 7 the peak injection pressure exceeds the minimum confining stress. This would indicate that the rate of fluid injection is sufficient to cause tensile parting of the sand during the test.

The pattern of dye found in fracture sample 4 after the test appears to show a distinct curved surface which reaches from the injection zone to the edge of the sample. A significant zone of leak off on both sides of this plane is also evident. This test may be interpreted as a tensile parting which propagates rapidly to the edge of the sample followed by leak off as additional fluid is pumped into the sample. This flow away from the parting may be occurring along thin shear surfaces which may form due to shear strain caused by the volume change associated with the formation of the parting. (It is noted that shear strength tests performed on undisturbed tube samples taken from the fracture samples display strongly dilatant behaviour during shear, Appendix II). The change in local stresses in the sample caused by the dilatant volume change may also account for the curved shape of the main parting.

In Test 7, the rate and total volume of injection was half that used in Test 4. The dye in the sample after the test was found to have migrated only a short distance from the well. In this test, it would appear that the lower injection rate was sufficient to initiate the tensile parting but it was not sufficient to sustain its propagation.

Tests 5 and 6 were carried out at one quarter the injection rate employed in Test 4. These tests gave almost identical peak injection pressures. The pattern of dye in the Test 5 sample shows the formation of a large number of surfaces on which flow had taken place. This may indicate the sample is undergoing shear deformation.

Fracture Test 8 was carried under stress conditions to induce a vertical fracture (σ_h = 400 kPa, σ_v = 600 kPa and u = 200 kPa), the injection rate was equal to that used in Test 7 (10 ml/s). In contrast to Test 7, in this test the peak injection pressure did not exceed the minimum confining stress (Figure 6.1). This may indicate that the boundary stresses applied to the sample may also be a factor in whether tensile parting takes place during injection.

It is noted that the pattern of dye in Test sample 8 was similar to that observed in Test sample 5. Assuming a uniform stress state in the samples, tensile parting could not occur in these samples because the injection pressure was always less than the confining pressure. Both Test 5 and 8 show a distinct cupped, or conical, zone of dye penetration. It is possible that this feature is the result of preferential fluid flow due to shear deformation, which would occur on planes of maximum stress obliquity.

Figure 6.2 is a plot of injection pressure versus time for Fracture Tests 4 through 8. Although no detail analyses were carried out on these results, it may be noted that the results obtained from Fracture Tents 5 and 6 are virtually identical. As discussed, previously, these tests were carried out under the same stress and fluid injection conditions. This demonstrates the repeatability of test methods and procedures.

7.0 CONCLUSIONS AND RECOMMENDATIONS

The data from the large scale fracture simulations have provided valuable insight into the mechanisms of fracture in uncemented sands. Different mechanisms appear to occur depending on the injection rate used in the test. The exact mechanisms may not be known, but the different dyed patterns observed in the tests suggest that different mechanisms occurred.

In general the penetration of dye into the sample during the fracture tests was significant. Surfaces or bands of dye were detected in several tests at or near the boundaries of the sample even though the amount of dyed fluid injected into the sample was very small. For example in Fracture Test 5, 20 ml of fluid was injected into a sample volume of 1.3 m^3, which is only 0.002% by volume. Dye in this sample was found near the boundaries of this sample. The permeability of the sand to the viscous pore fluid is such that, at an injection pressure of 240 kPa, i.e. the maximum observed in this test, the volume of fluid that would flow into the sample is only about 1 ml. In fact 20 ml were injected so it must be assumed that the sand was locally in a failure stress state during injection. Thus, it was a "fracture test", not a permeability test.

Fundamentally there are two mechanisms of failure that are possible in uncemented sands when subjected to fluid injection: tensile failure (or parting) and shear failure. Tensile failure will occur when the rate of fluid injection into a uncemented sand mass exceeds the rate of flow that can occur through the interconnected pores in the sand. If the fluid pressure at this injection rate is greater than the total minor principal stress there can be tensile stress in the sand matrix. Since an uncemented sand will not support such stresses, the sand grains will be forced apart and a parting will propagate through the sand mass.

Shear failure occurs when the shear forces at a sand grain contact exceeds the shear resistance at the contact. Increases in the pore fluid pressure from fluid injection into the sand mass results in a decrease in the normal forces at contacts between sand grains and therefore a reduction in shear resistance. When the shear resistance falls below the shear force the sand grains slide relative to one another. In dense sands the shear sliding results in a less densely packed array of sand grains. The volume of the void spaces in the sand mass is increased (this is termed shear dilation) and the sand is therefore more permeable along the shear surfaces. It is noted that tensile and shear failure mechanisms may not occur independently of one another. When the injection rate is greater than the flow rate through the pores, but the pressure is less than the minor principal total stress, a tensile parting is unlikely to occur, but some combination of localized shearing and parting may take place.

The dye patterns observed in Phase 1 appear to show evidence of both parting and shear failure. The failure process appears to depend on the injection rate and boundary conditions. However further large scale fracture tests and pertinent numerical modelling is necessary to fully understand the role of these failure mechanisms in the hydraulic fracturing phenomenon in uncemented sands. This modelling should include the assessment of factors such as stress inhomogeneities and leakoff and fabric inhomogeneities.

Based on the tests reported in this study, the next phases of the study should include the tests to examine the following:

1. The effect of the initial stress conditions on fracture propagation. The purpose of these tests would be to examine the mode of oil sands failure during fluid injection. A series of tests would be carried out at constant injection rate, the stress difference applied to the sample would be varied in each test. All these tests would be carried out at K_o values either greater

than one or at K_o values less than one. The relationship between fracture patterns and K_o values would be examined to assess the relative influence tensile and shear failure mechanisms have on fracture propagation.

2. The effect of fluid injection rate on fracture propagation. The object of these tests would be to determine if fracture processes and patterns are consistent with those predicted by leak off dominated fracture models. The same volume of fluid would be injected into the sample at higher and/or lower rates. The stresses applied to the sample would be the same for each test. These tests would further quantify the relationship developed during Phase 1 testing.

3. The effect of injection of a different fluid from the pore fluid to induce the hydraulic fracture. In the field it is common to inject steam into oil sands which are saturated with bitumen and water. The injection fluid is thus less viscous than the pore fluid. In addition, the injection fluid may or may not be miscible with the pore fluid.

GOLDER ASSOCIATES LTD.

PROFESSIONAL ENGINEER ALBERTA K.M. KOSAR

KM Kosar
K.M. Kosar, P. Eng.

for KM Kosar
K. Been, P. Eng
Associate

PERMIT TO PRACTICE
GOLDER ASSOCIATES LTD.
Signature
Date Aug 2/91
PERMIT NUMBER: P 5122
The Association of Professional Engineers, Geologists and Geophysicists of Alberta

Table 4.1
Summary of Hydraulic Fracture Test Program

Task 1 – Laboratory Simulation of Horizontal Fracture Propagation

Test No.	Vertical Stress (kPa)	Horizontal Stress (kPa)	Pore Fluid Pressure (kPa)	Ko	Injection Rate (ml/s)	Injection Volume (ml)	Supplementary Tests			
							B Test	Permeability (Darcys)	Drained Loading	Injectivity
1	400	600	—	—	96.0	927	—	—	no	no
2	Test aborted due to fitting leak									
3	460	493	432	2.2	93.5	907	—	—	no	no
4	400	600	200	2.0	20.0	80	0.3	—	yes	no
5	400	600	200	2.0	5.0	20	0.3	—	yes	no
6	400	600	200	2.0	5.0	18	0.3	1.5	yes	yes
7	400	600	200	2.0	10.0	40	0.3	4.4	yes	yes

Task 2 – Effect of Initial Stress Condition on Fracture Propagation

Test No.	Vertical Stress (kPa)	Horizontal Stress (kPa)	Pore Fluid Pressure (kPa)	Ko	Injection Rate (ml/s)	Injection Volume (ml)	Supplementary Tests			
							B Test	Permeability (Darcys)	Drained Loading	Injectivity
8	600	400	200	0.5	10.0	40	0.3	2.8	yes	yes

PROJECT No. 902-2013 DRAWN RK REVIEWED KMK DATE APR 91

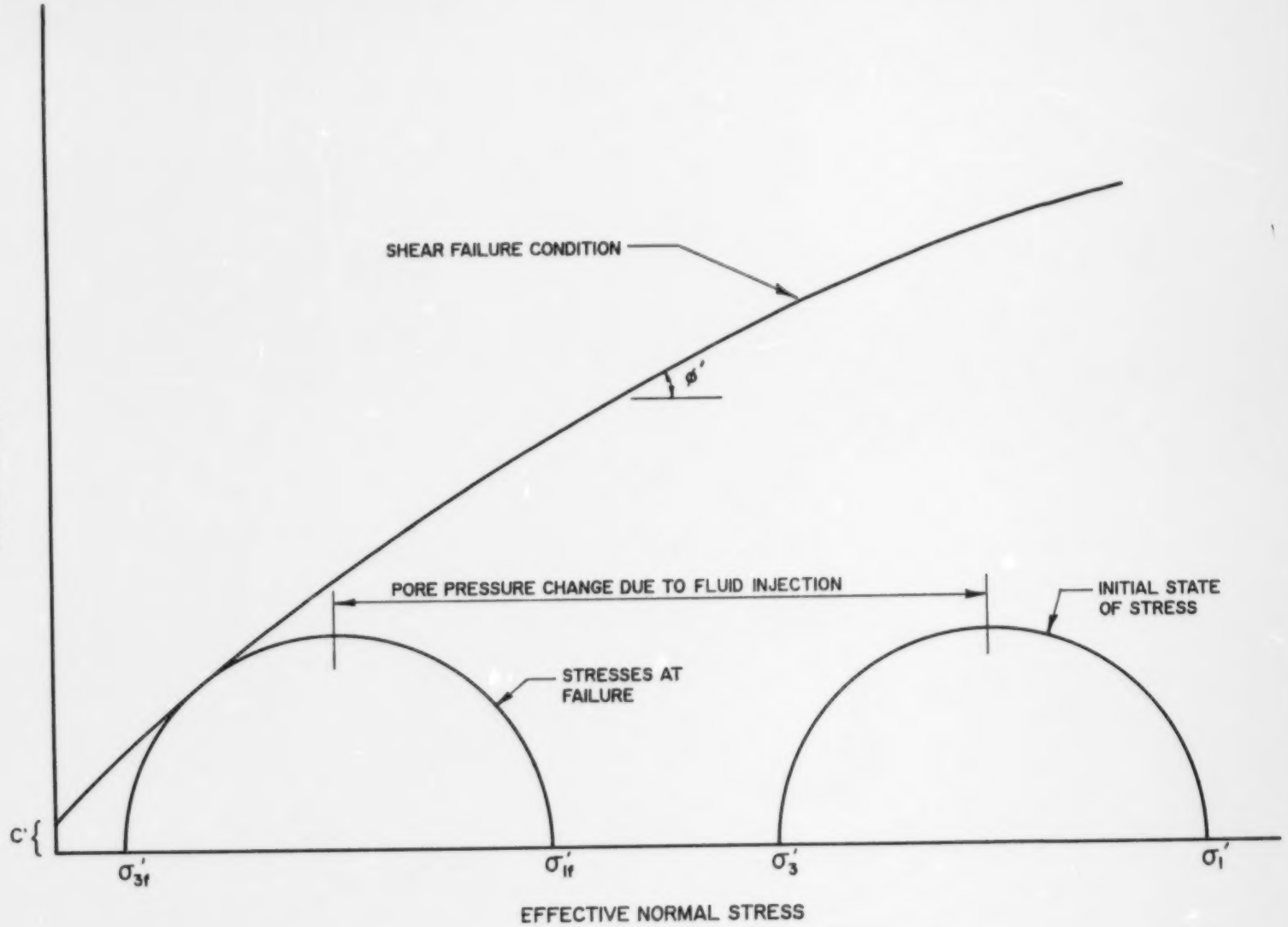

SHEAR FAILURE DUE TO FLUID INJECTION

Figure 1.1

Golder Associates

DRAINED TRIAXIAL TEST ON McMURRAY FORMATION OIL SANDS AT IN SITU STRESSES

Figure 2.1

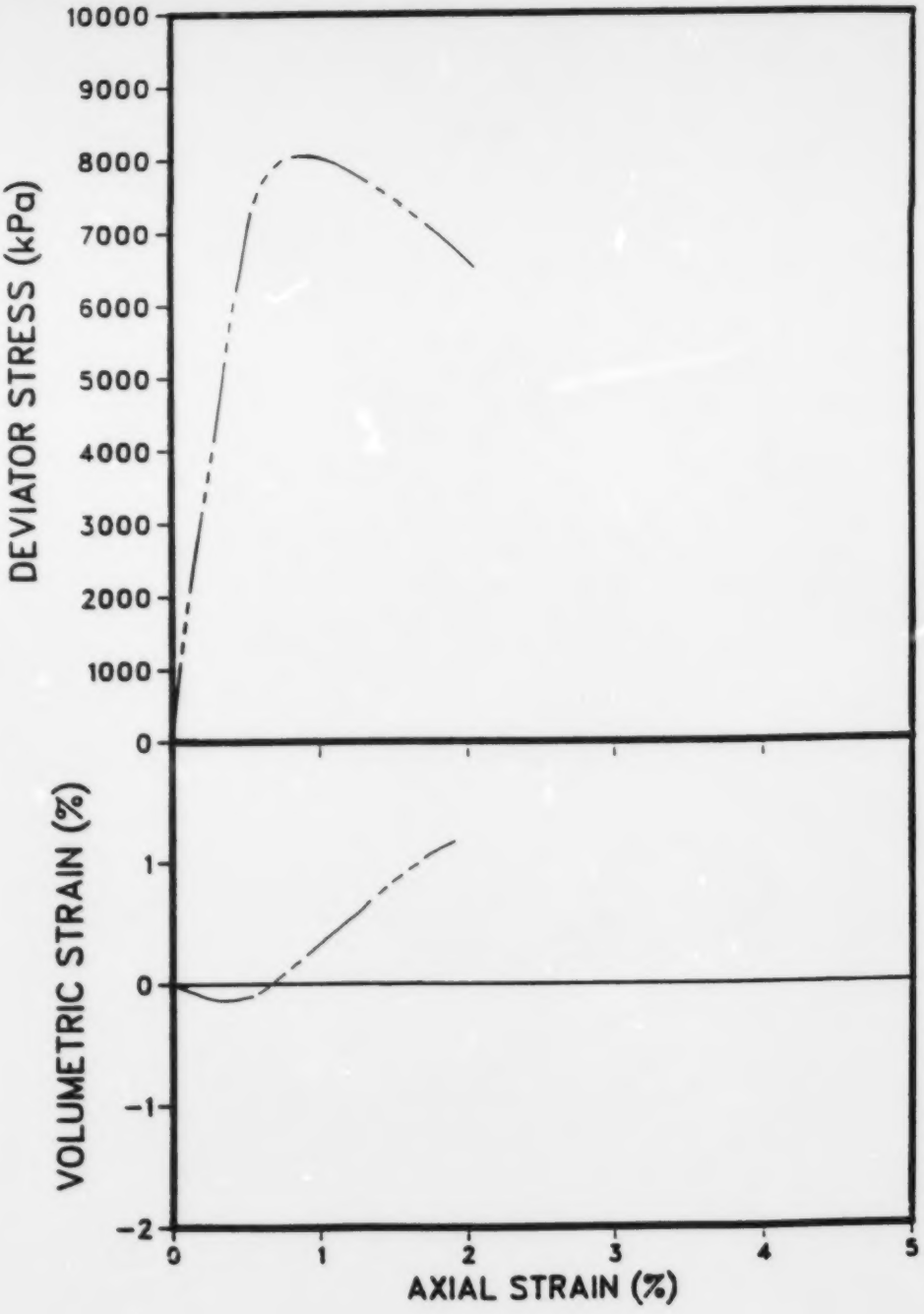

PROJECT No. 902-2013 DRAWN RR REVIEWED _____ DATE APR 91

Golder Associates

TYPICAL DRAINED TRIAXIAL TEST ON DENSE QUARTZITIC SAND AT 350 kPa

Figure 2.2

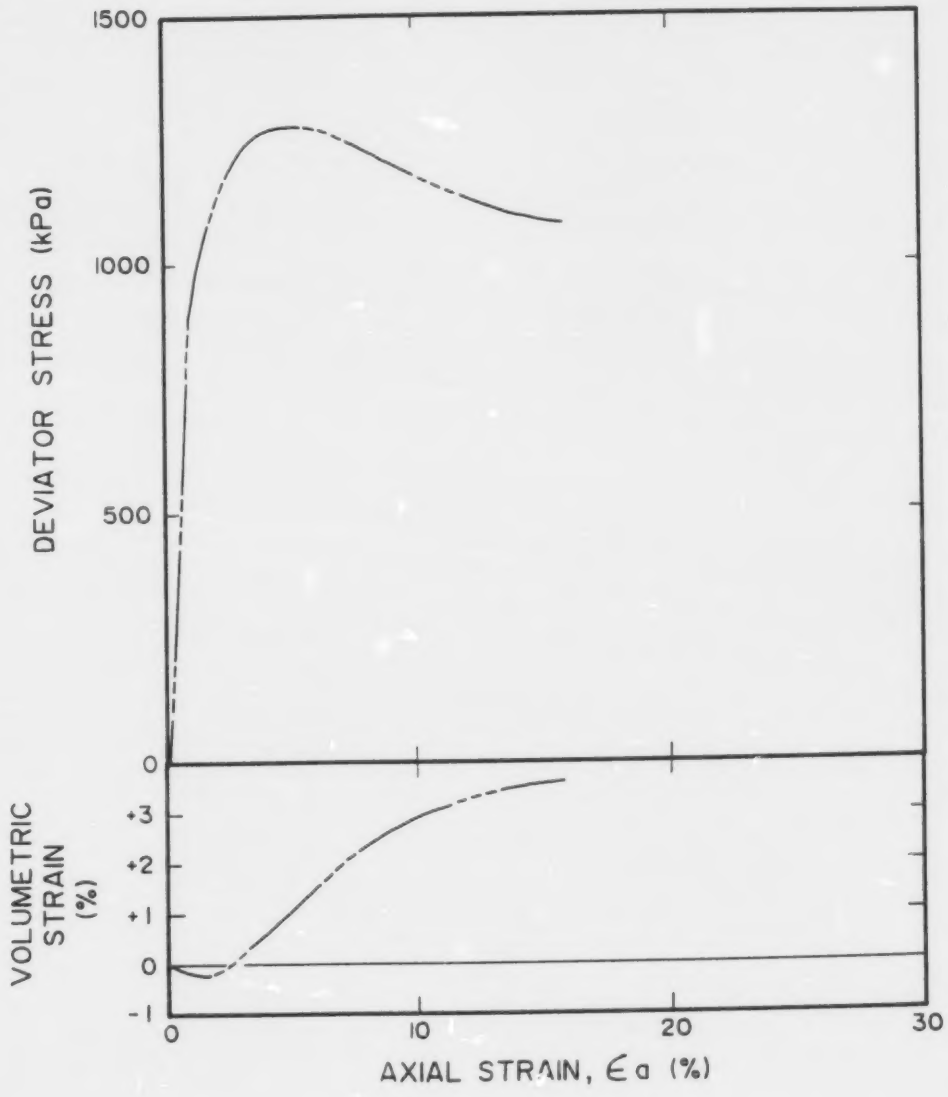

PROJECT No. 902-2013 DRAWN RR REVIEWED _____ DATE APR 91

PROJ. No. 122-2068 DRAWN EC REVIEWED DATE 13 Feb 90

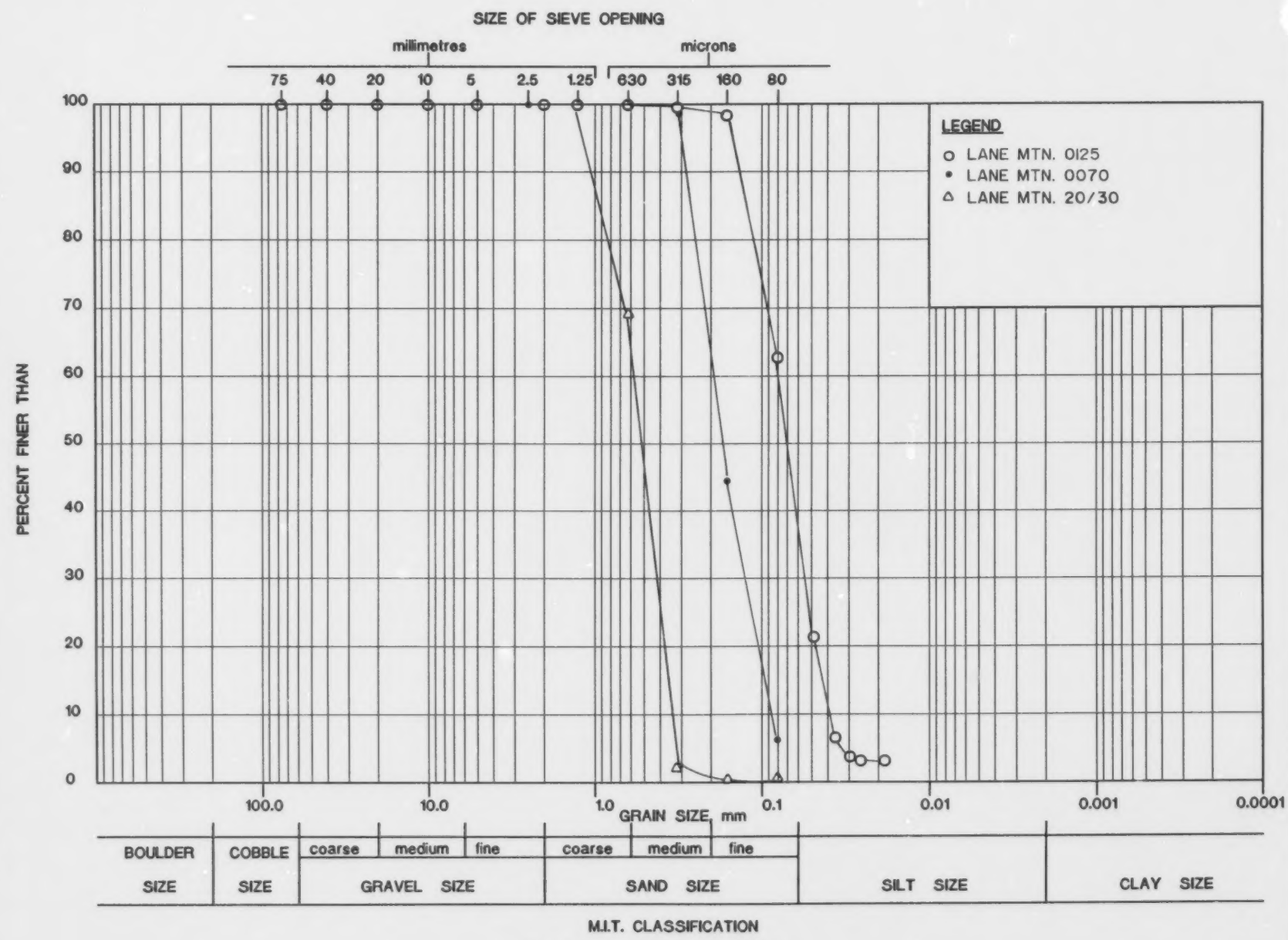

GRAIN SIZE DISTRIBUTION
LANE MTN SAND

Figure 2.3

Golder Associates

PRO No. 1-22-0.2.5 DRAWN EC REVIEWED DATE 12 FEB 87

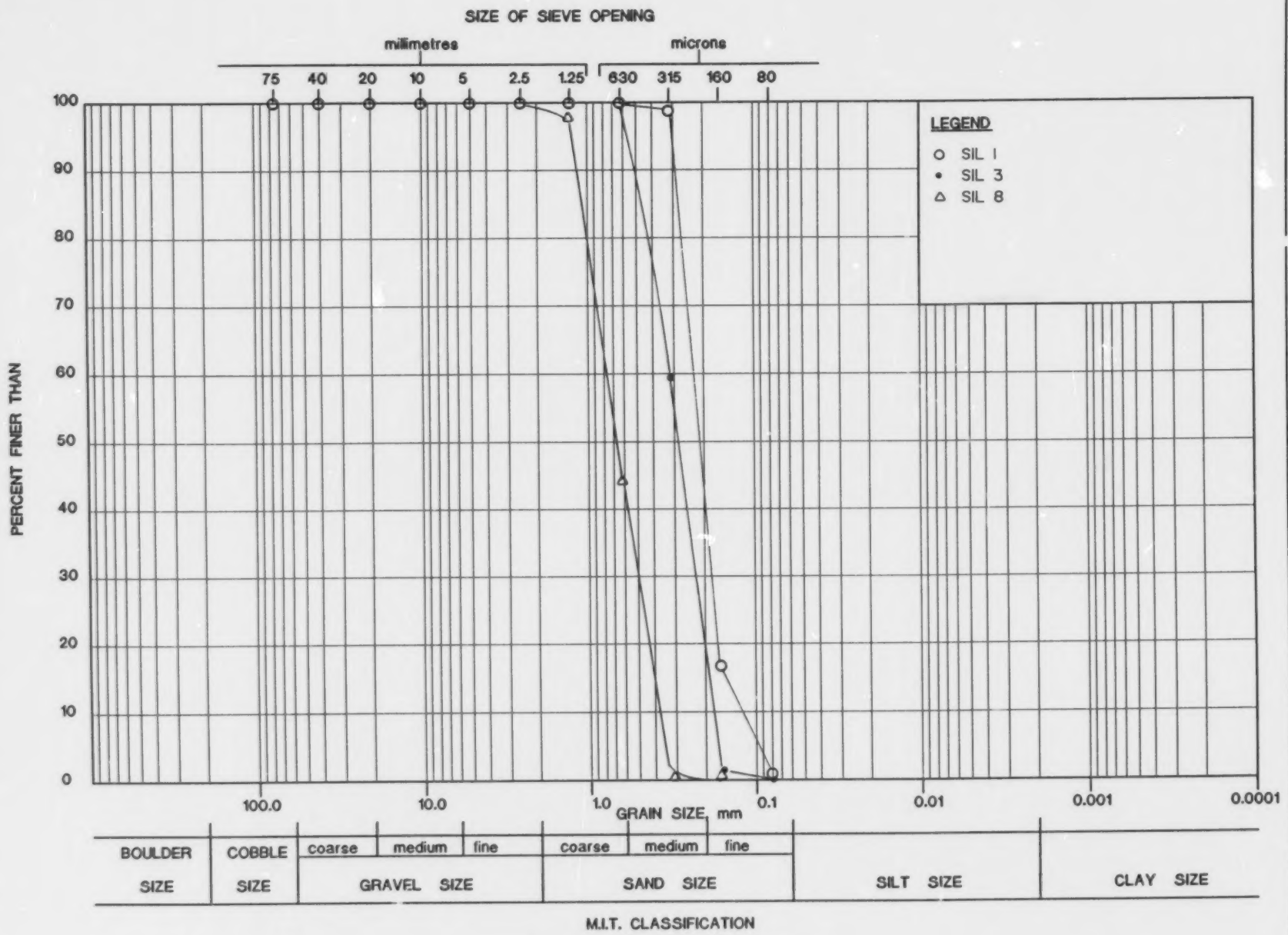

GRAIN SIZE DISTRIBUTION
SIL SAND

Figure 2.4

Golder Associates

VISOSITY OF VISCOUS PORE FLUIDS | **Figure 2.5**

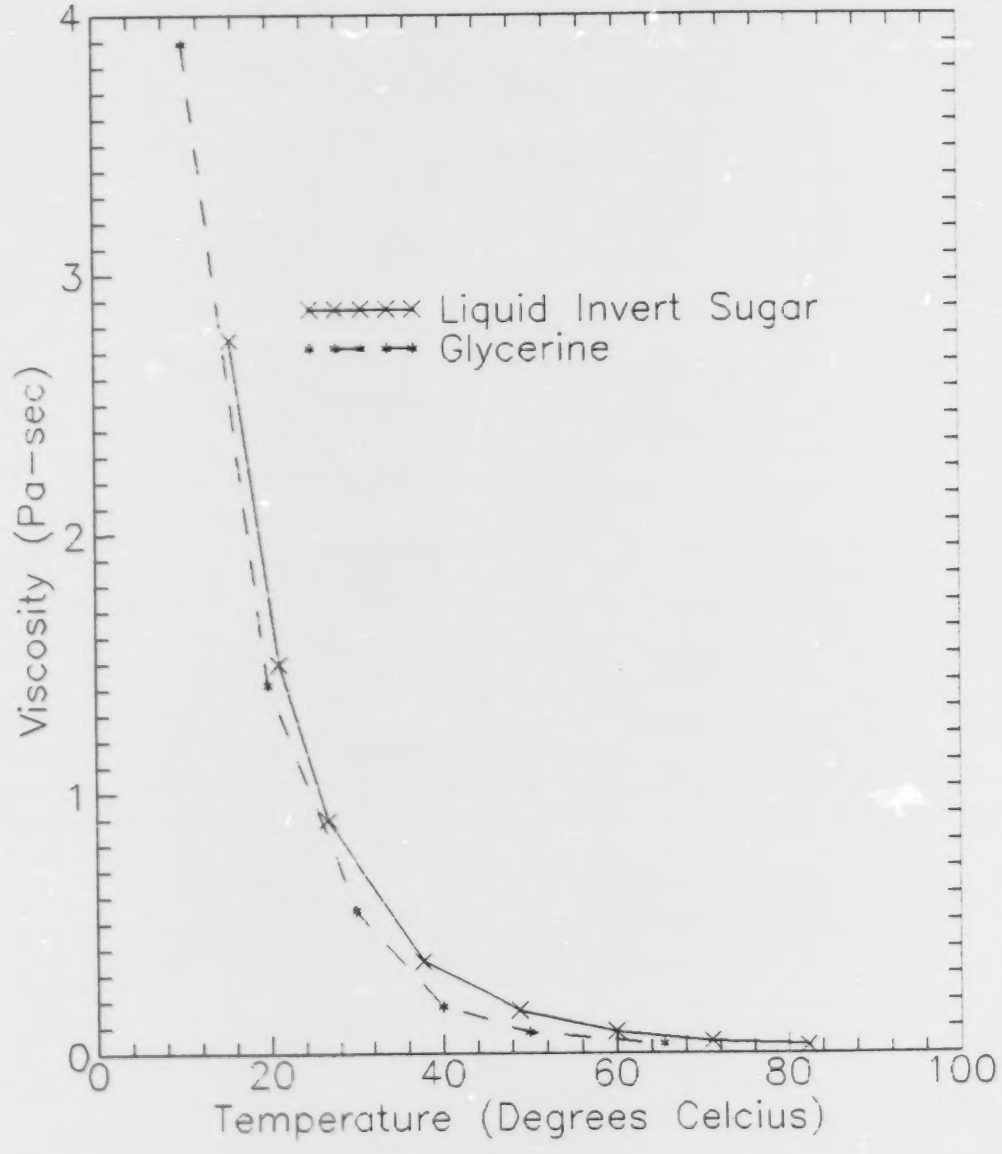

PROJECT No. 902-2013 DRAWN RR REVIEWED ____ DATE APR 91

PERMEABILITY TEST ON GLYCERINE IMPREGNATED SAND

Figure 2.6

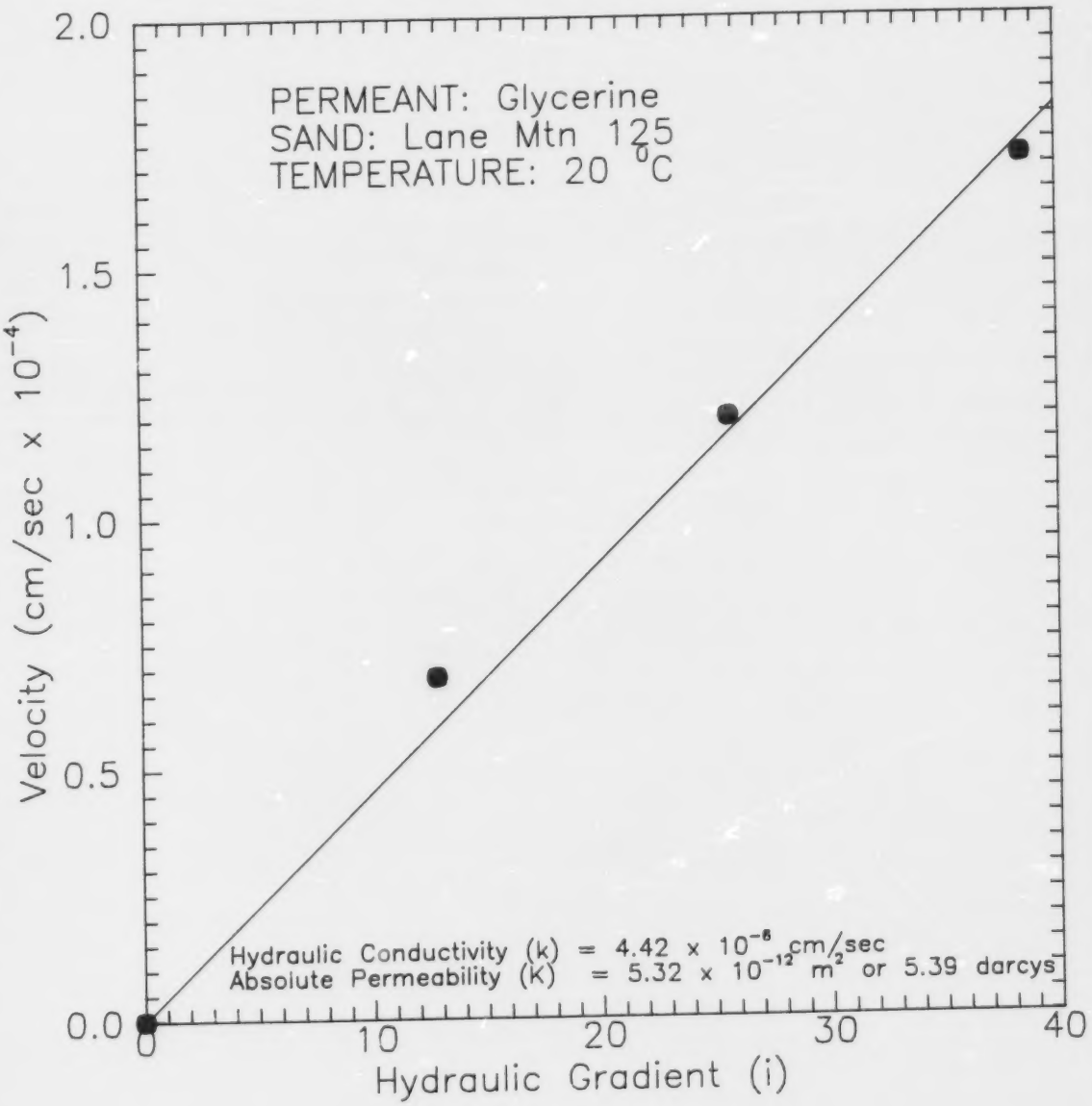

PROJECT No. 902-2013 DRAWN CG REVIEWED ____ DATE APR 91

Golder Associates

PREDICTED INJECTION RATE FOR GLYCERINE IMPREGNATED SAND

Figure 2.7

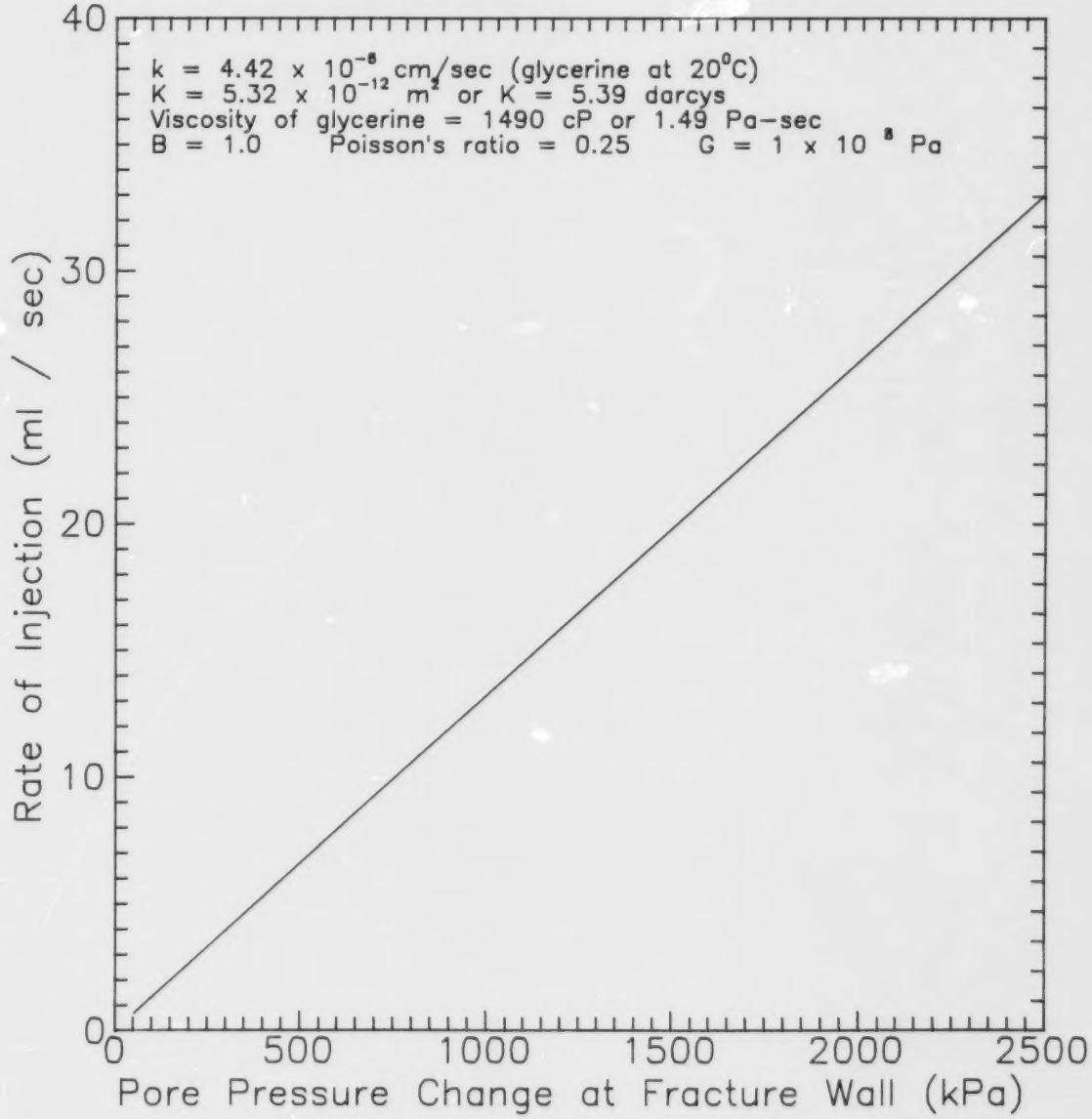

PROJECT No. 902-2013 DRAWN CG REVIEWED DATE APR 91

SATURATION TESTS ON GLYCERINE IMPREGNATED LANE Mtn 125 SAND

Figure 2.8

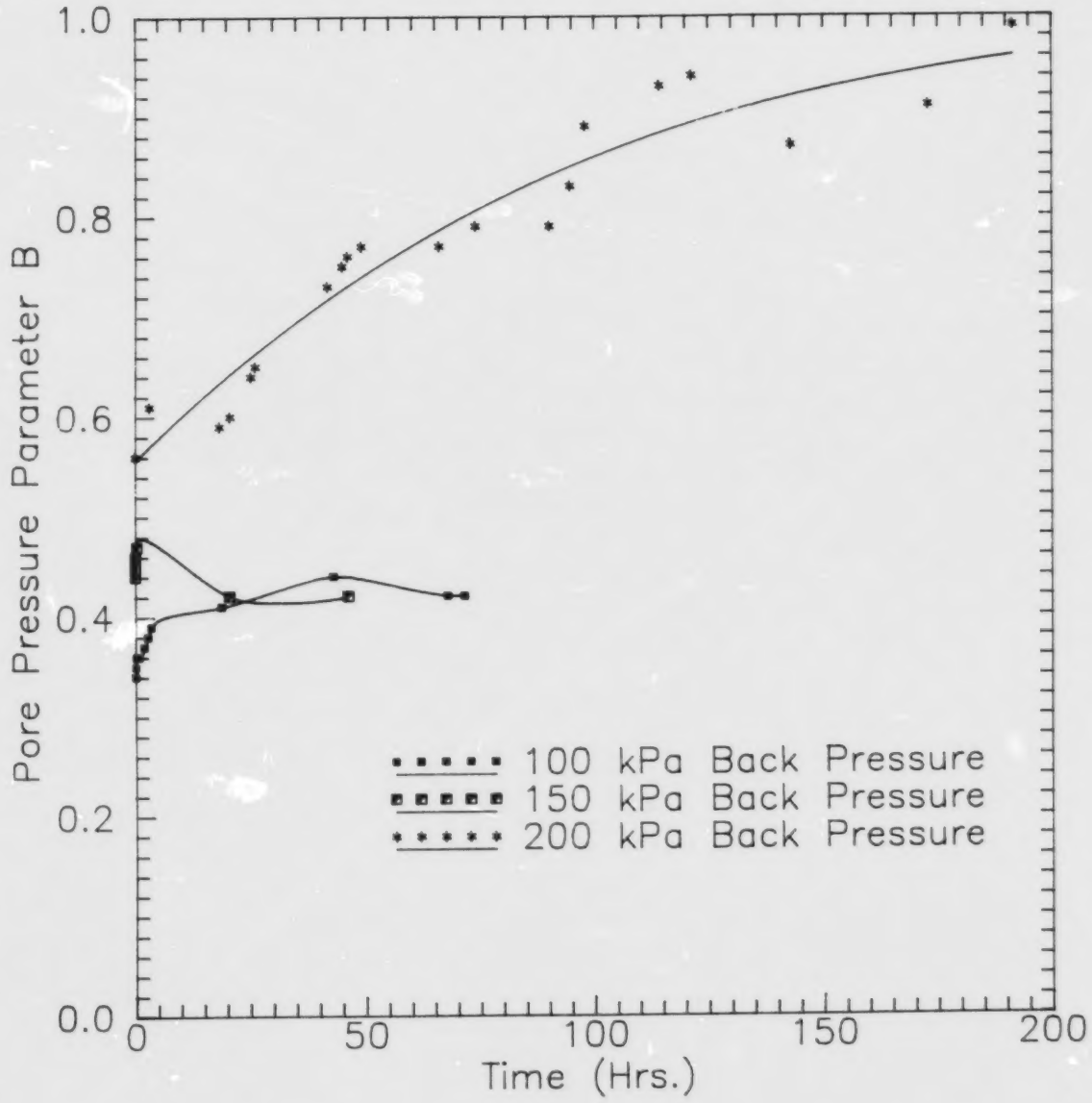

PROJECT No. 902-2013 DRAWN CG REVIEWED DATE JUNE 90

Golder Associates

INJECTION/DIFFUSION TEST | **Figure 2.9**

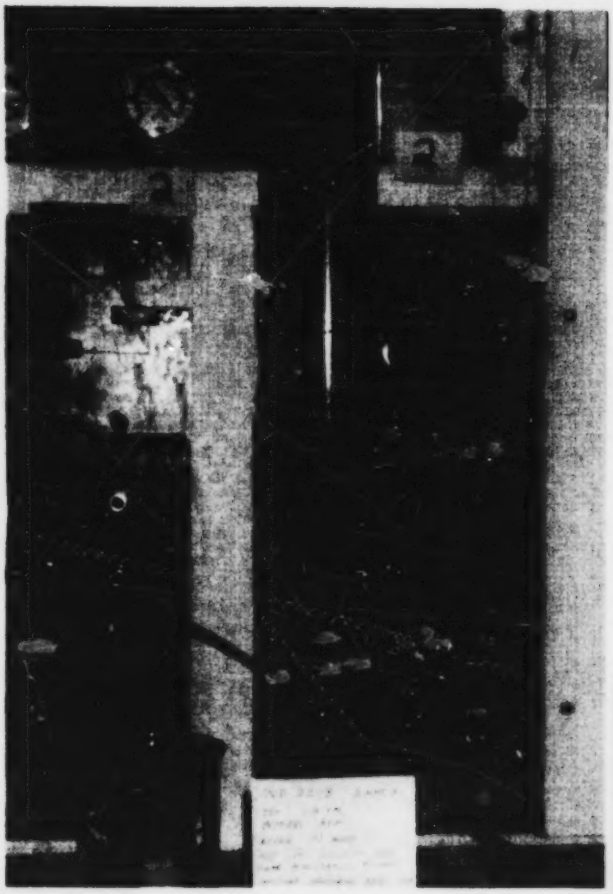

UNDER NORMAL LIGHT

UNDER BLACK LIGHT

PROJECT No. 902-2013 DRAWN CG REVIEWED _____ DATE APR 91

LARGE TRIAXIAL STRESS CHAMBER

Figure 3.1

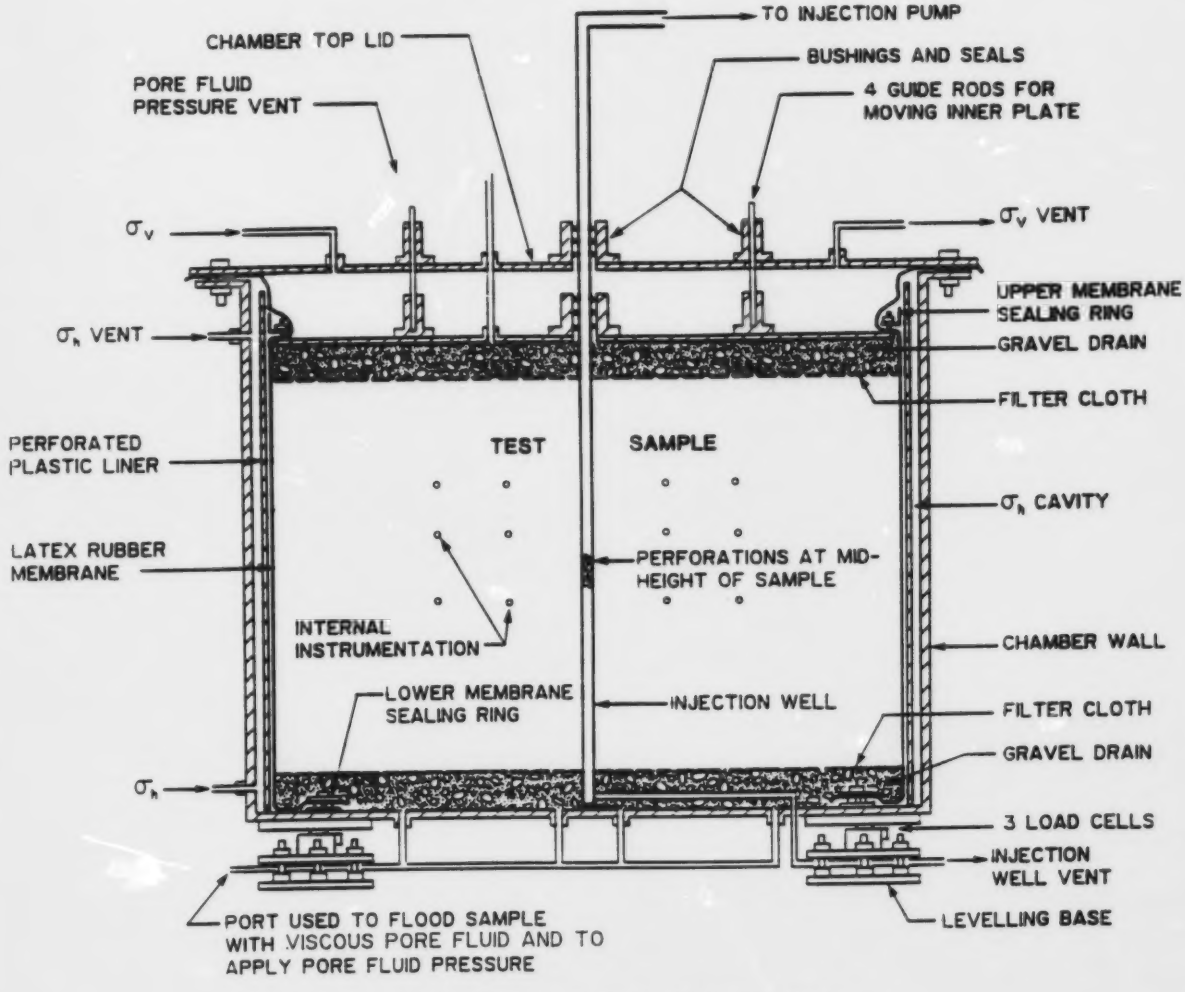

NOTE: SCHEMATIC ONLY - SOME DETAIL NOT SHOWN

PROJECT No. 902-2013 DRAWN RR REVIEWED _____ DATE APR 91

PRESSURE CONTROL BOARD	Figure 3.2

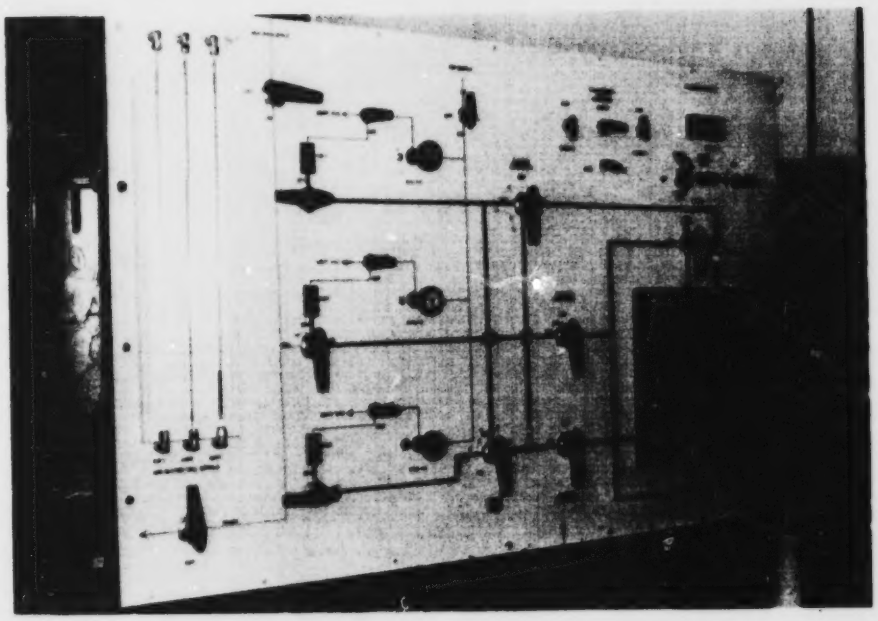

PROJECT No. 902-2013 DRAWN CG REVIEWED _____ DATE APR 91

CROSS SECTION OF INJECTION WELL AT MID-HEIGHT OF SAMPLE

Figure 3.3

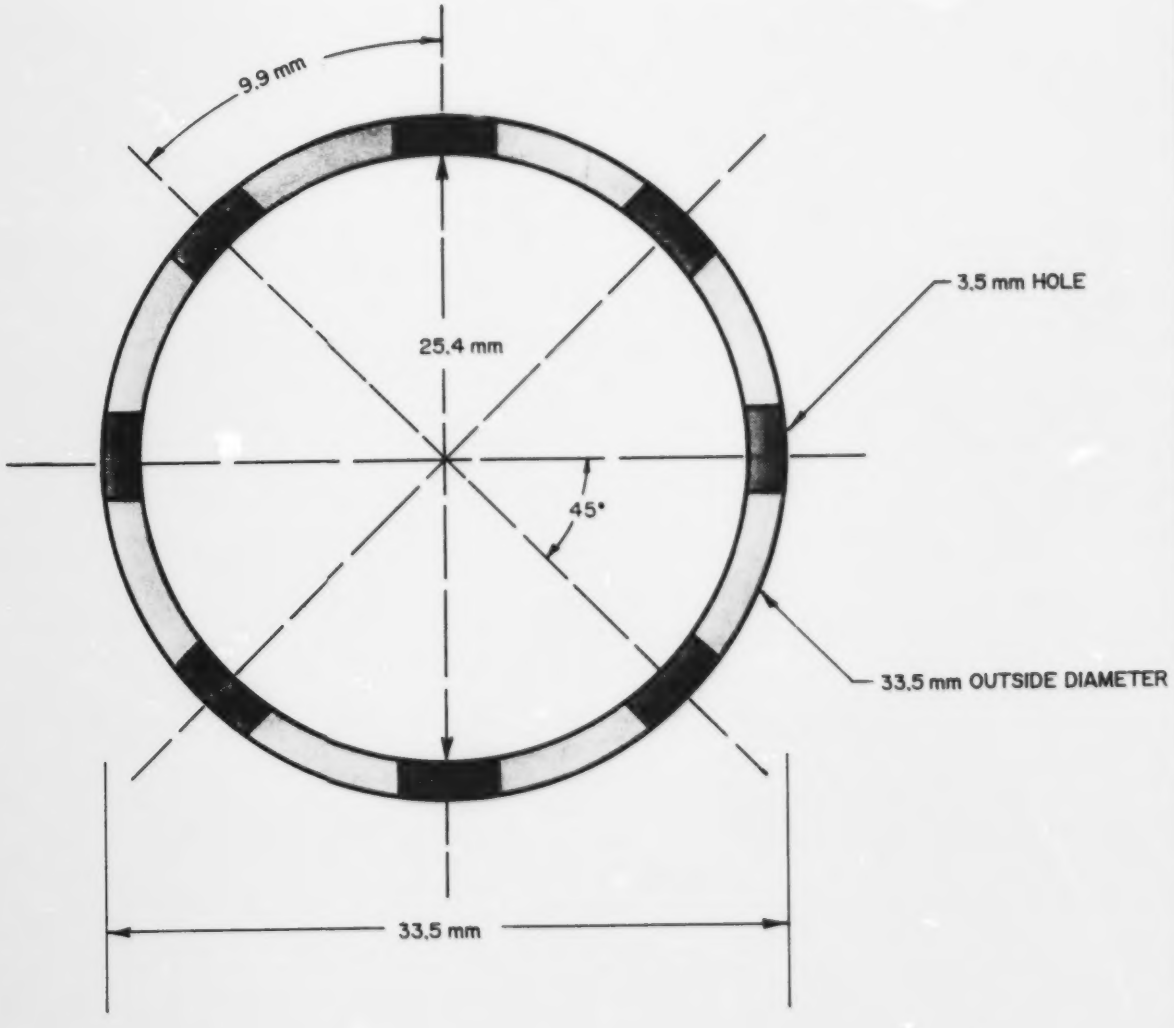

8 ROWS ON 6.4 mm CENTERS

PROJECT No. 902-2013 DRAWN CG REVIEWED _____ DATE JUNE 90

CONSTANT FLOW PUMP	Figure 3.4

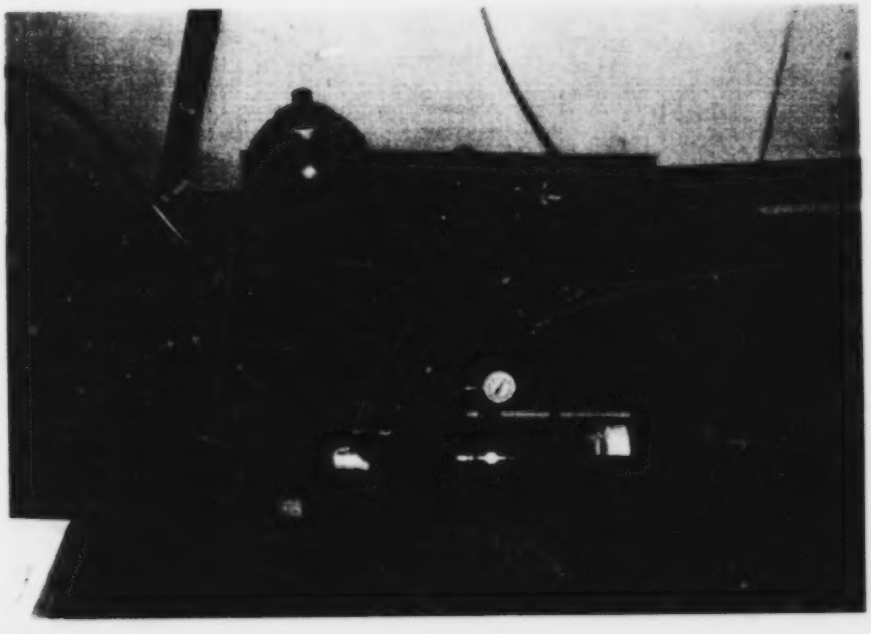

PROJECT No. 902-2013 DRAWN CG REVIEWED _____ DATE APR 91

PROJECT No. 902-2013 DRAWN CG REVIEWED _____ DATE JUNE 90

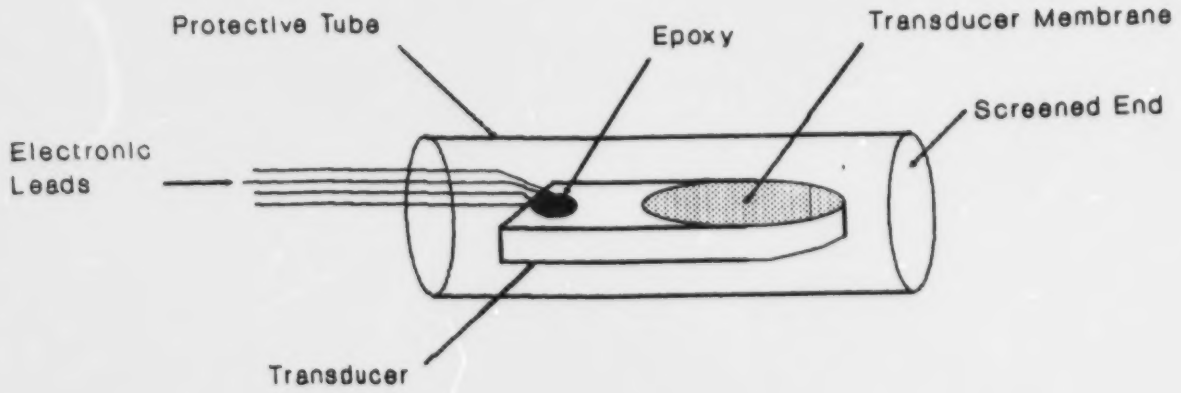

PIEZOMETER DETAIL

Figure 3.5

Golder Associates

PHOTOGRAPH OF PIEZOMETER	Figure 3.6

PROJECT No. 902-2013 DRAWN CG REVIEWED _____ DATE APR 91

INJECTION WELL DETAIL

Figure 3.7

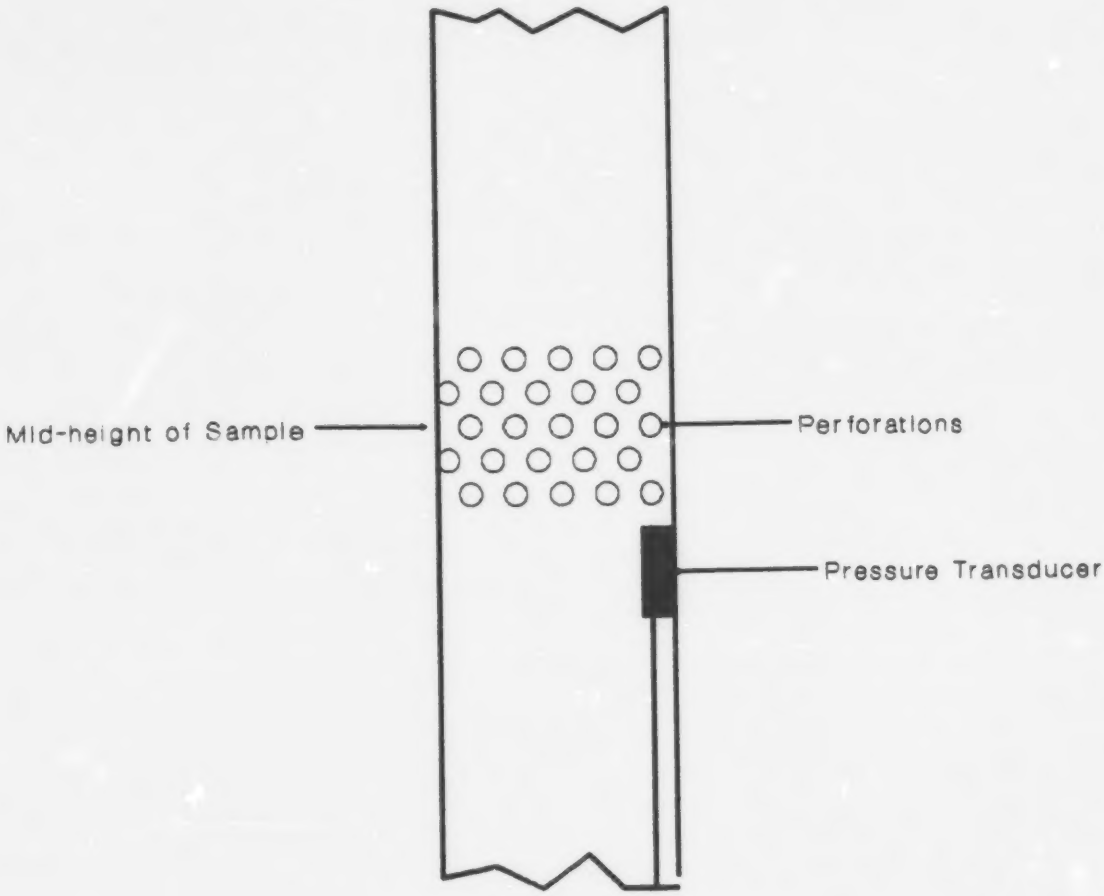

PROJECT No. 902-2013 DRAWN CG REVIEWED _____ DATE JUNE 90

Golder Associates

PROJECT No. 902-2013 DRAWN CG REVIEWED _____ DATE JUNE 90

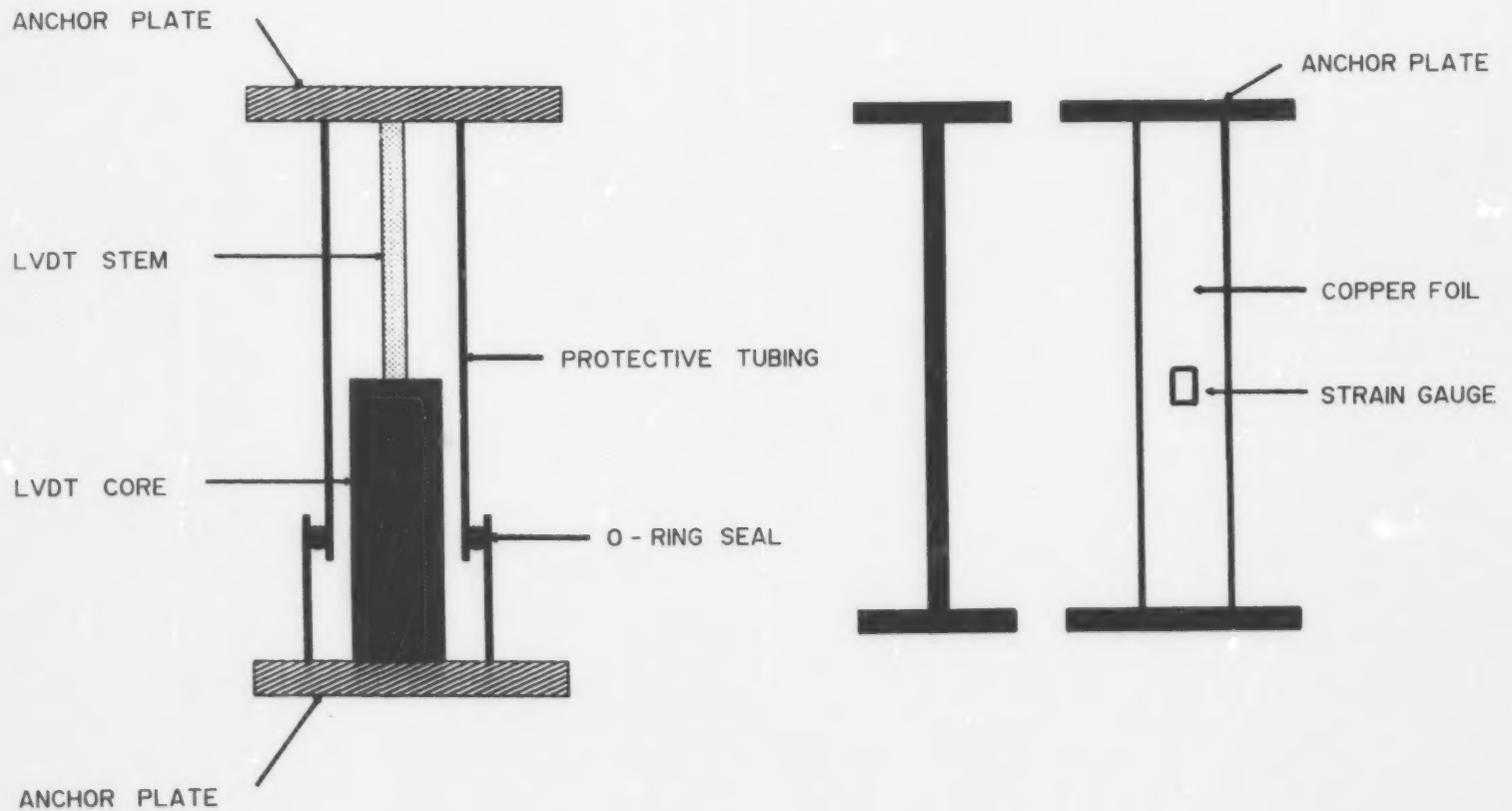

EXTENSOMETER DETAIL

Figure 3.8

Golder Associates

INTERNAL DEFORMATION MEASURING DEVICES

Figure 3.9

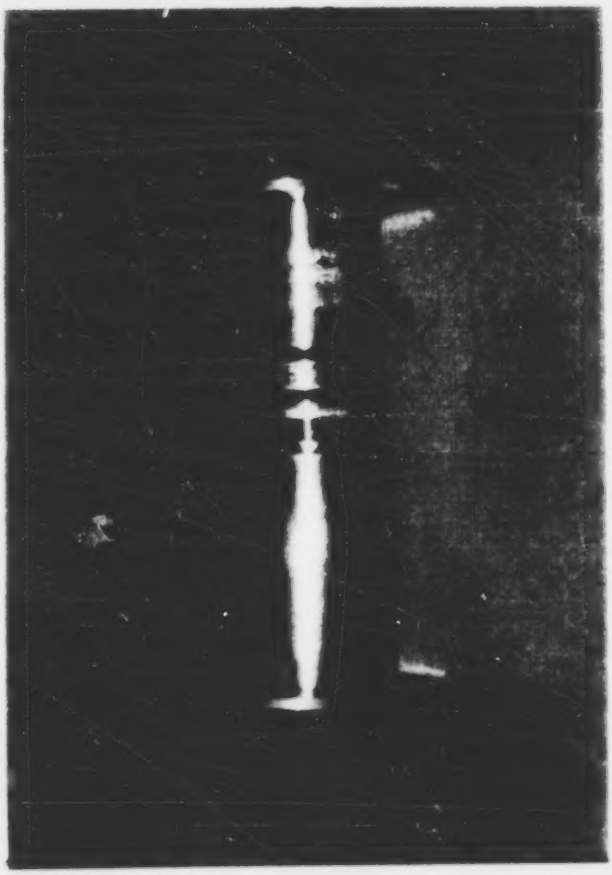

LVDT EXTENSOMETER ASSEMBLY

LVDT

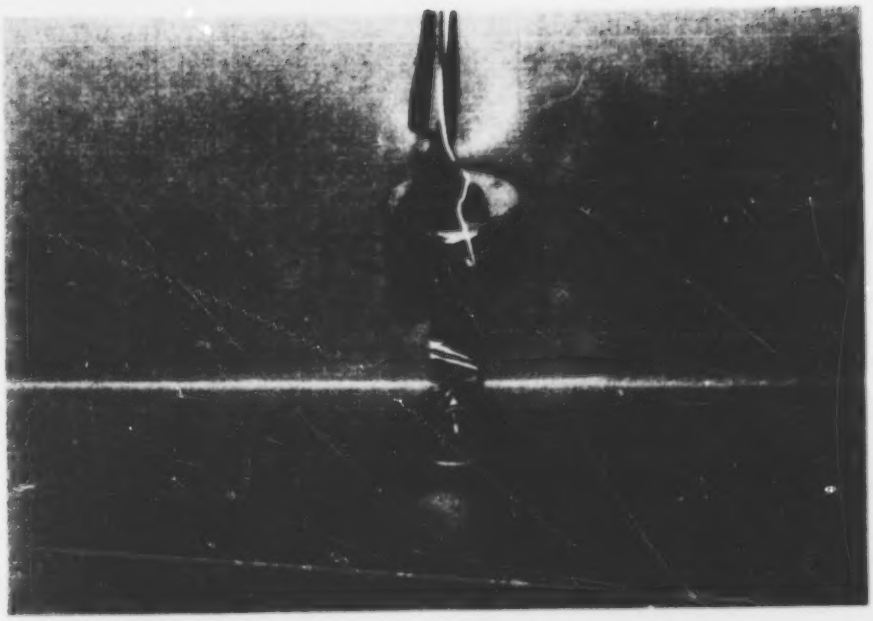

STRAIN GAUGE FOIL EXTENSOMETER

PROJECT No. 902-2013 DRAWN CG REVIEWED DATE APR 91

PHOTOGRAPH OF LARGE TRIAXIAL CHAMBER	Figure 3.10

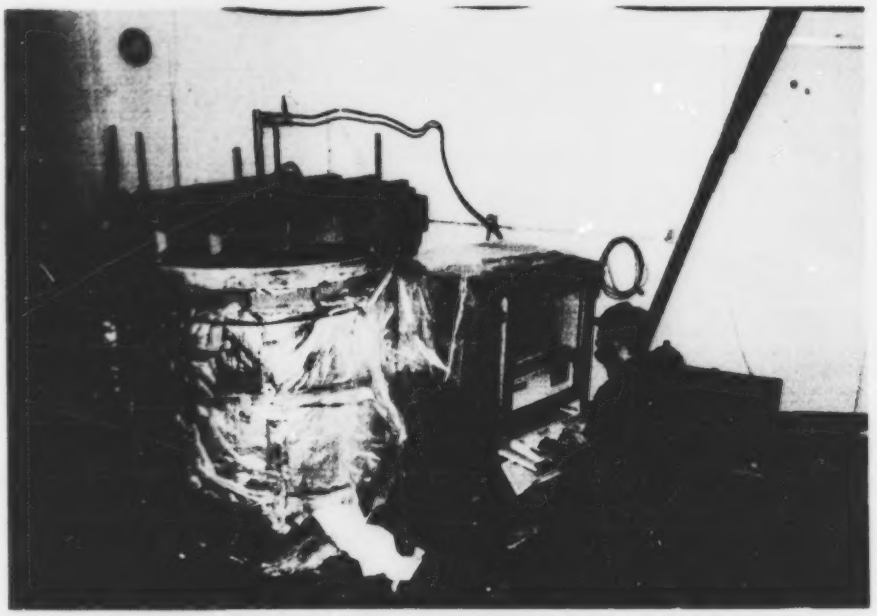

PROJECT No. 902-2013 DRAWN CG REVIEWED _____ DATE APR 91

PLUVIATION OF SAND INTO STRESS CHAMBER

Figure 3.11

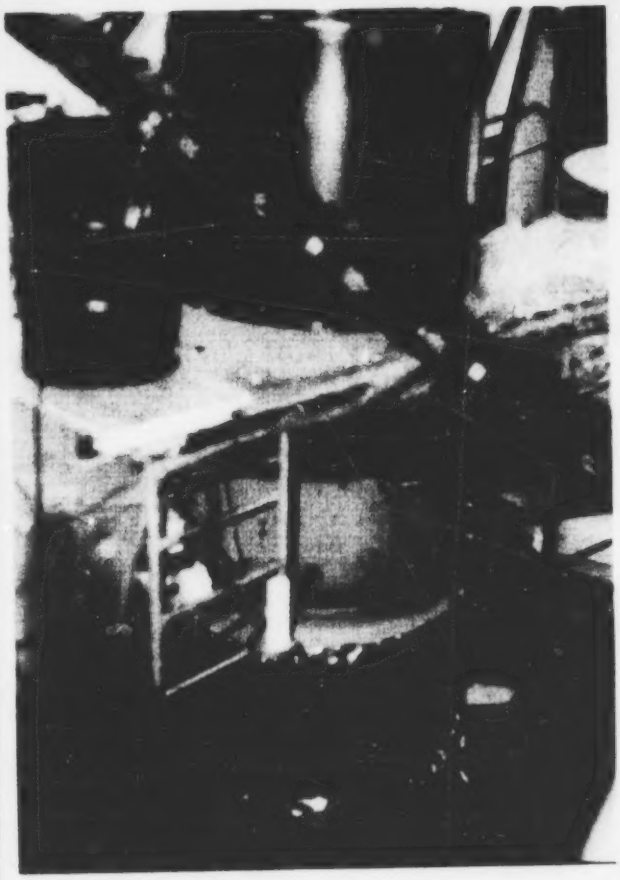

THE SAND IS LOADED IN A HOPPER WHICH IS ERECTED DIRECTLY OVER THE TRIAXIAL CHAMBER.

THE SAND IS PLUVIATED INTO THE CHAMBER SLOWLY TO PRODUCE A DENSE, HOMOGENEOUS SAMPLE. A PLASTIC CURTAIN AROUND THE CHAMBER DURING PLUVIATION LIMITS THE AMOUNT OF AIRBORNE PARTICLES IN THE LABORATORY.

PROJECT No. 902-2013 DRAWN CG REVIEWED _____ DATE APR 91

PROJECT No. 902-2013 DRAWN CG REVIEWED _____ DATE JUNE 90

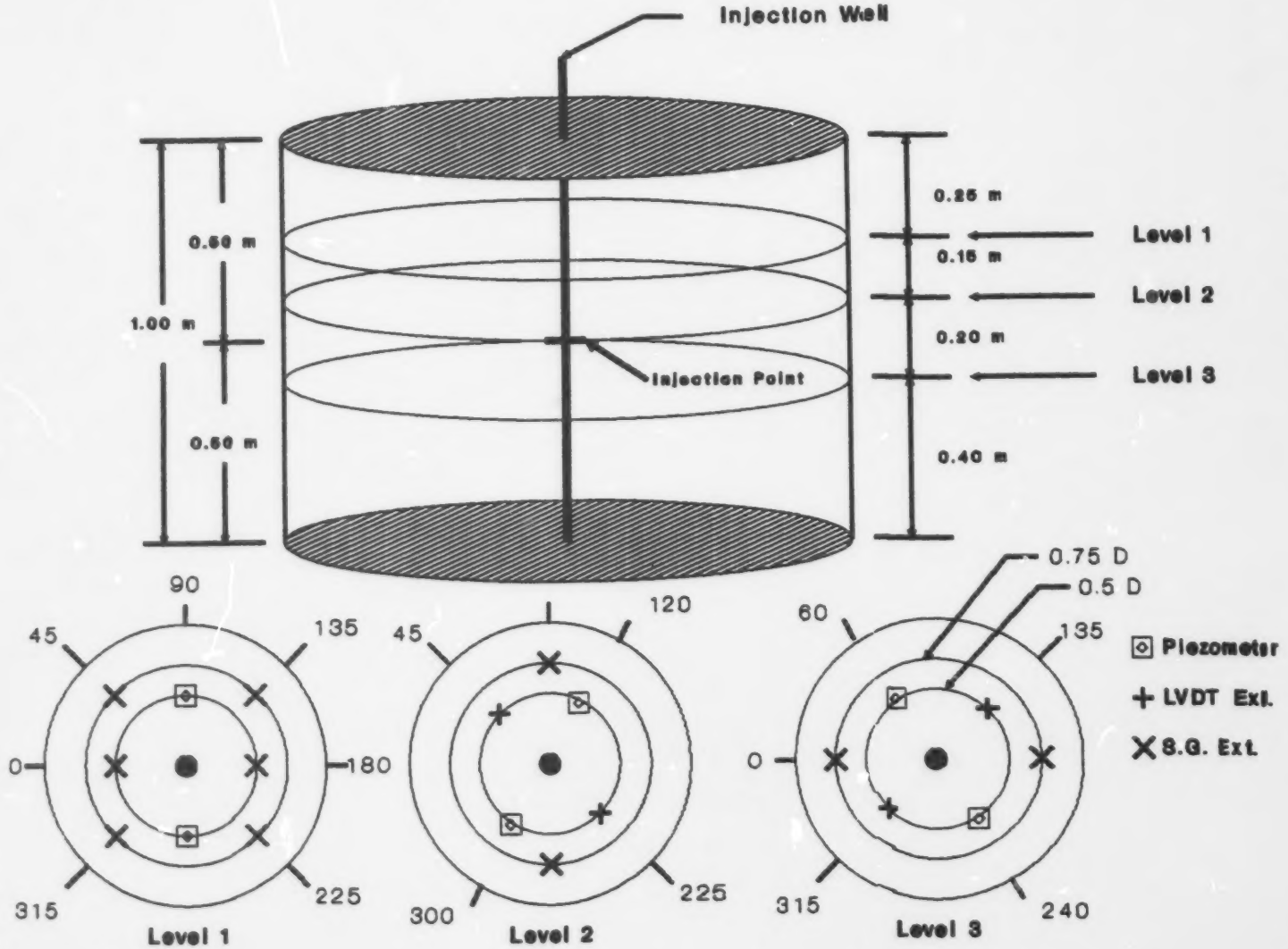

INSTRUMENTATION DETAIL FOR FRACTURE SIMULATIONS

Figure 3.12

Golder Associates

LOWER DRAINAGE BOUNDARY	Figure 3.13

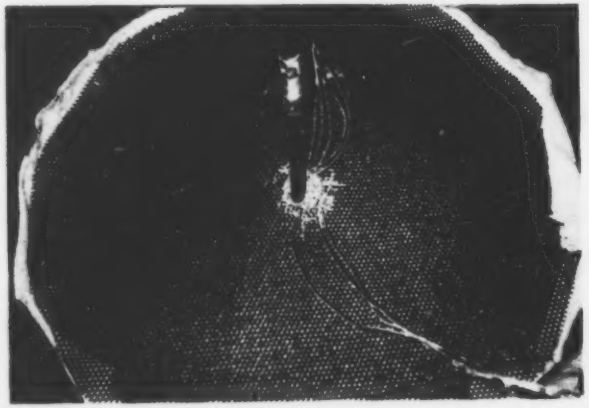

a) GEONET

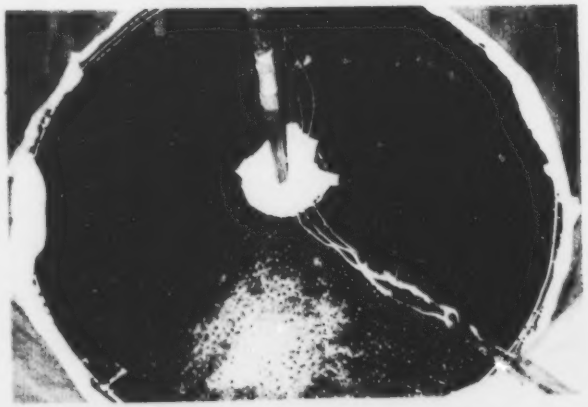

b) HIGH DENSITY POLYETHENE

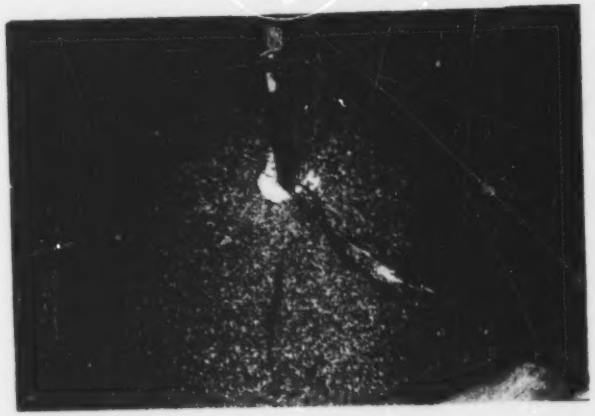

c) GRAVEL AND SCREEN

Golder Associates			
PROJECT: 902-2013	DRAWN BY: CG	DATE: APR 91	REVIEWED:

DELINIATION OF FLUORESCENT DYE DURING EXCAVATION FOR DIGITIZING PROCESS

Figure 3.14

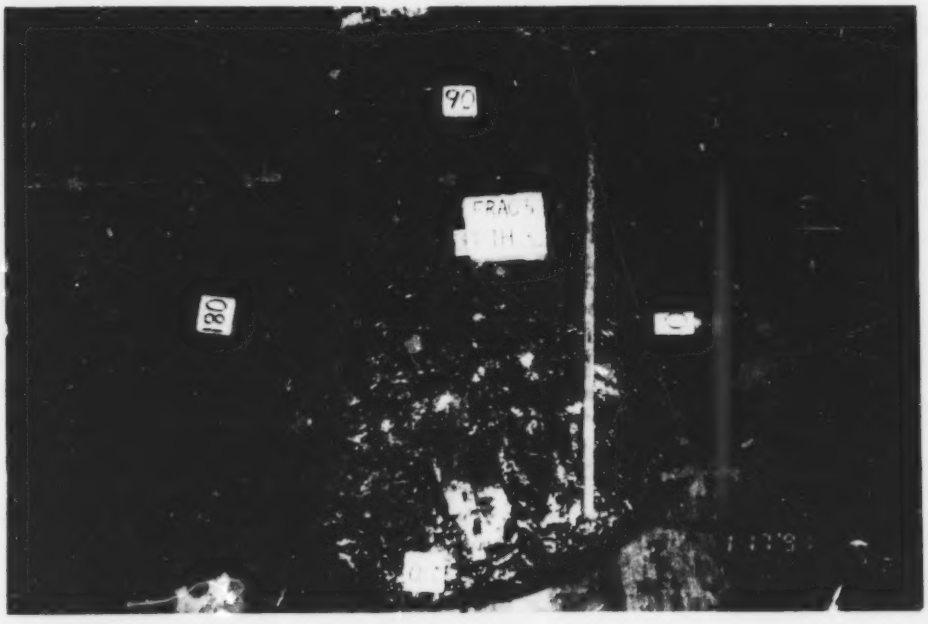

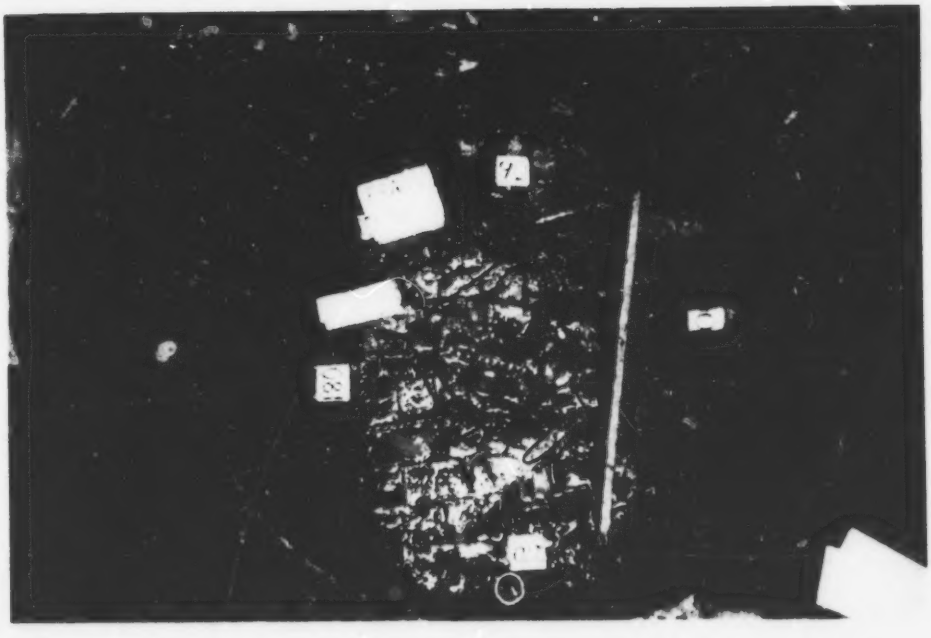

PROJECT No. 902-2013 DRAWN CG REVIEWED _____ DATE APR 91

PROJECT No. 902-2013 DRAWN RR REVIEWED _____ DATE OCT 90

INSTRUMENTATION

- ○ PIEZOMETER
- △ LVDT EXTENSOMETER
- □ STRAIN GAUGE FOIL EXTENSOMETER

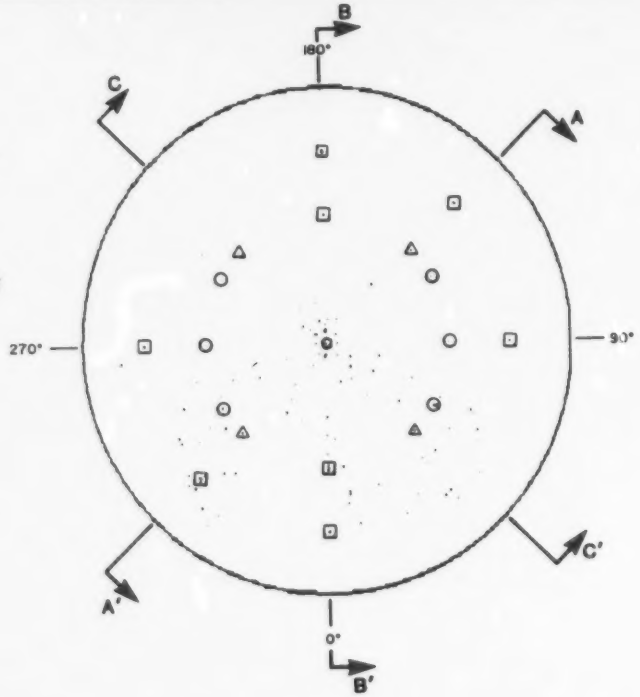

A) PLAN VIEW

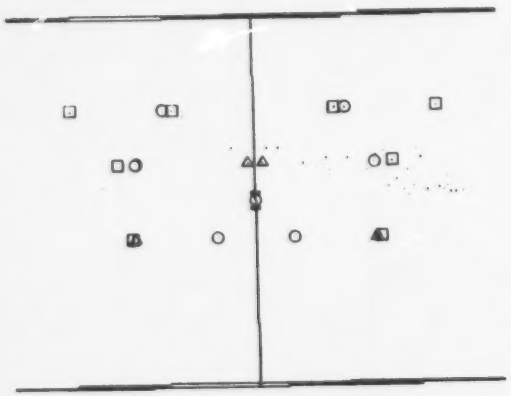

B) SECTION A - A'

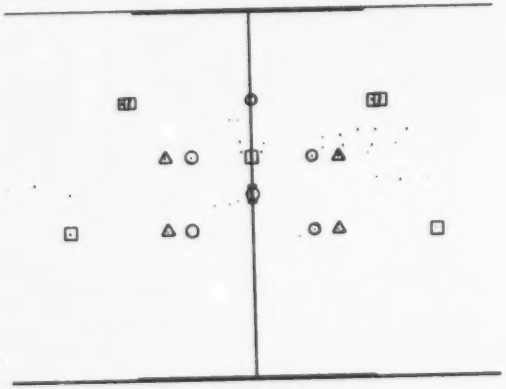

C) SECTION B - B'

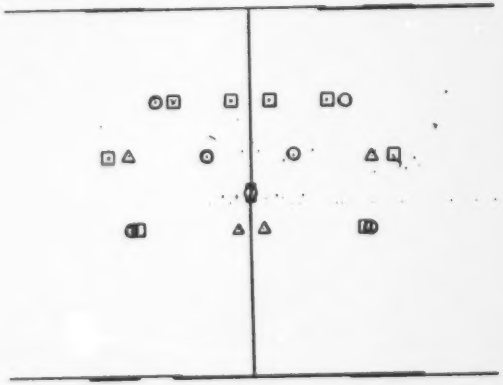

D) SECTION C - C'

LOCATION OF FLUORECENT DYE AFTER INJECTION - TEST 1

Figure 4.1

Golder Associates

RESPONSE OF LVDT EXTENSOMETERS AND FLUID INJECTION RECORD - TEST 1

Figure 4.2

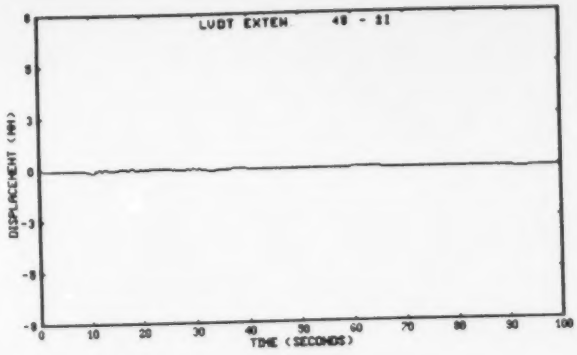

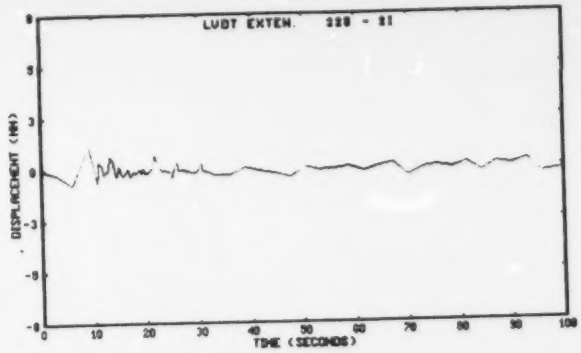

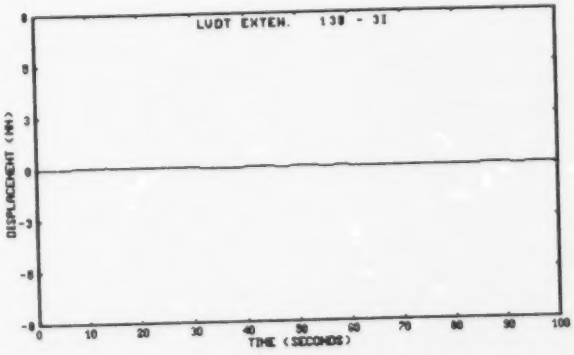

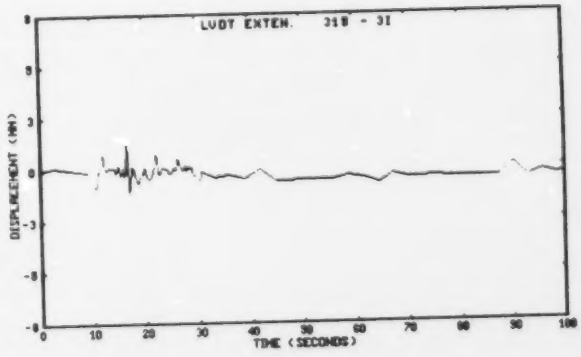

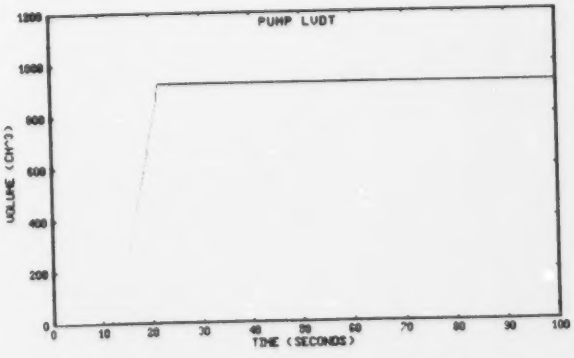

PROJECT No. 902-2013 DRAWN RR REVIEWED ____ DATE OCT 90

RESPONSE OF STRAIN GAUGE FOIL EXTENSOMETERS - TEST 1

Figure 4.3

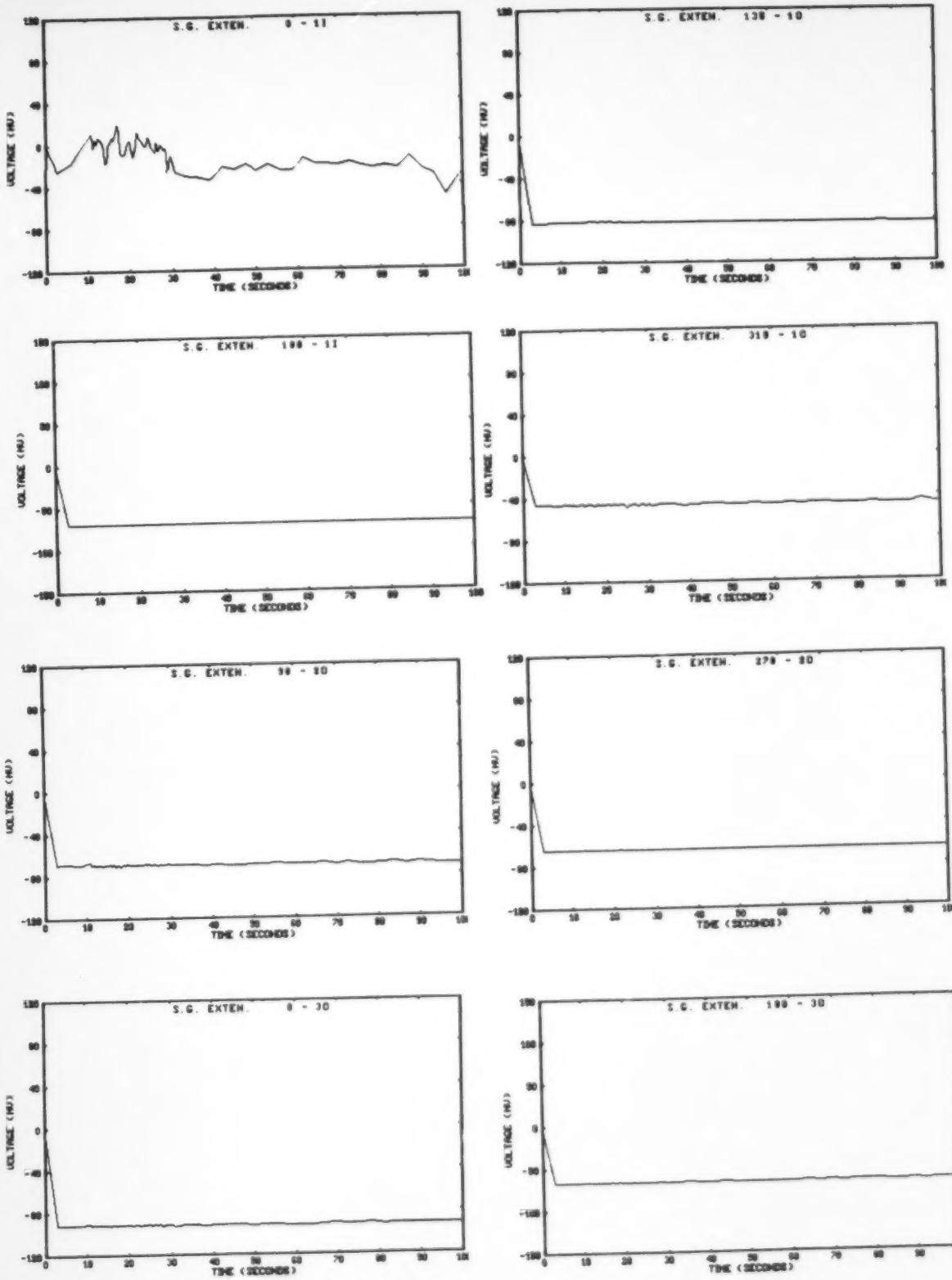
S.G. EXTEN. 0 - 11
S.G. EXTEN. 130 - 10
S.G. EXTEN. 190 - 11
S.G. EXTEN. 310 - 10
S.G. EXTEN. 90 - 20
S.G. EXTEN. 270 - 20
S.G. EXTEN. 0 - 30
S.G. EXTEN. 190 - 30
VOLTAGE (MV)
TIME (SECONDS)

PROJECT No. 902-2013 DRAWN RR REVIEWED _____ DATE OCT 90

Golder Associates

RESPONSE OF PIEZOMETERS - TEST 1

Figure 4.4a

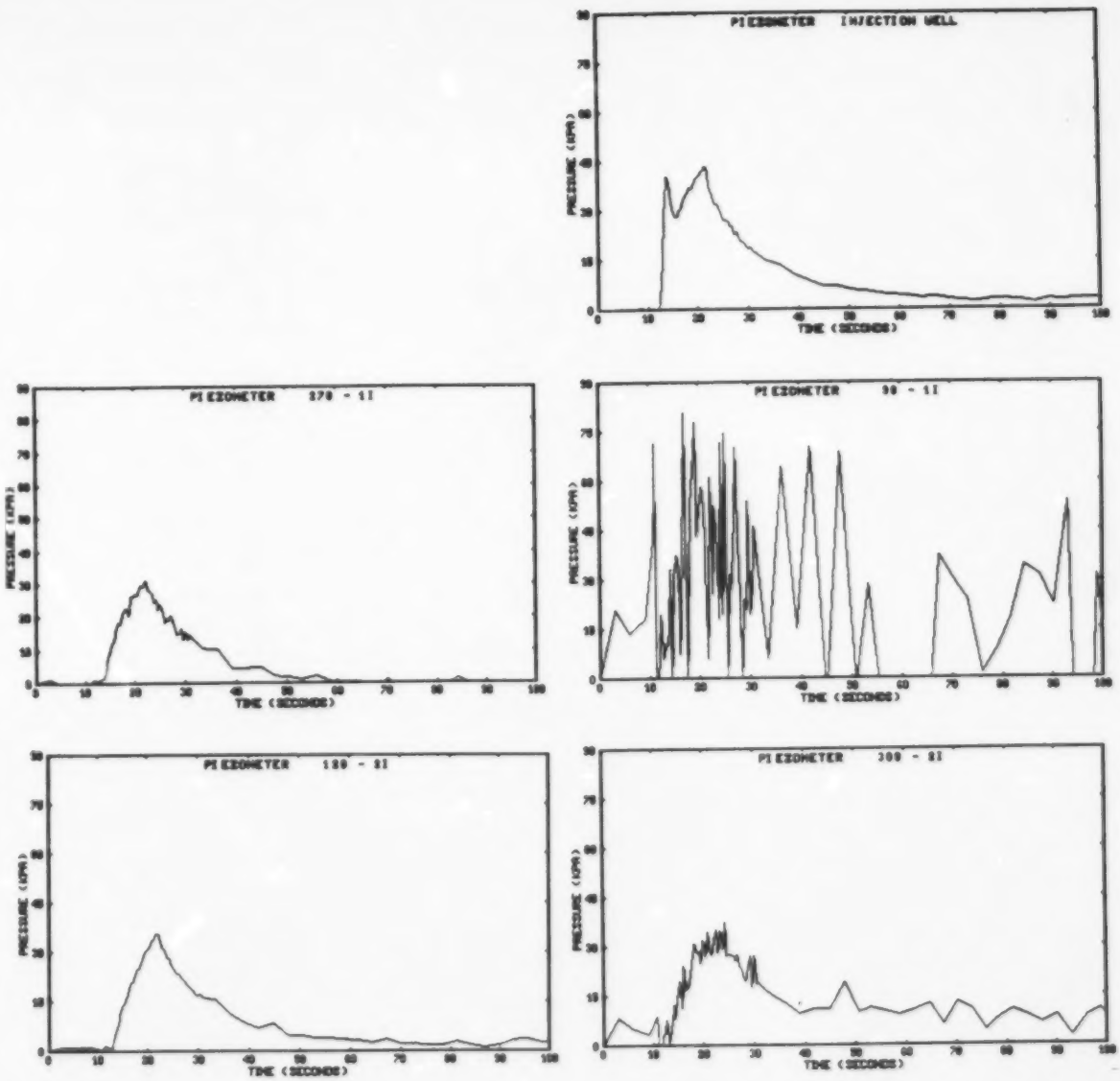

PROJECT No. 902-2013 DRAWN RR REVIEWED _____ DATE OCT 90

RESPONSE OF PIEZOMETERS - TEST 1

Figure 4.4b

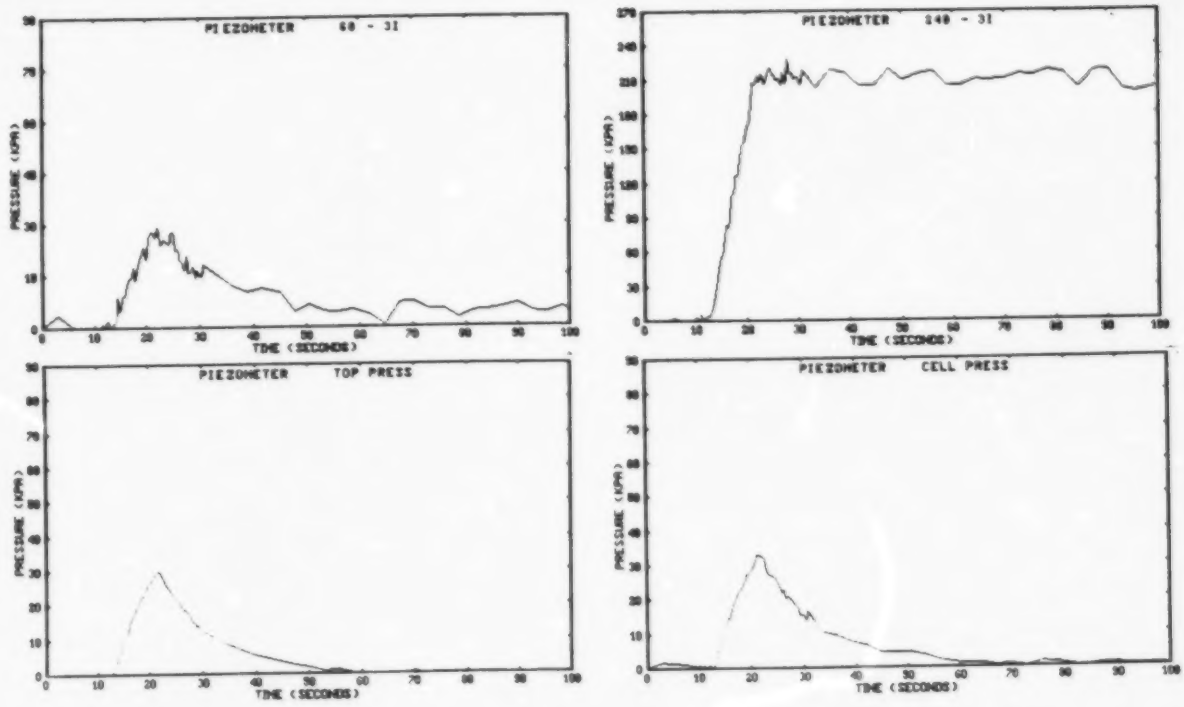

PROJECT No. 902-2013 DRAWN RR REVIEWED _____ DATE OCT 90

PROJECT No. 902-2013 DRAWN RR REVIEWED _____ DATE OCT 90

INSTRUMENTATION

- ○ PIEZOMETER
- △ LVDT EXTENSOMETER
- □ STRAIN GAUGE FOIL EXTENSOMETER

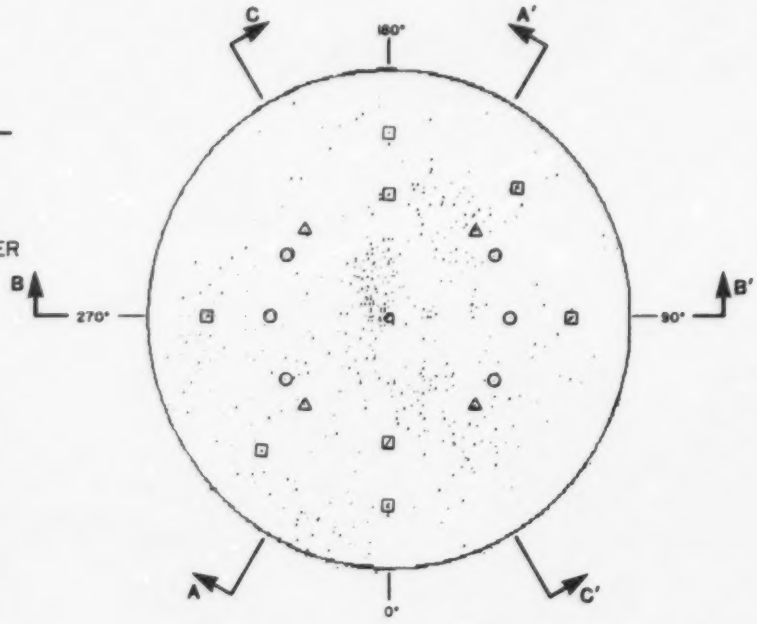

A) PLAN VIEW

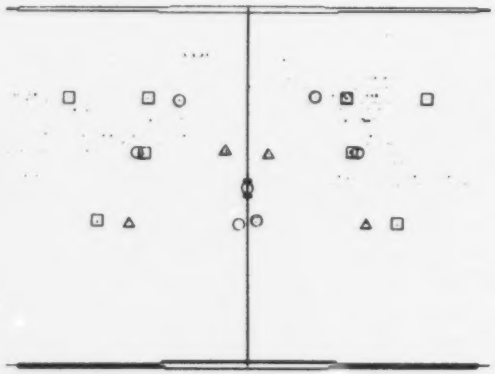

B) SECTION A - A'

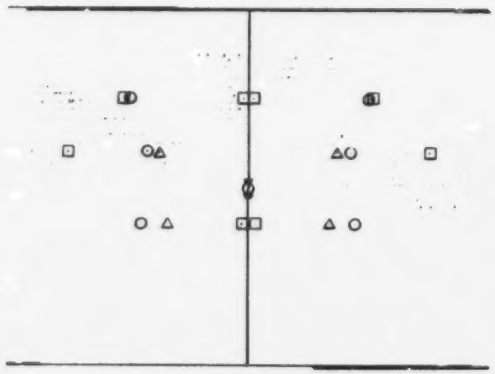

C) SECTION B - B'

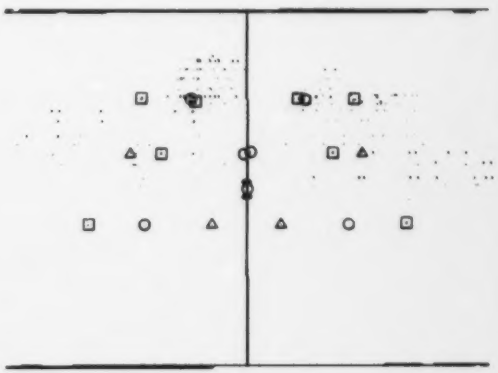

D) SECTION C - C'

LOCATION OF FLUORECENT DYE AFTER INJECTION - TEST 3

Figure 4.5

Golder Associates

RESPONSE OF LVDT EXTENSOMETERS AND FLUID INJECTION RECORD - TEST 3

Figure 4.6

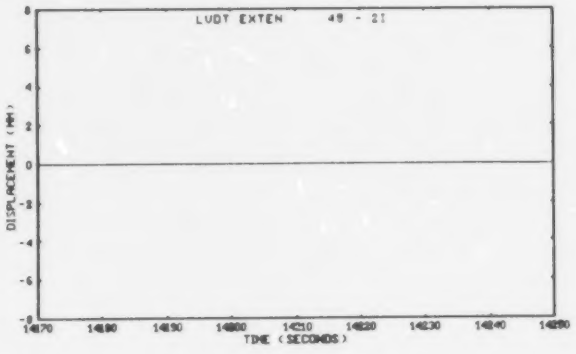

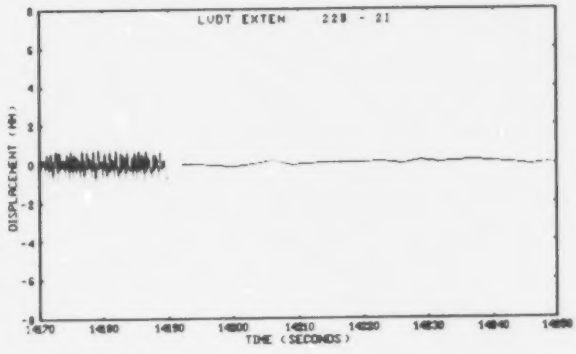

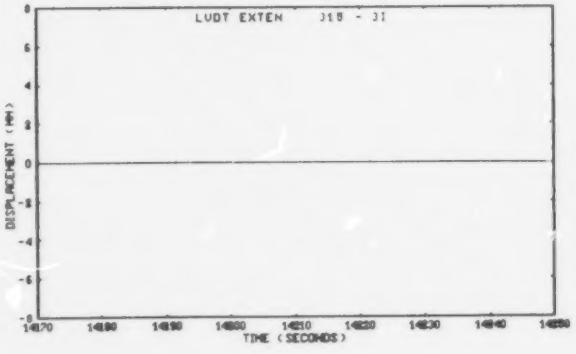

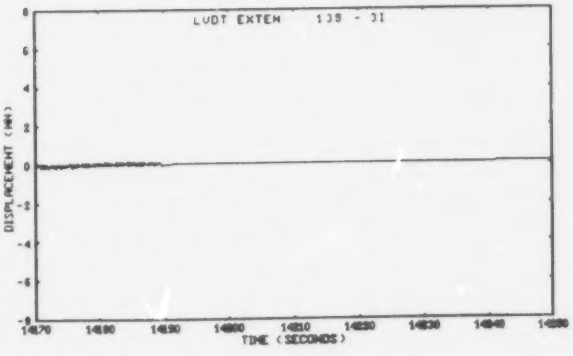

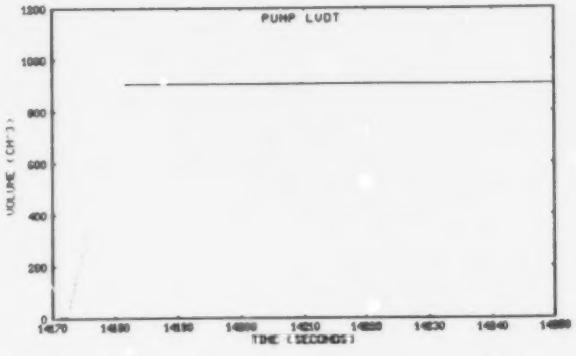

PROJECT No. 902-2013 DRAWN RR REVIEWED _____ DATE OCT 90

RESPONSE OF STRAIN GAUGE FOIL EXTENSOMETERS - TEST 3

Figure 4.7

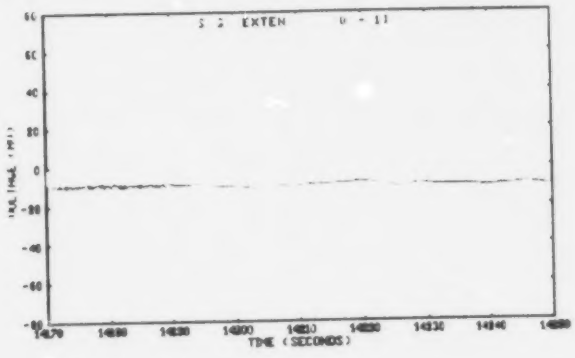

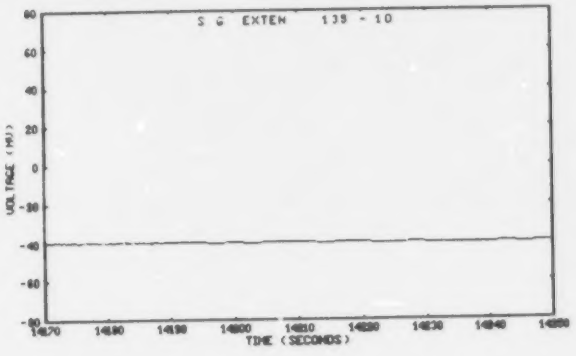

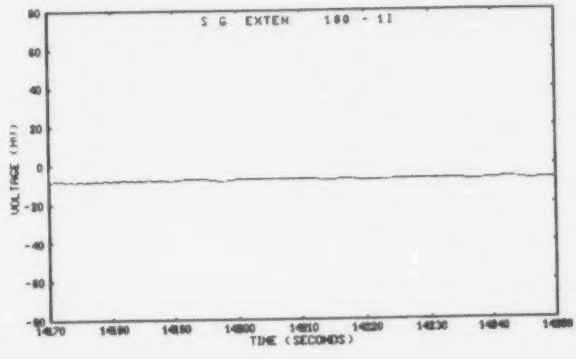

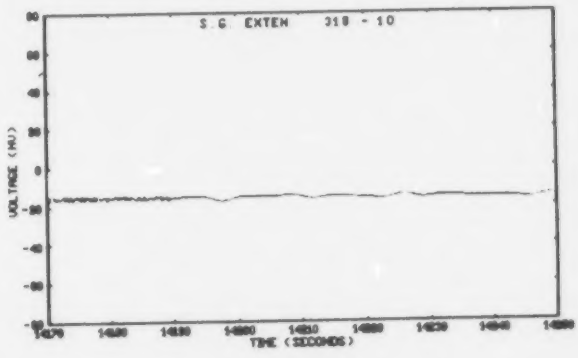

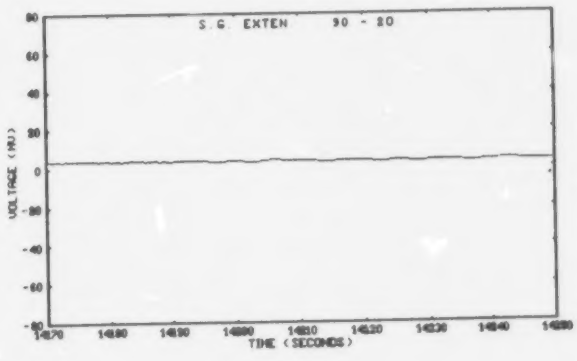

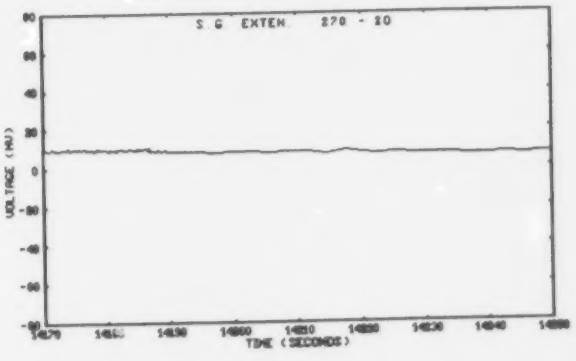

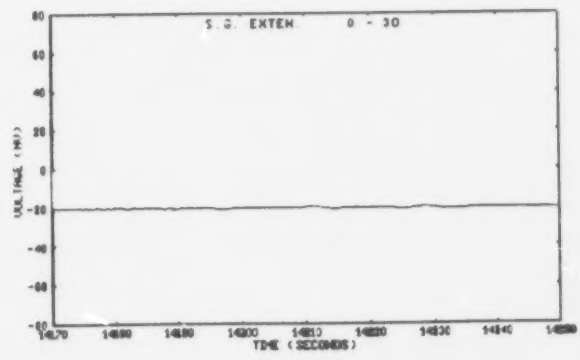

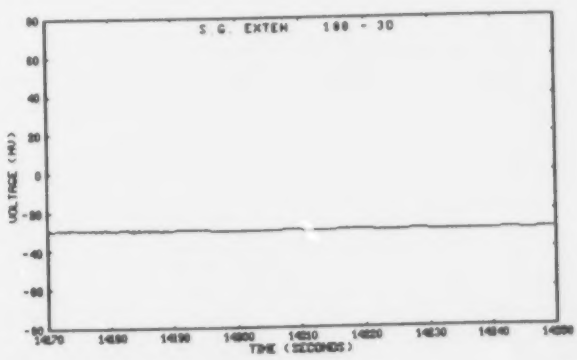

PROJECT No. 902-2013 DRAWN RR REVIEWED _____ DATE OCT 90

Golder Associates

RESPONSE OF PIEZOMETERS - TEST 3

Figure 4.8a

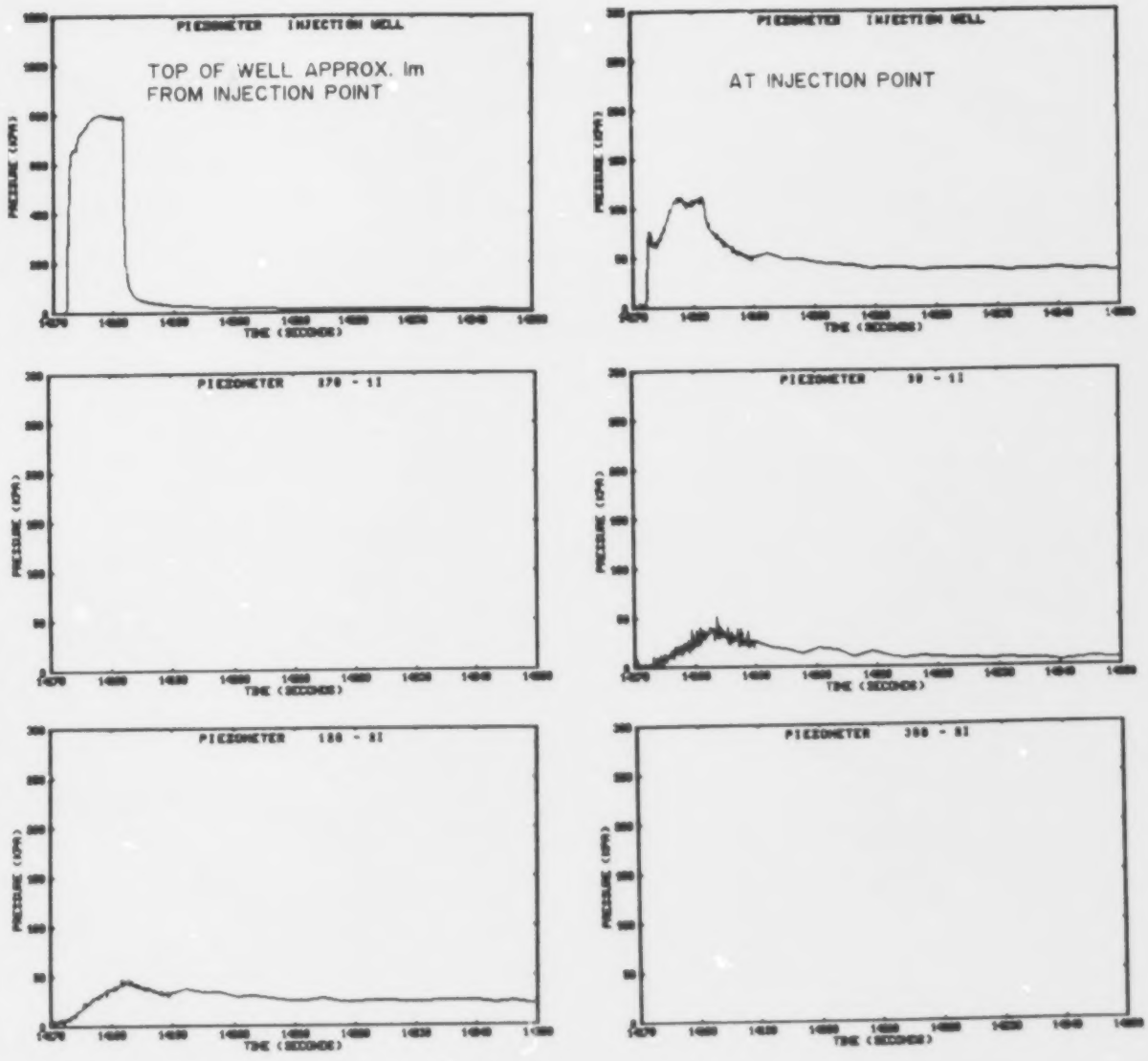

PROJECT No. 902-2013 DRAWN RR REVIEWED _____ DATE OCT 90

RESPONSE OF PIEZOMETERS - TEST 3

Figure 4.8b

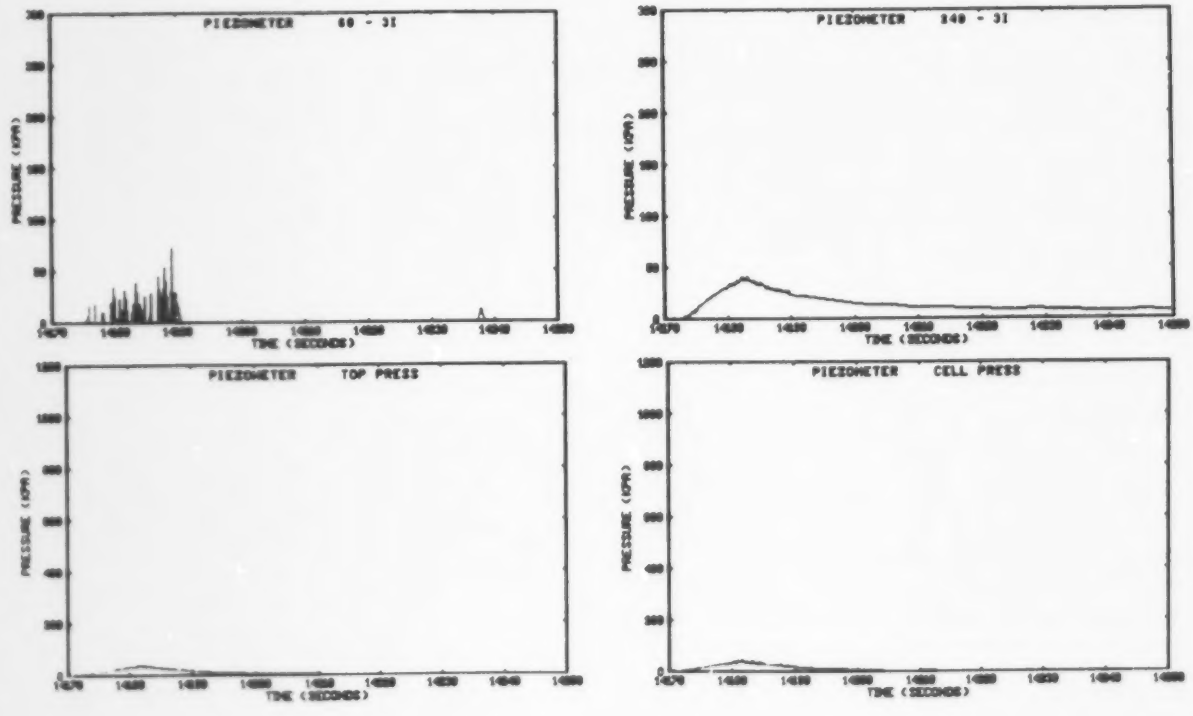

PROJECT No. 902-2013 DRAWN RR REVIEWED _____ DATE OCT 90

LOCATION OF FLUORECENT DYE AFTER INJECTION - TEST 4

Figure 4.9

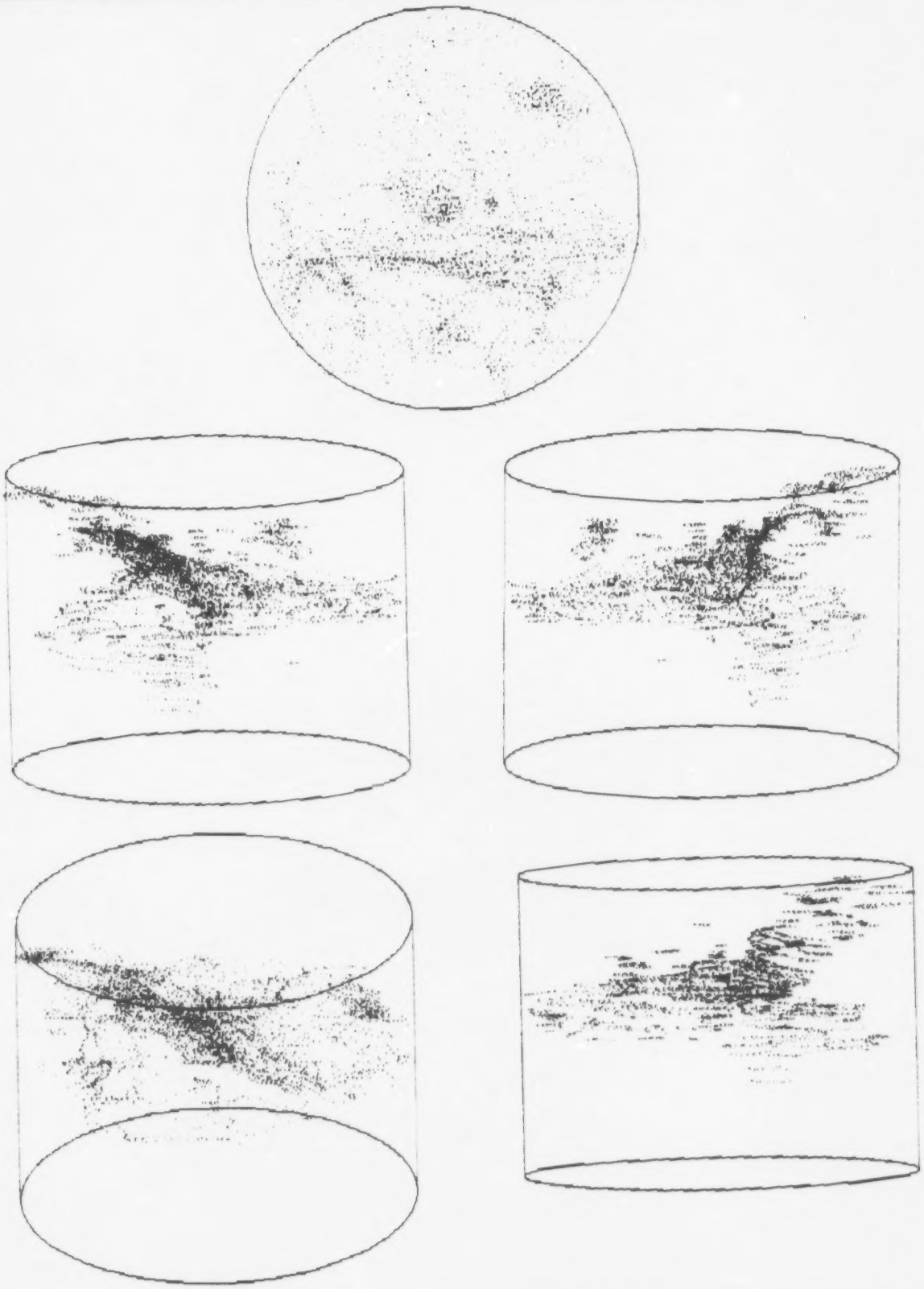

PROJECT No. 902-2013 DRAWN RR REVIEWED ____ DATE APR 91

Golder Associates

RESPONSE OF LVDT EXTENSOMETERS AND FLUID INJECTION RECORD - TEST 4

Figure 4.10

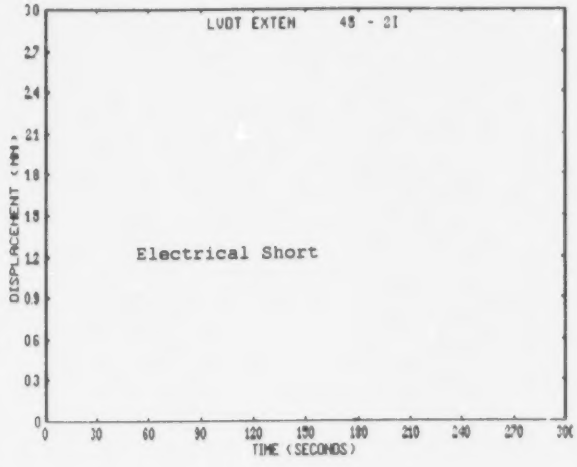

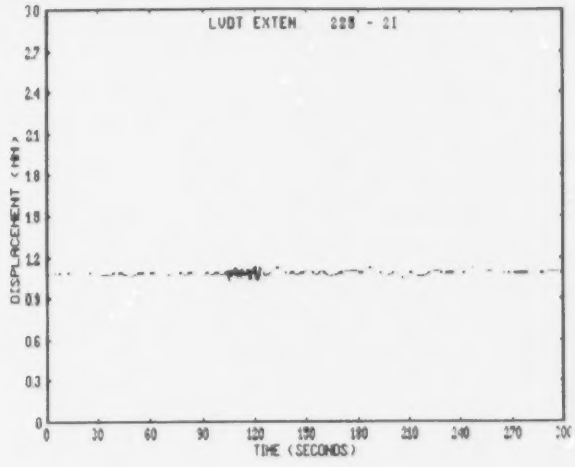

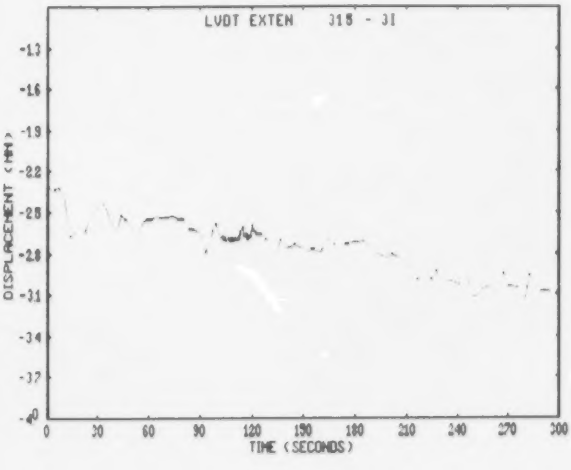

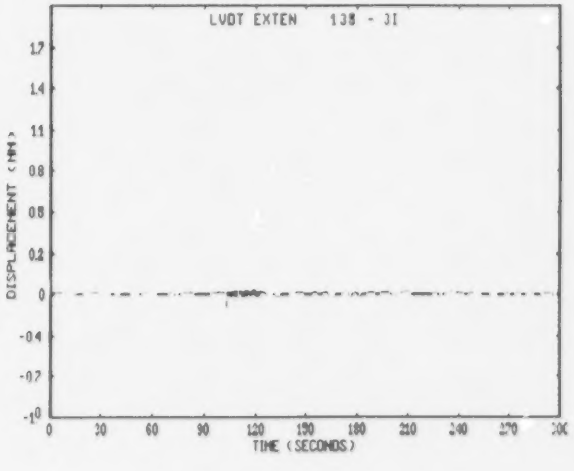

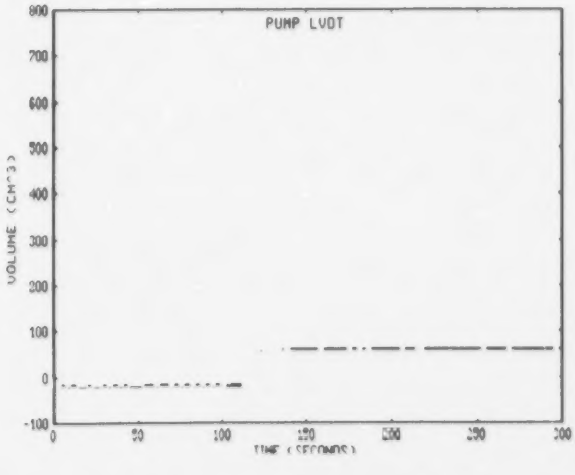

PROJECT No. 902-2013 DRAWN RR REVIEWED _____ DATE APR 91

RESPONSE OF PIEZOMETERS - TEST 4

Figure 4.11

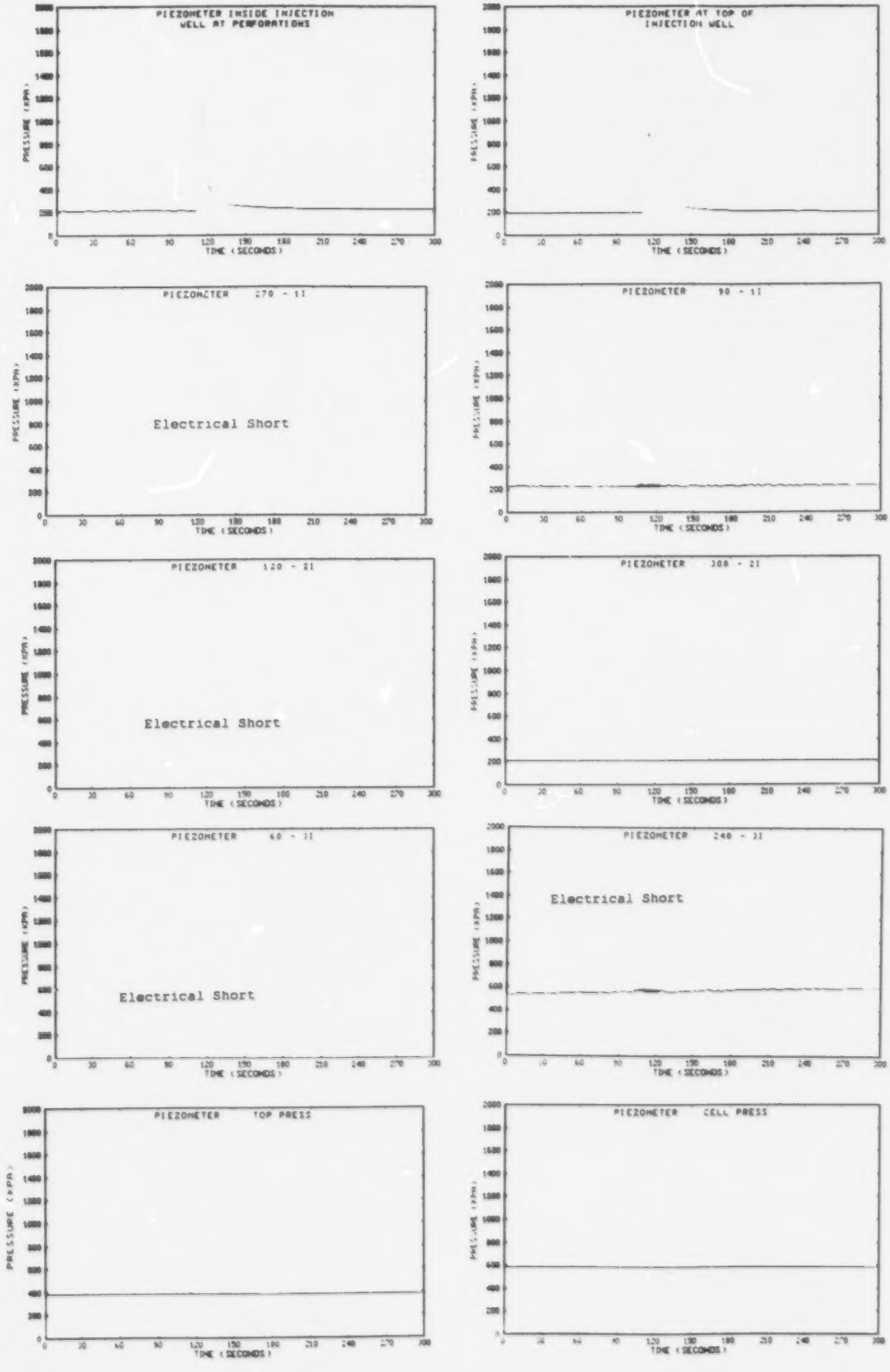

PROJECT No. 902-2013 DRAWN RR REVIEWED _____ DATE APR 91

INJECTION CURVES - FRACTURE - TEST 4

Figure 4.12

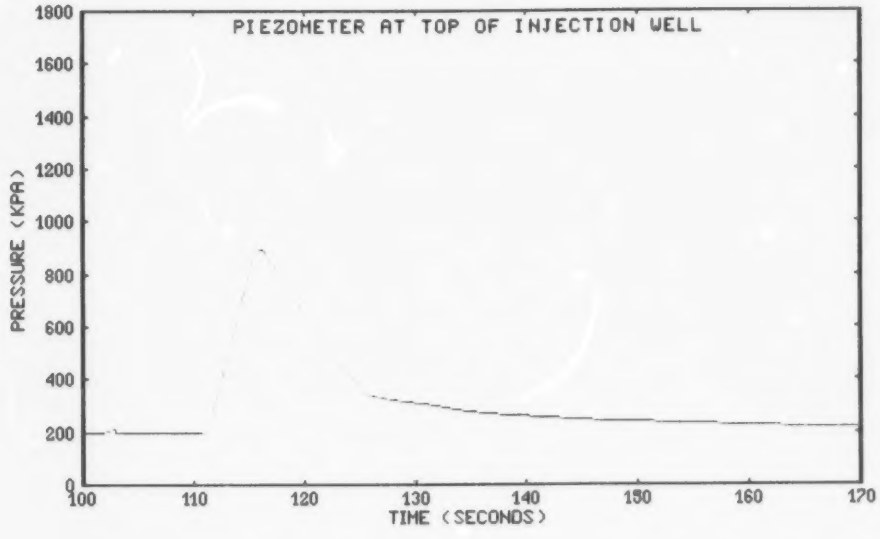

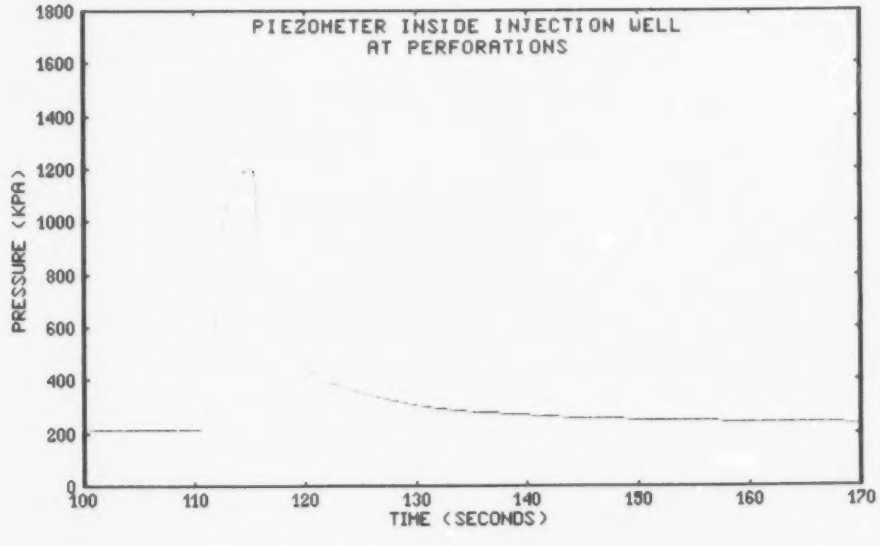

PROJECT No. 902-2013 DRAWN RR REVIEWED _____ DATE APR 91

DRAINED LOADING - TEST 5

Figure 4.13

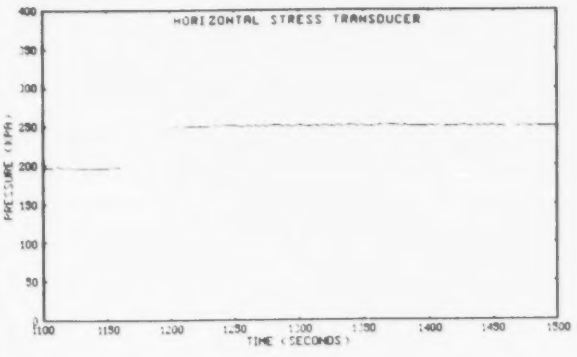

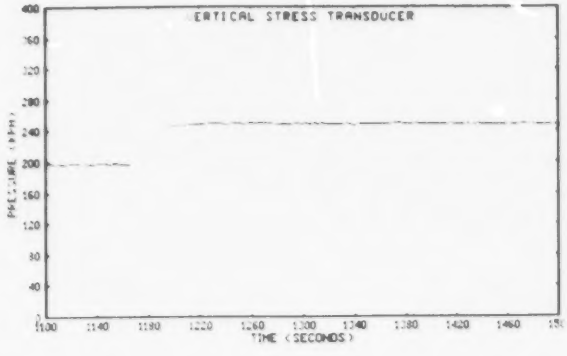

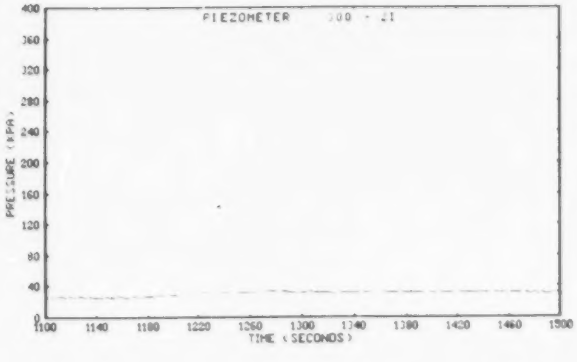

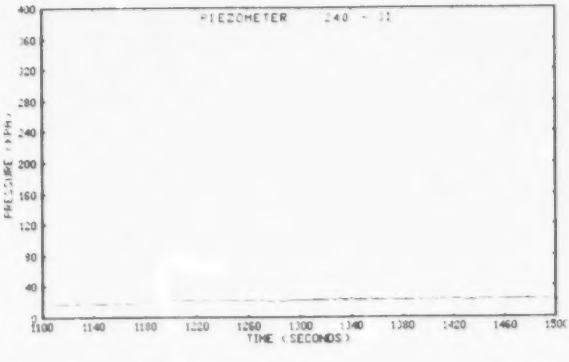

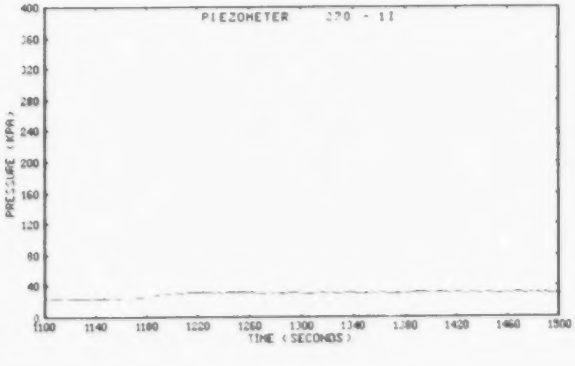

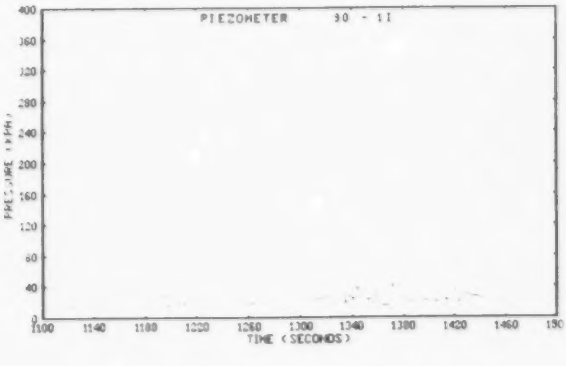

PROJECT No. 902-2013 DRAWN RR REVIEWED _____ DATE APR 91

B TEST - TEST 5

Figure 4.14

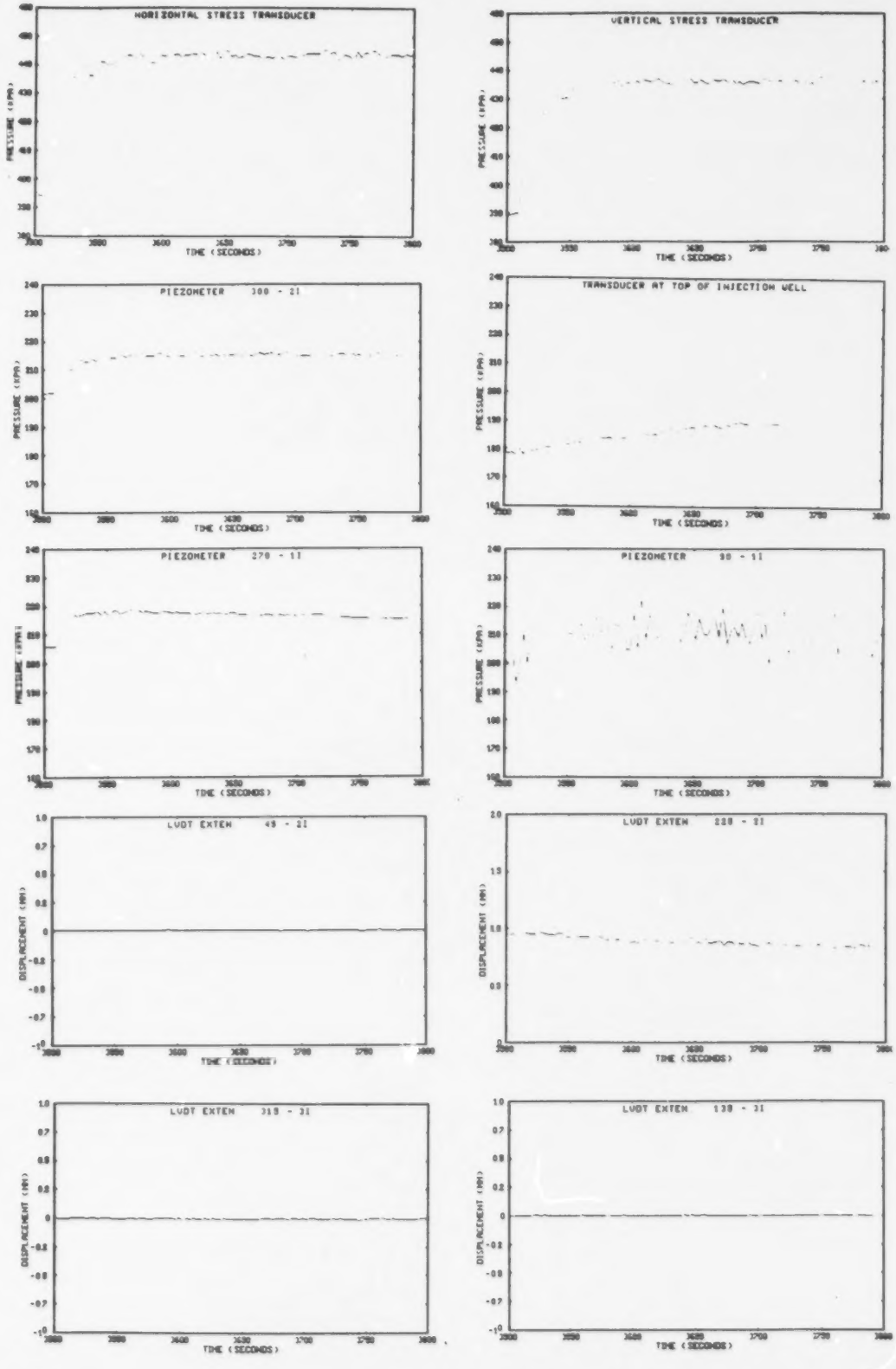

PROJECT No. 902-2013 DRAWN RR REVIEWED _____ DATE APR 91

LOCATION OF FLUORENCENT DYE AFTER INJECTION - TEST 5

Figure 4.15

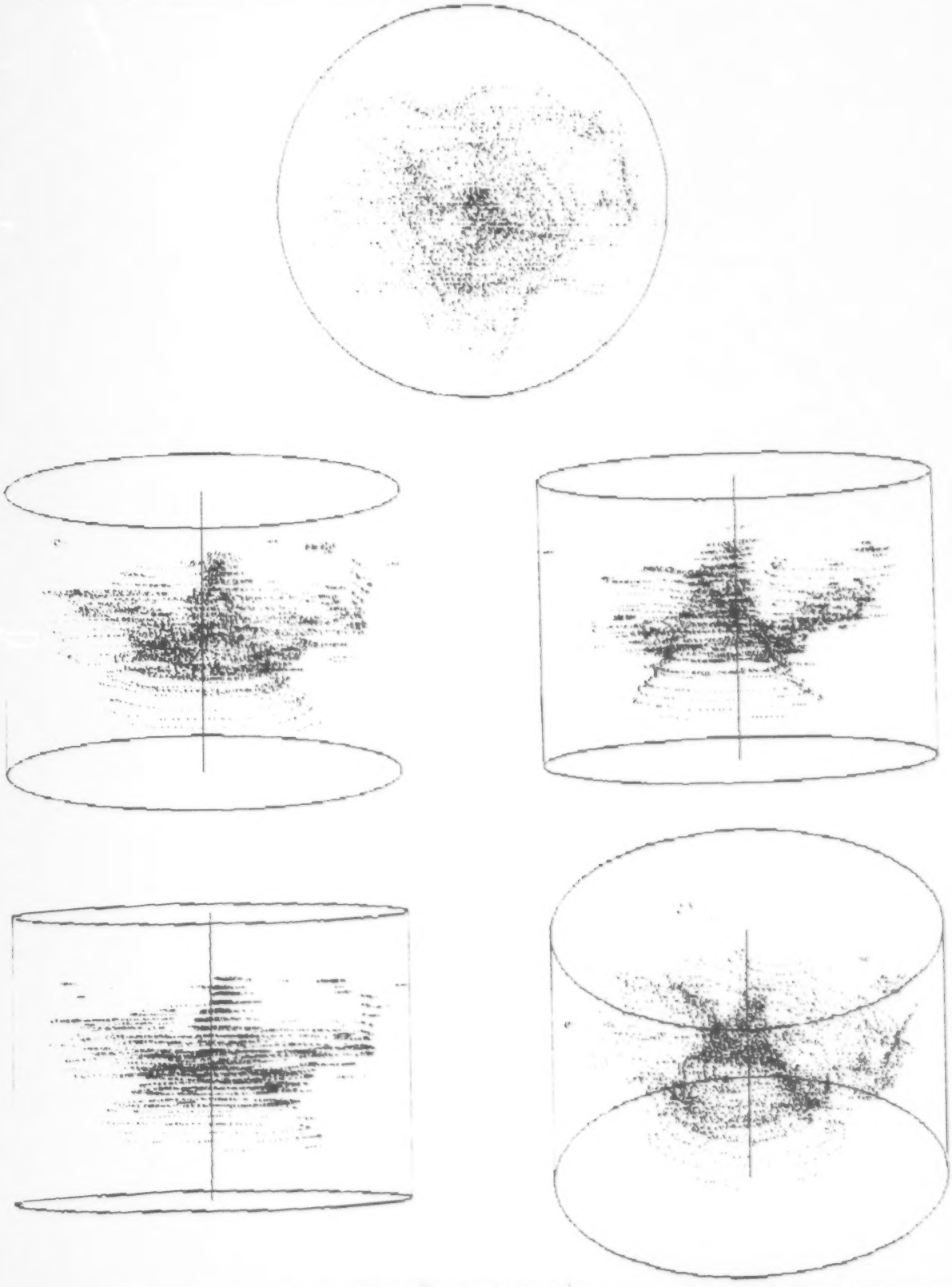

PROJECT No. 902-2013 DRAWN RR REVIEWED _____ DATE APR 91

Golder Associates

RESPONSE OF LVDT EXTENSOMETERS AND FLUID INJECTION RECORD - TEST 5

Figure 4.16

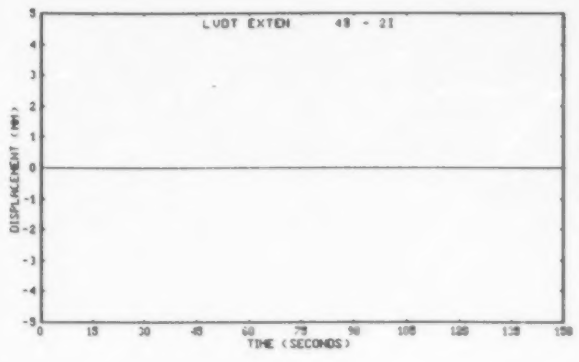

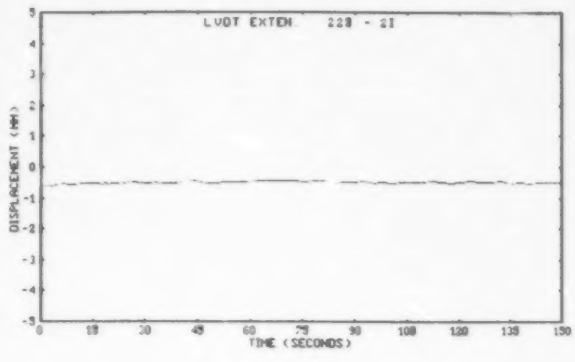

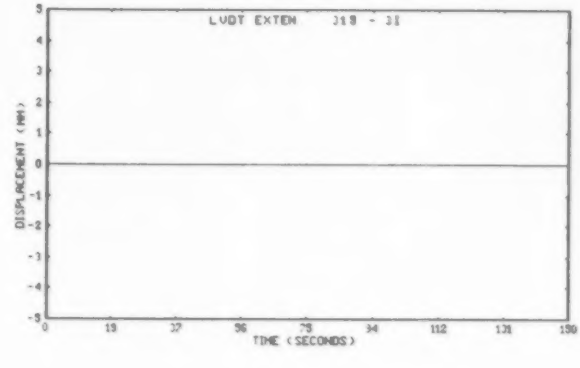

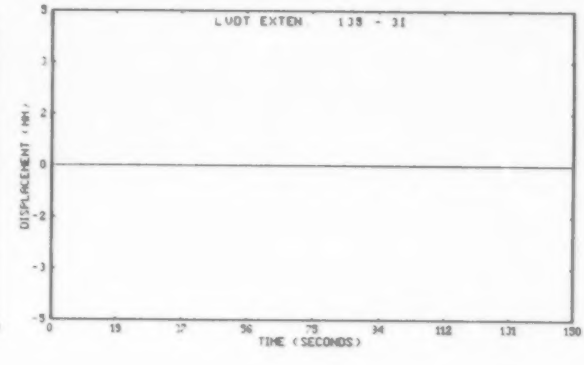

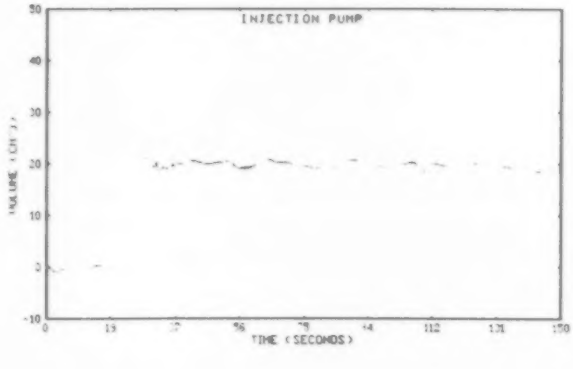

PROJECT No. 902-2013 DRAWN RR REVIEWED ____ DATE APR 91

RESPONSE OF PIEZOMETERS - TEST 5

Figure 4.17

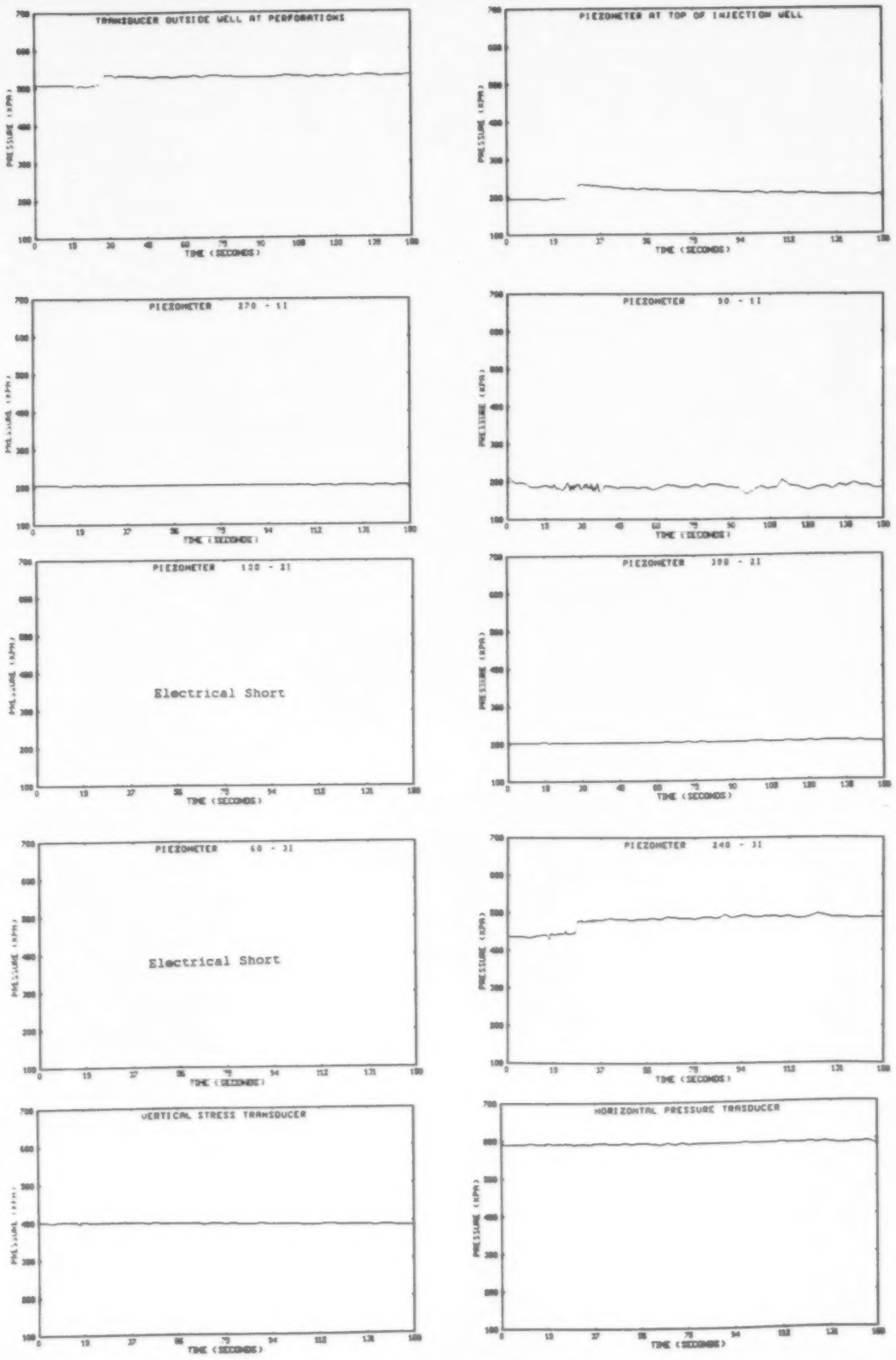

PROJECT No. 902-2013 DRAWN RR REVIEWED _____ DATE APR 91

PERMEABILITY TEST - TEST 6

Figure 4.18

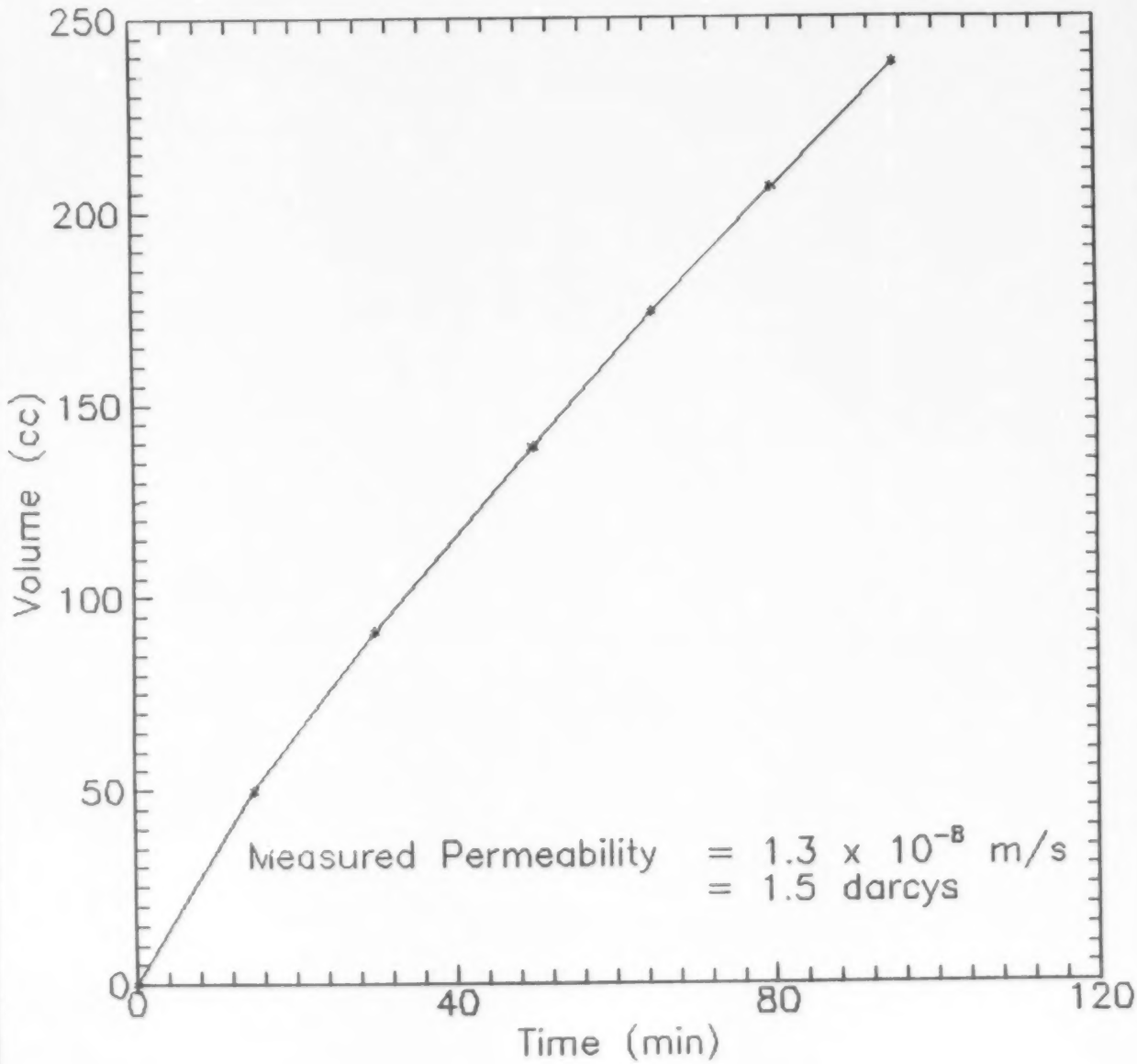

PROJECT No. 902-2013 DRAWN RR REVIEWED _____ DATE APR 91

Golder Associates

INJECTION TEST No. 1 - TEST 6

Figure 4.19

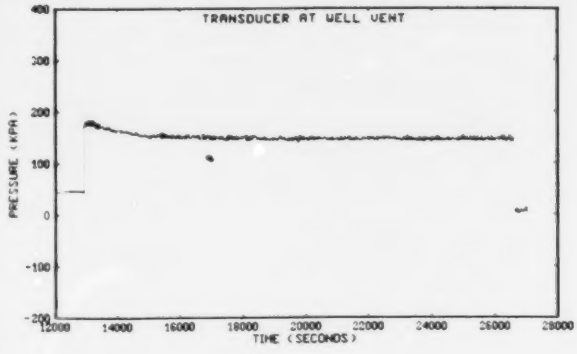

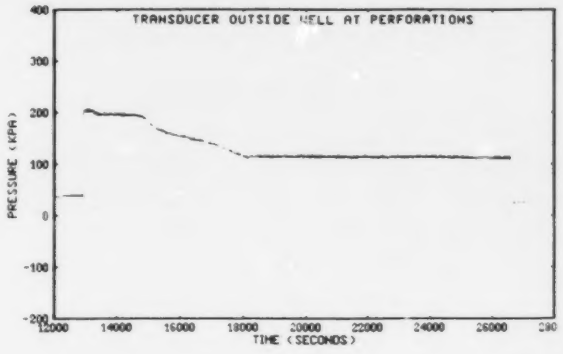

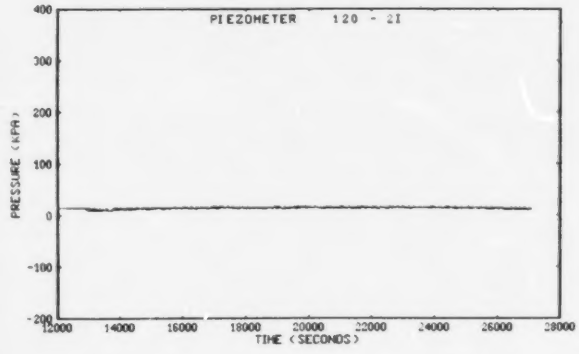

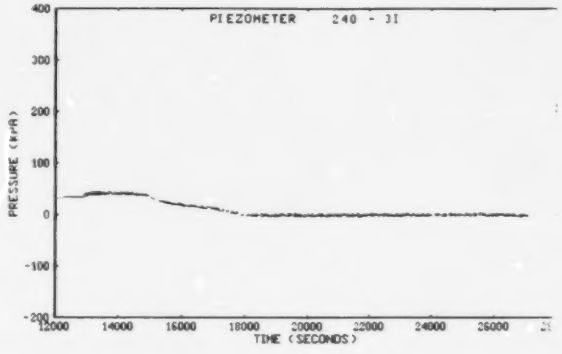

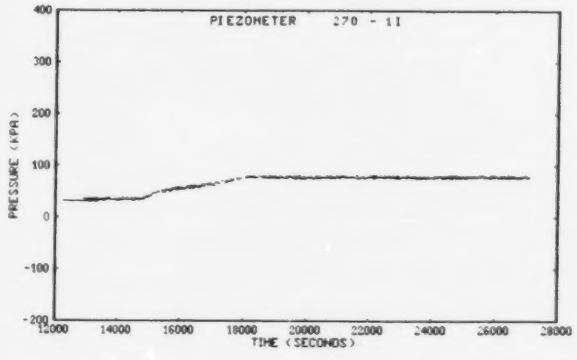

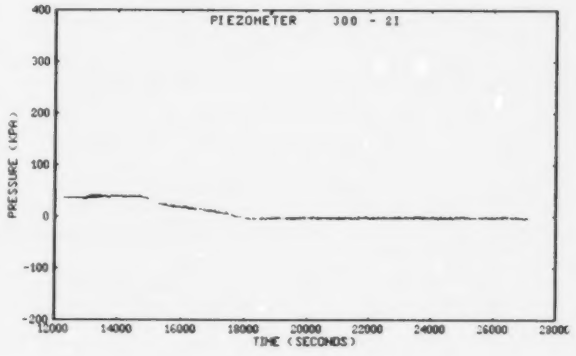

PROJECT No. 902-2013 DRAWN RR REVIEWED ____ DATE APR 91

INJECTION TEST No. 2 - TEST 6

Figure 4.20

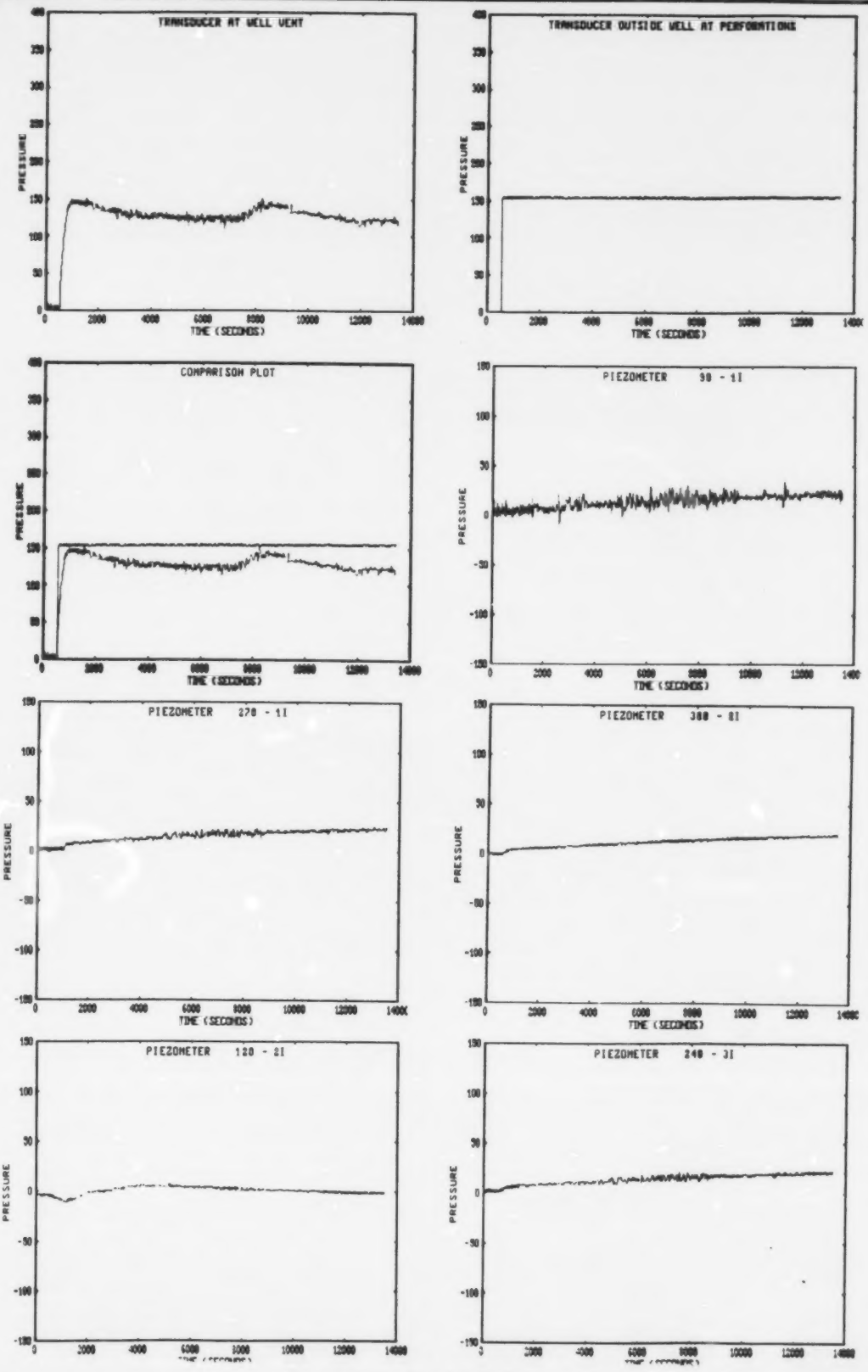

PROJECT No. 902-2013 DRAWN RR REVIEWED _____ DATE APR 91

DRAINED LOADING AND B TEST - TEST 6

Figure 4.21

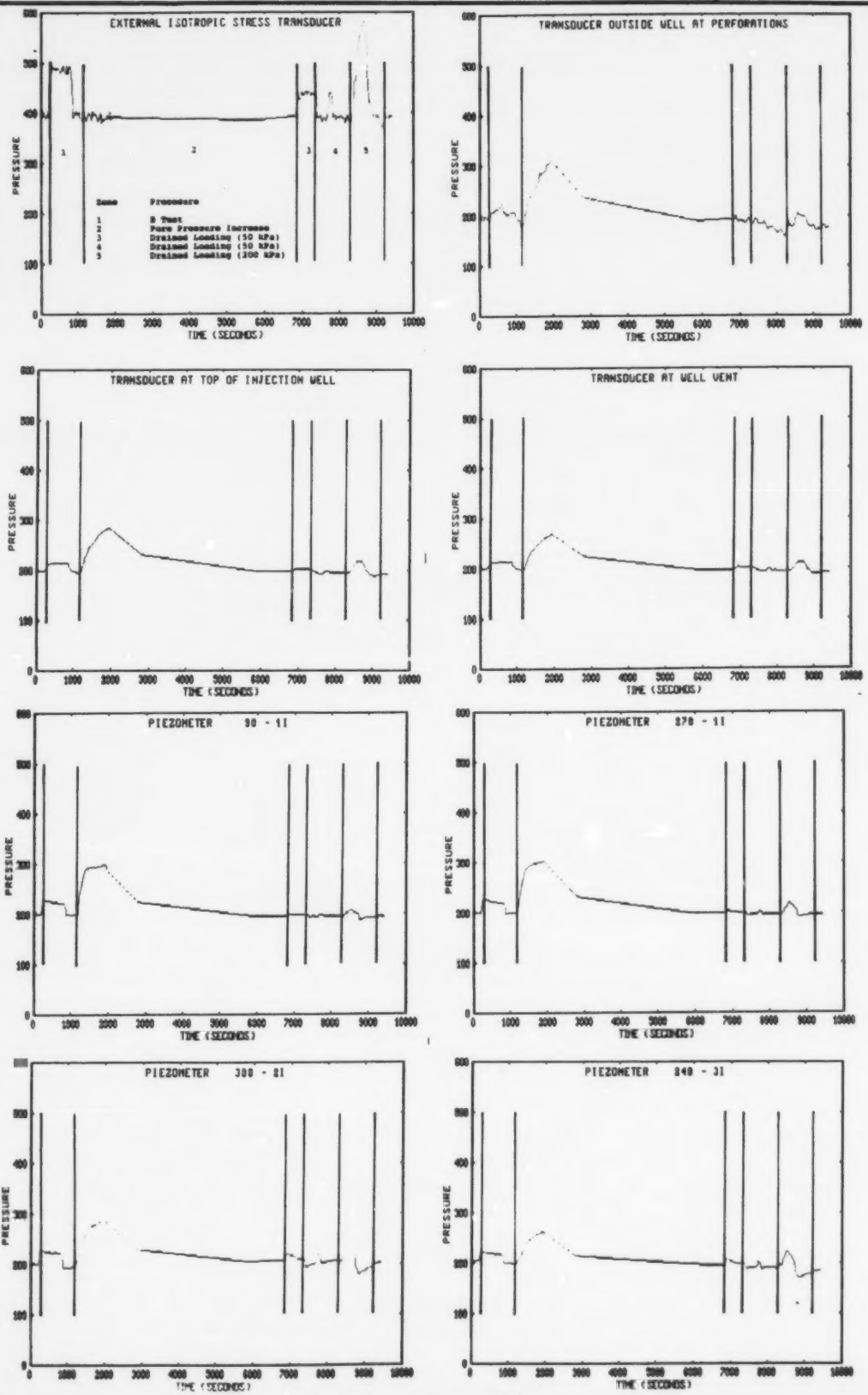

PROJECT No. 902-2013 DRAWN RR REVIEWED _____ DATE APR 91

LOCATION OF FLUORECENT DYE AFTER INJECTION - TEST 6

Figure 4.22

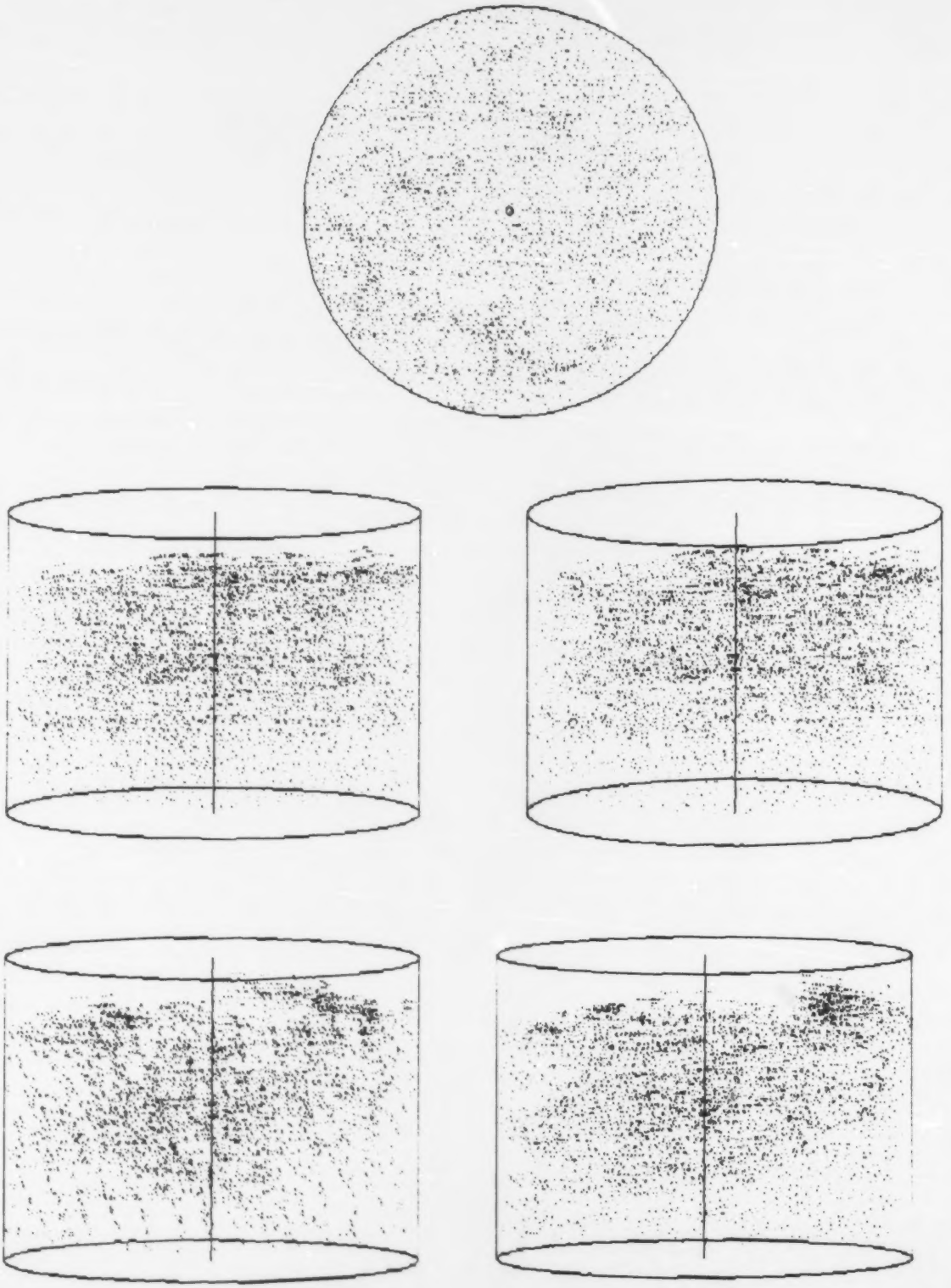

PROJECT No. 902-2013 DRAWN RR REVIEWED _____ DATE APR 91

Golder Associates

INJECTION PRESSURE CURVES - TEST 6

Figure 4.23

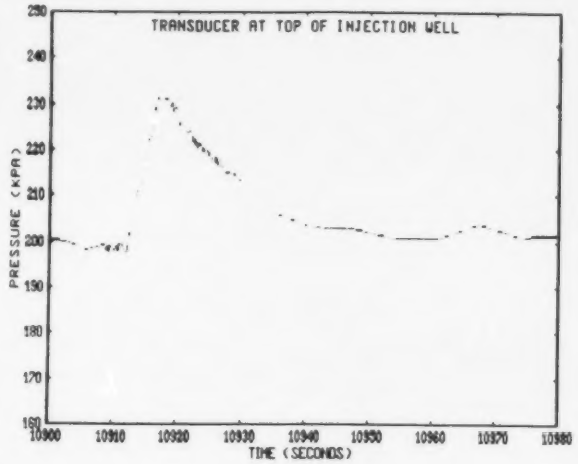

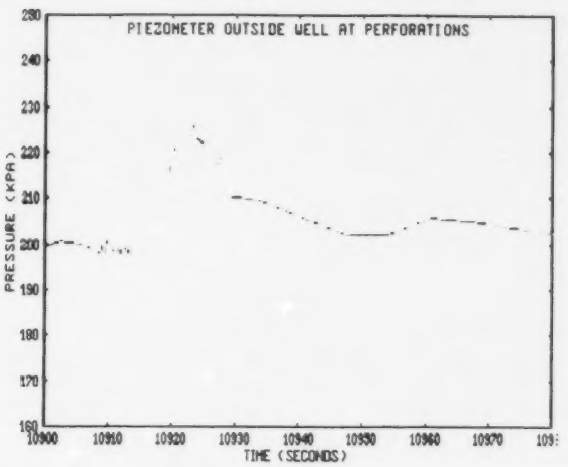

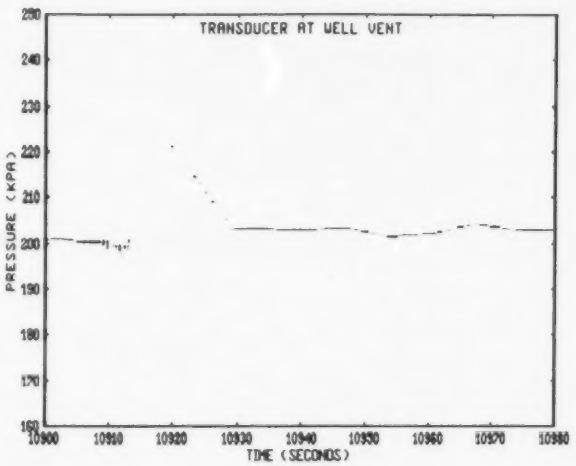

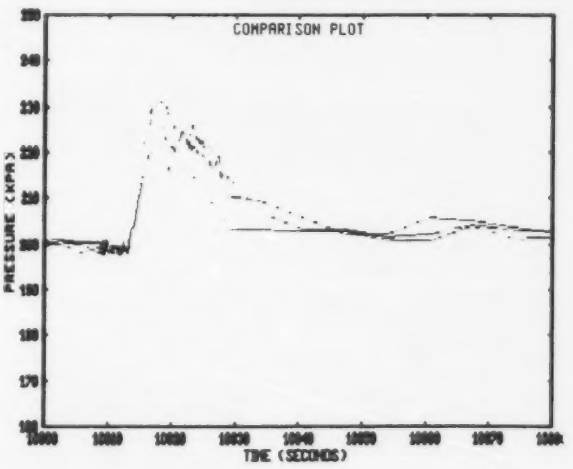

PROJECT No. 902-2013 DRAWN RR REVIEWED ____ DATE APR 91

RESPONSE OF PIEZOMETERS - TEST 6

Figure 4.24

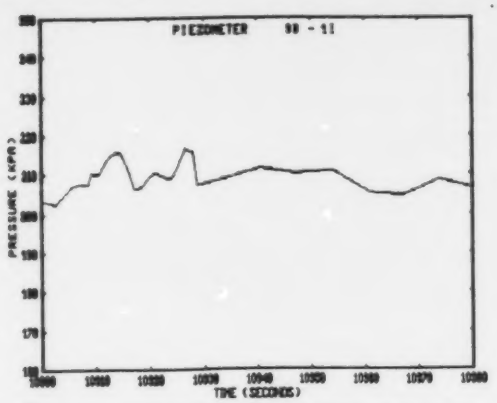

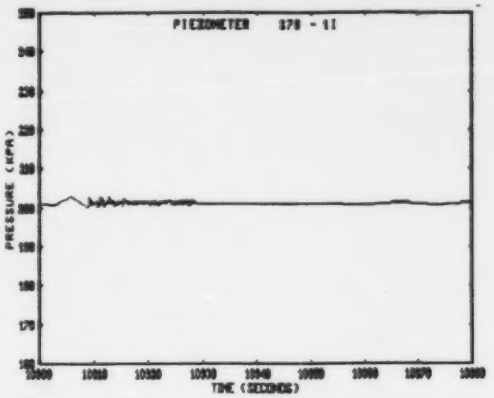

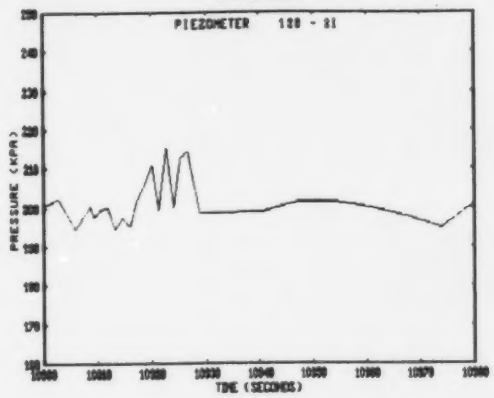

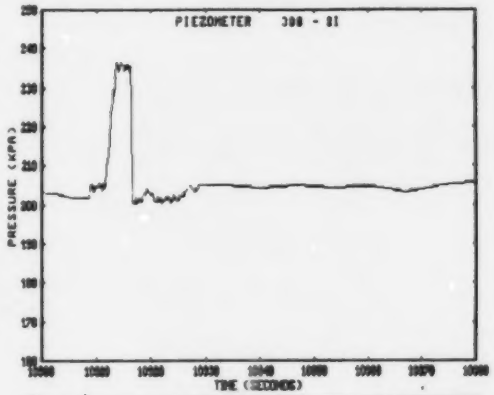

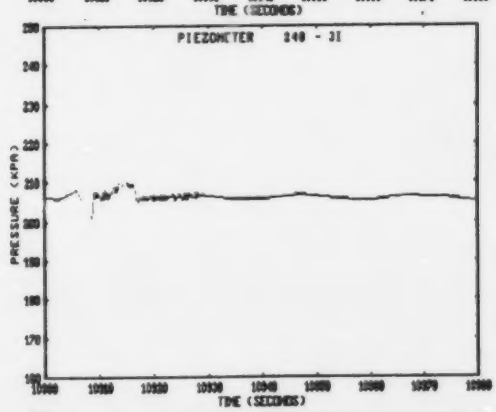

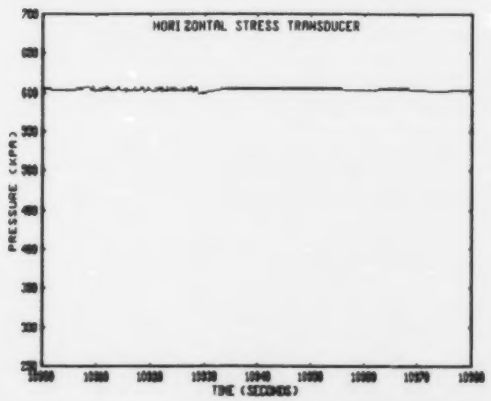

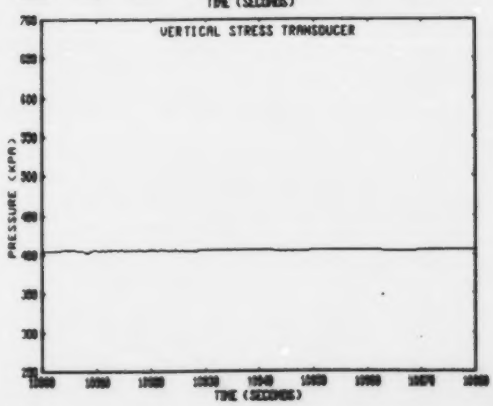

PROJECT No. 902-2013 DRAWN RR REVIEWED _____ DATE APR 91

Golder Associates

RESPONSE OF LVDT EXTENSOMETERS AND FLUID INJECTION RECORD - TEST 6

Figure 4.25

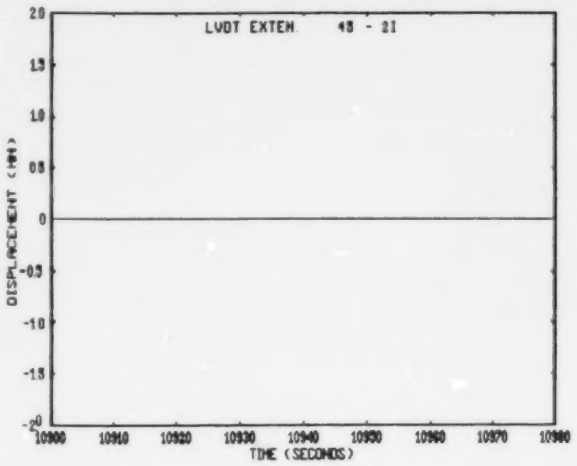

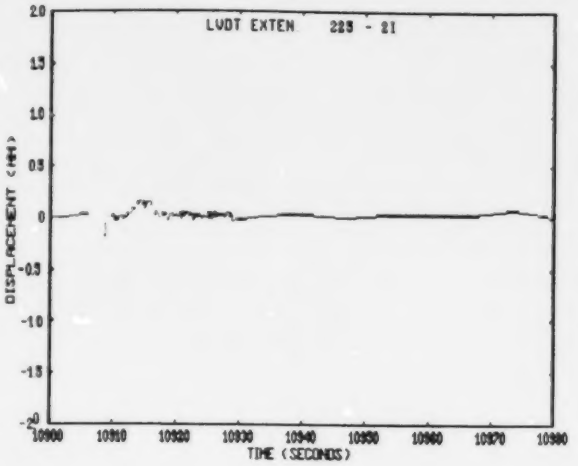

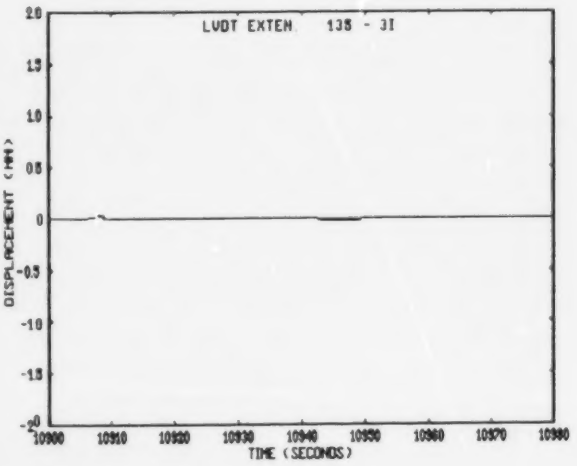

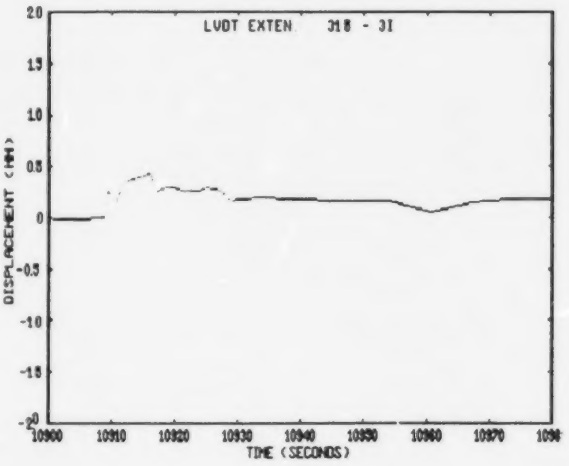

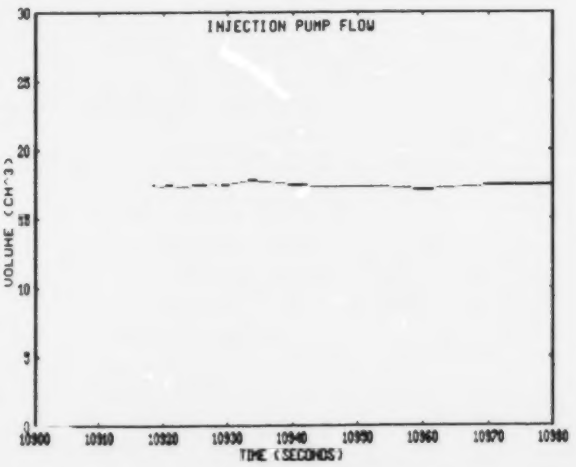

PROJECT No. 902-2013 DRAWN RR REVIEWED ____ DATE APR 91

INJECTION TEST - TEST 7

Figure 4.26

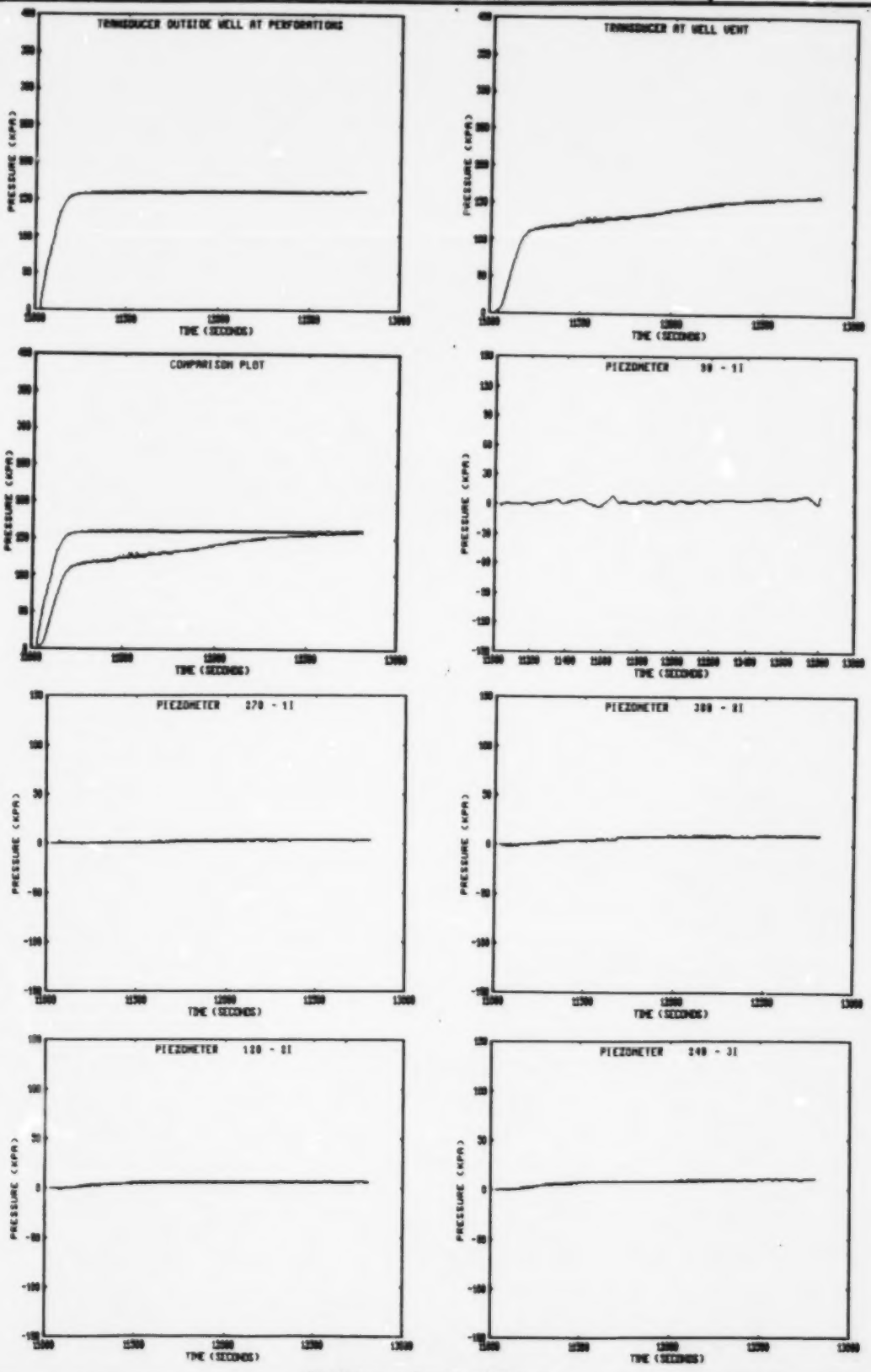

PROJECT No. 902-2013 DRAWN RR REVIEWED _____ DATE APR 91

LOCATION OF FLUORECENT DYE AFTER INJECTION - TEST 7

Figure 4.27

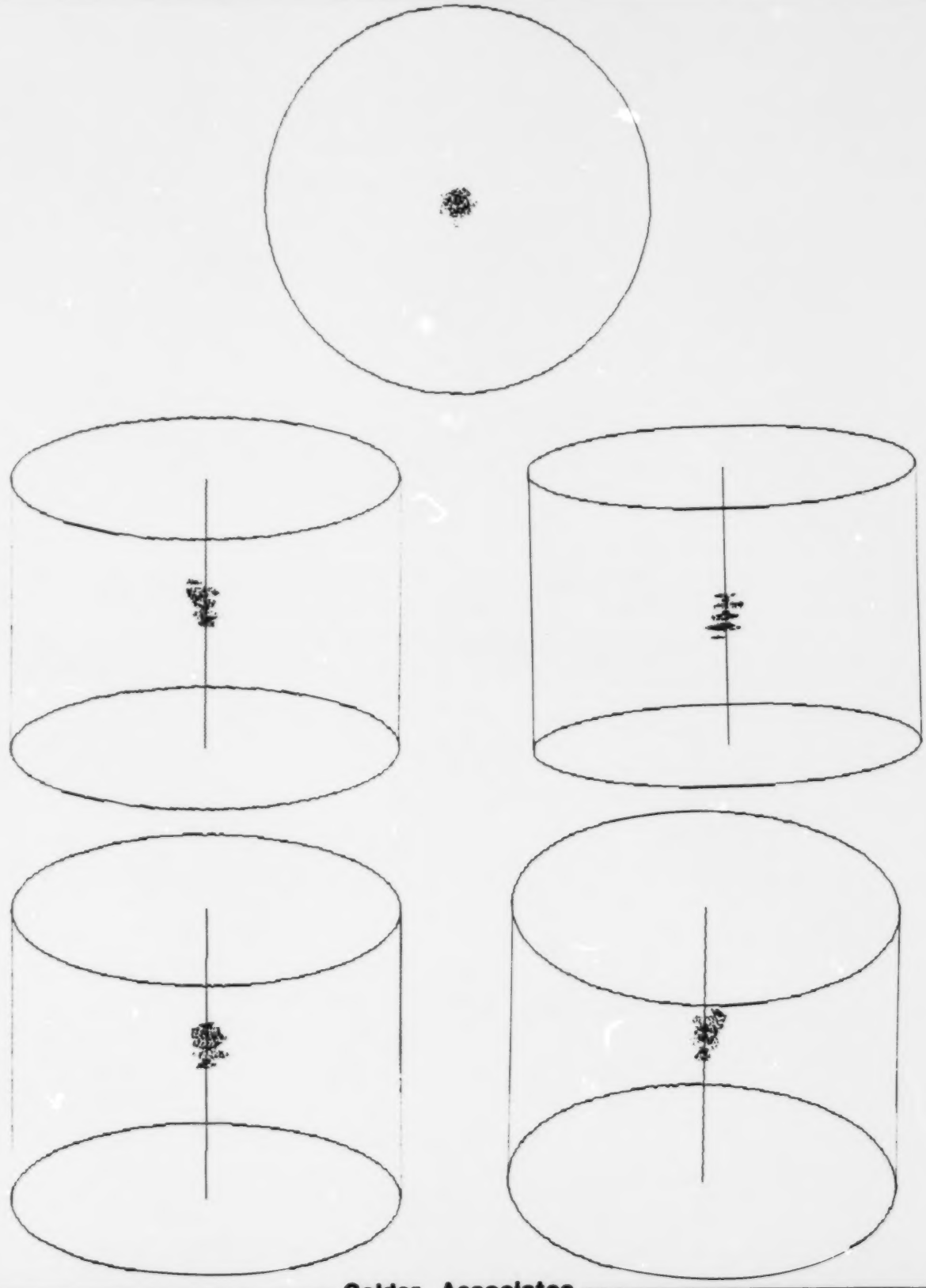

PROJECT No. 902-2013 DRAWN RR REVIEWED _____ DATE APR 91

Golder Associates

RESPONSE OF LVDT EXTENSOMETERS AND FLUID INJECTION RECORD - TEST 7

Figure 4.28

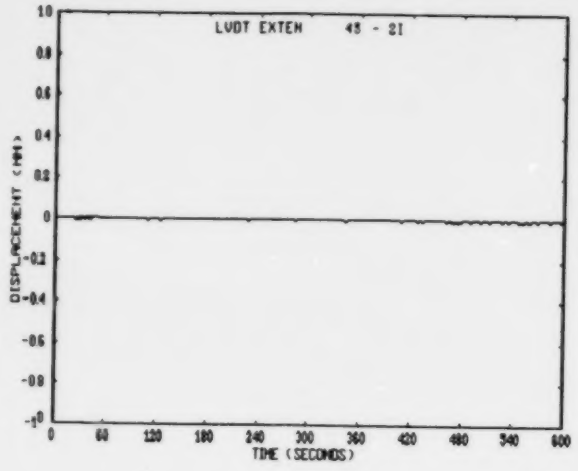

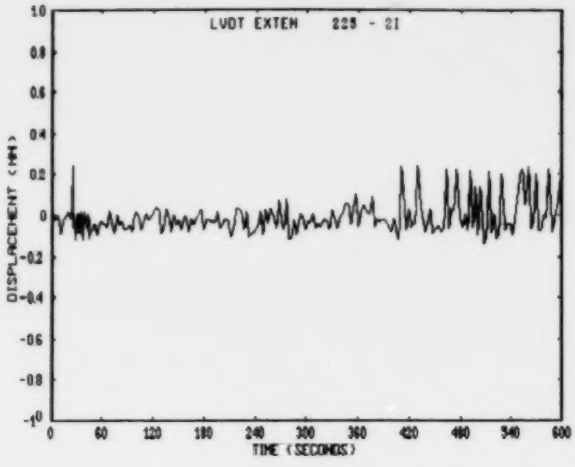

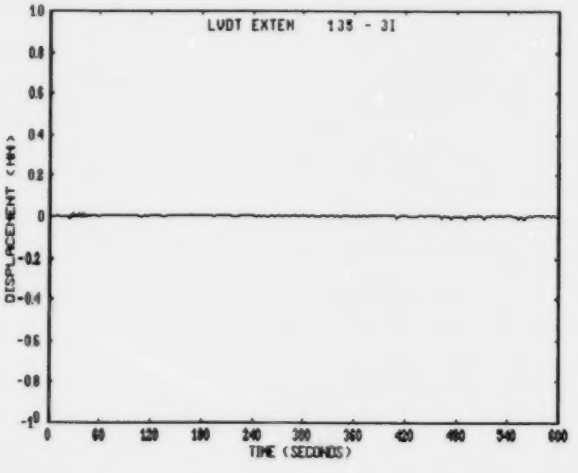

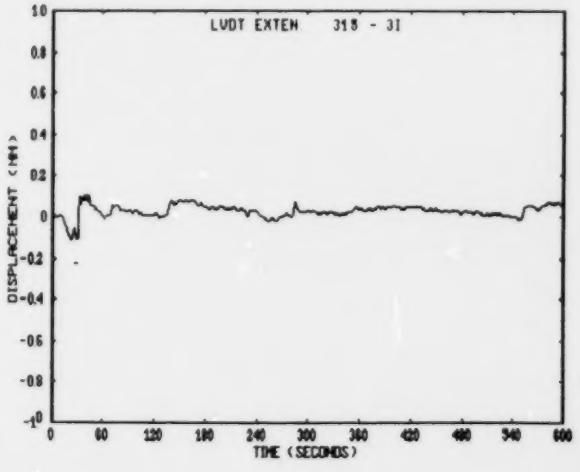

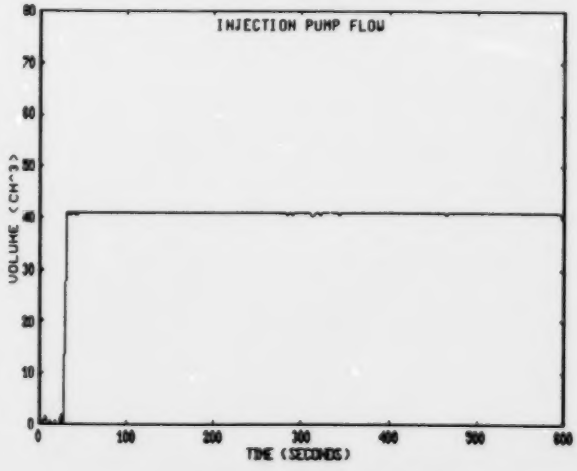

PROJECT No. 902-2013 DRAWN RR REVIEWED ____ DATE APR 91

RESPONSE OF PIEZOMETERS - TEST 7

Figure 4.29

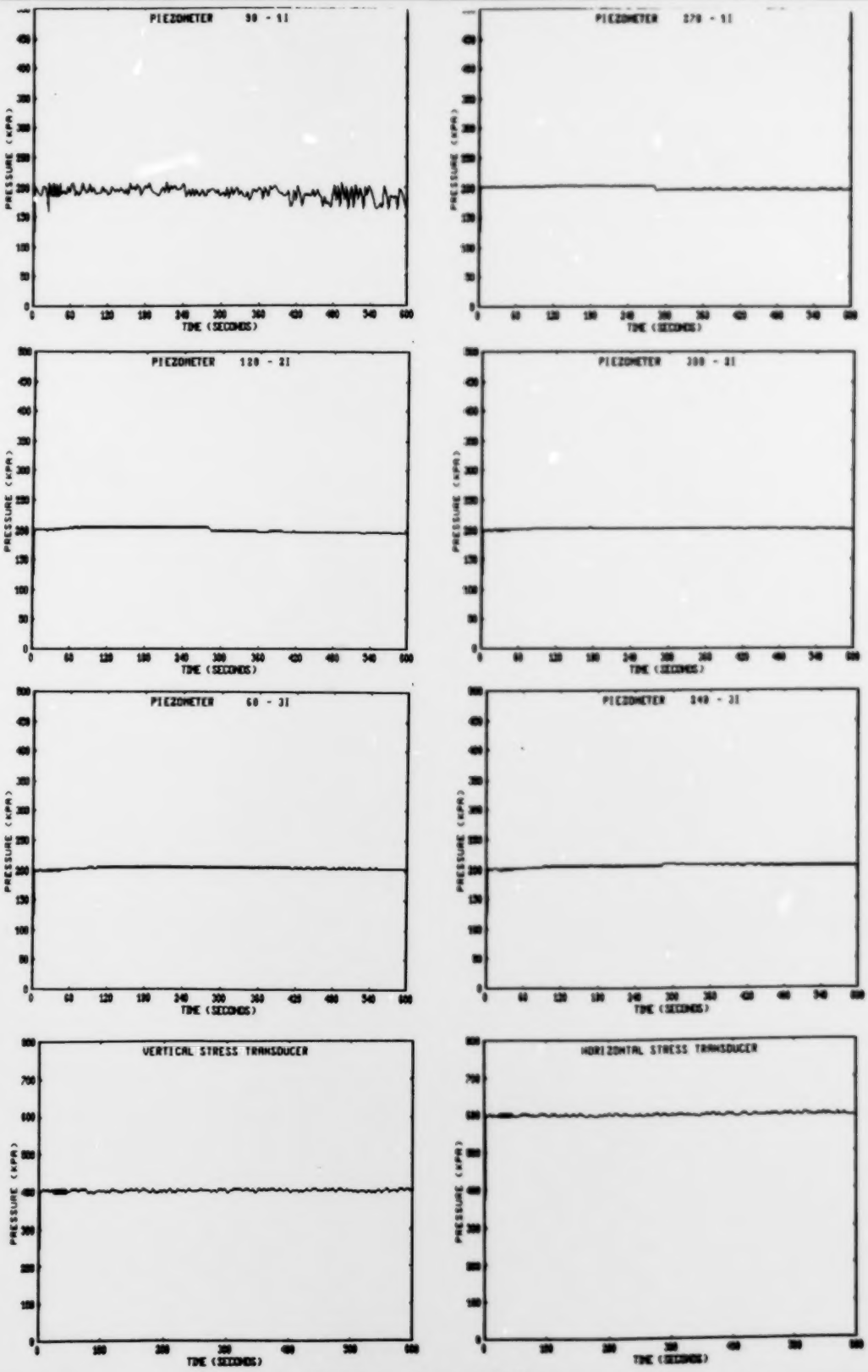

PROJECT No. 902-2013 DRAWN RR REVIEWED _____ DATE APR 91

INJECTION PRESSURE CURVES - TEST 7

Figure 4.30

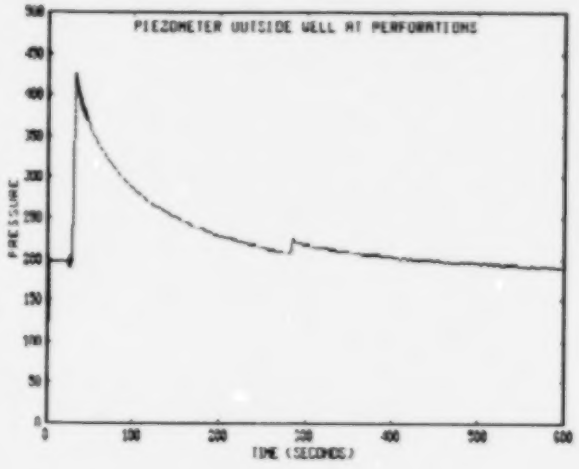

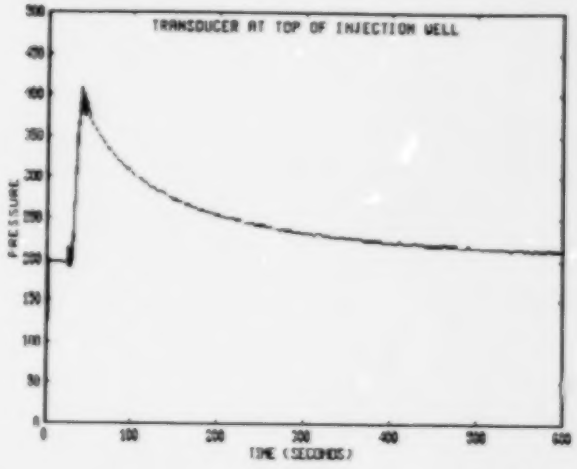

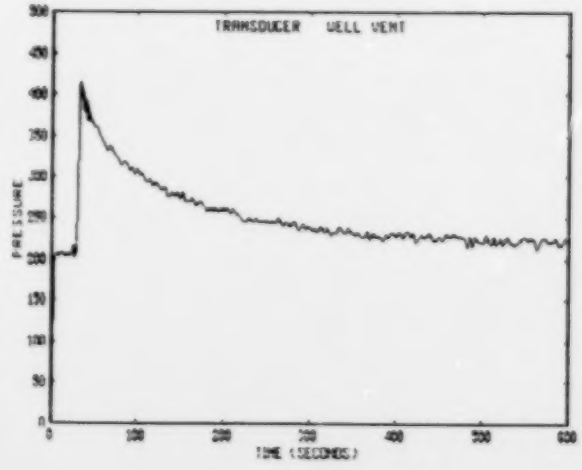

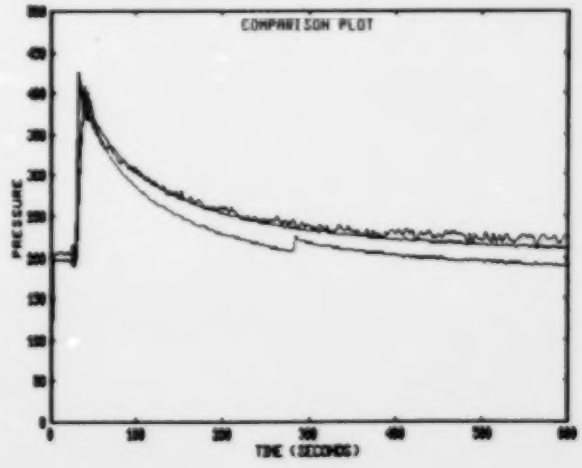

PROJECT No. 902-2013 DRAWN RR REVIEWED _____ DATE APR 91

PROJECT No. 902-2013 DRAWN RR REVIEWED _____ DATE APR 91

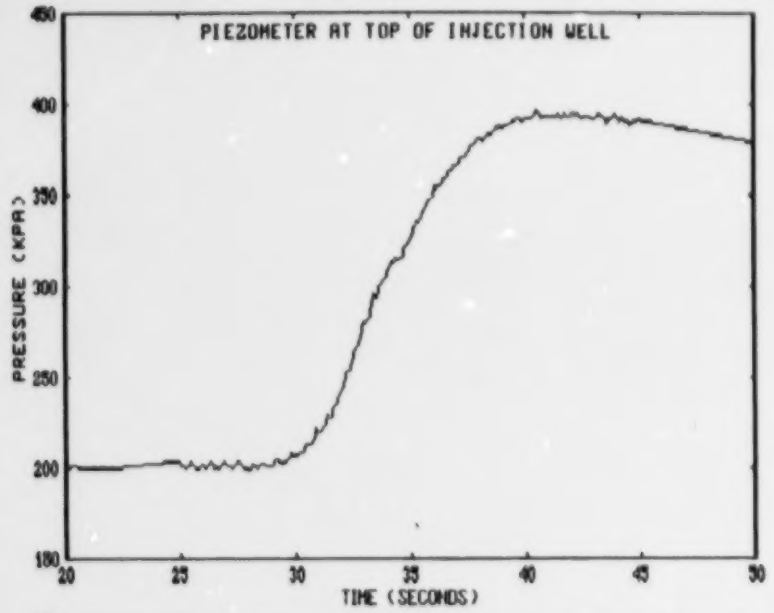

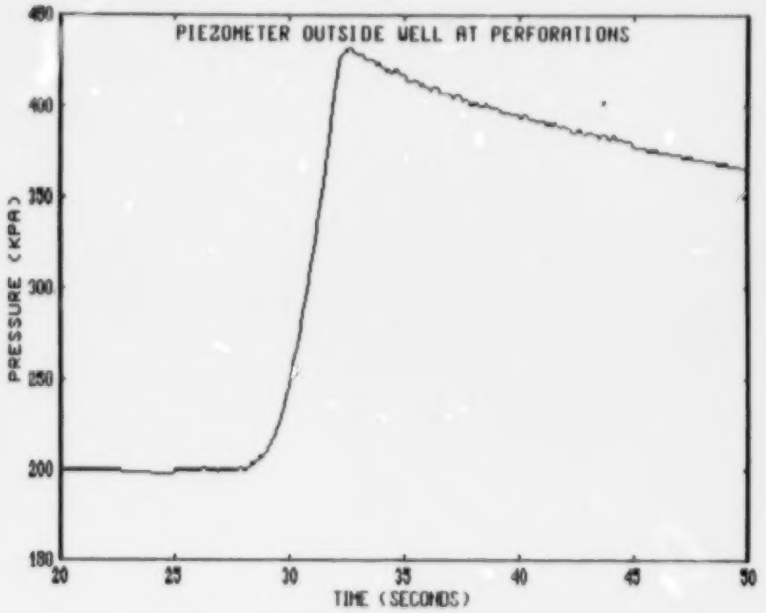

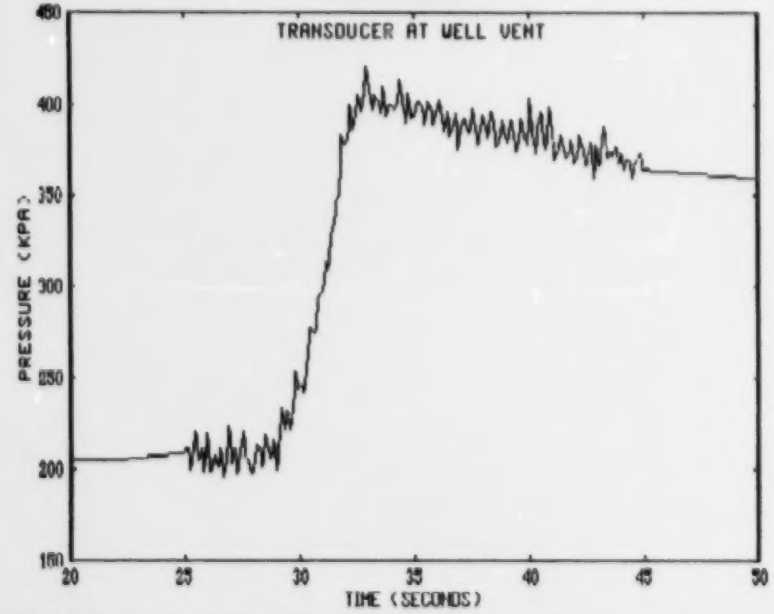

Golder Associates

INJECTION PRESSURE - TIME CURVES - TEST 7

Figure 4.31

DRAINED LOADING AND INJECTION TEST - TEST 8

Figure 4.32

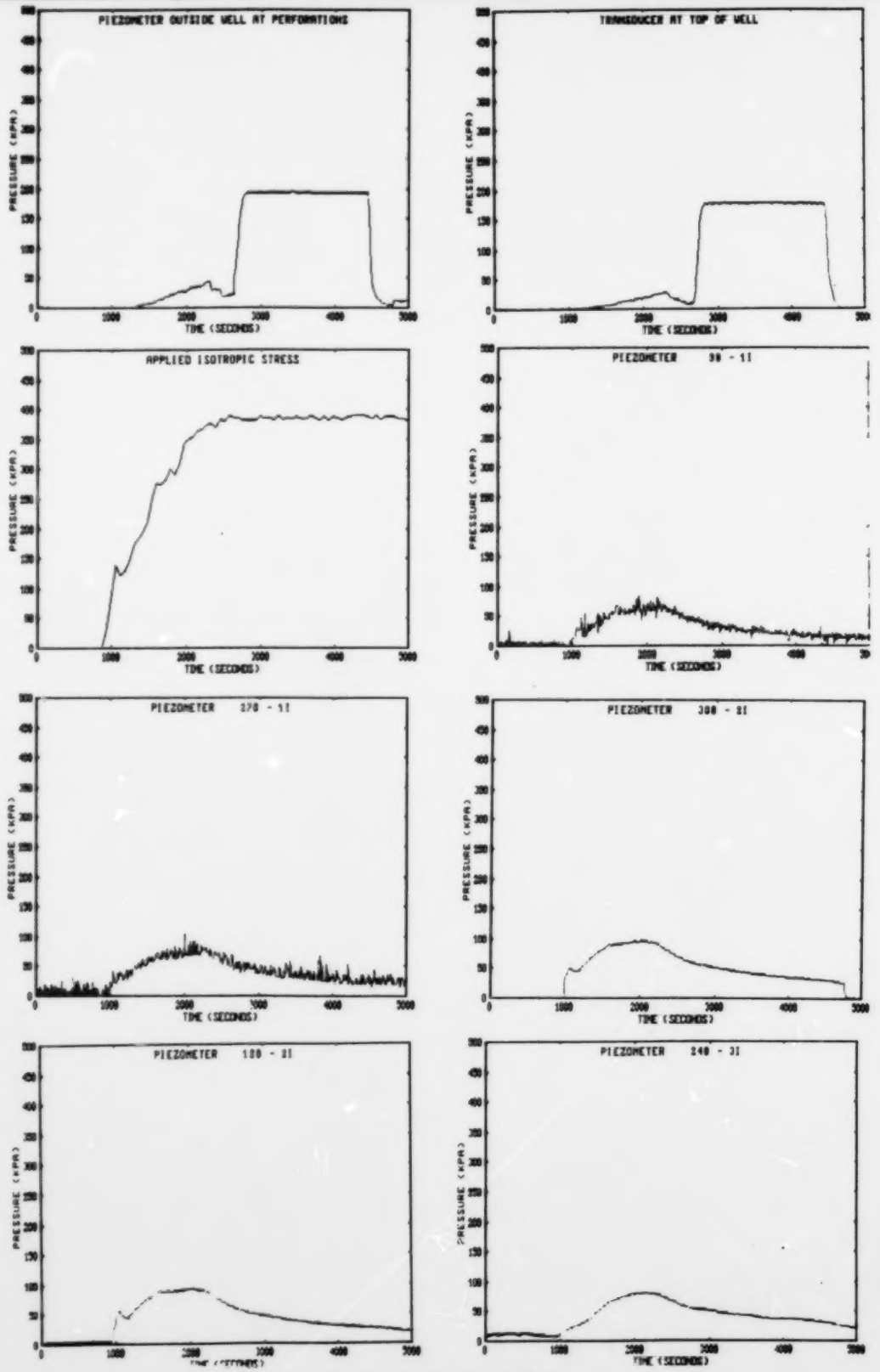

PROJECT No. 902-2013 DRAWN RR REVIEWED ____ DATE APR 91

LOCATION OF FLUORECENT DYE AFTER INJECTION - TEST 8

Figure 4.33

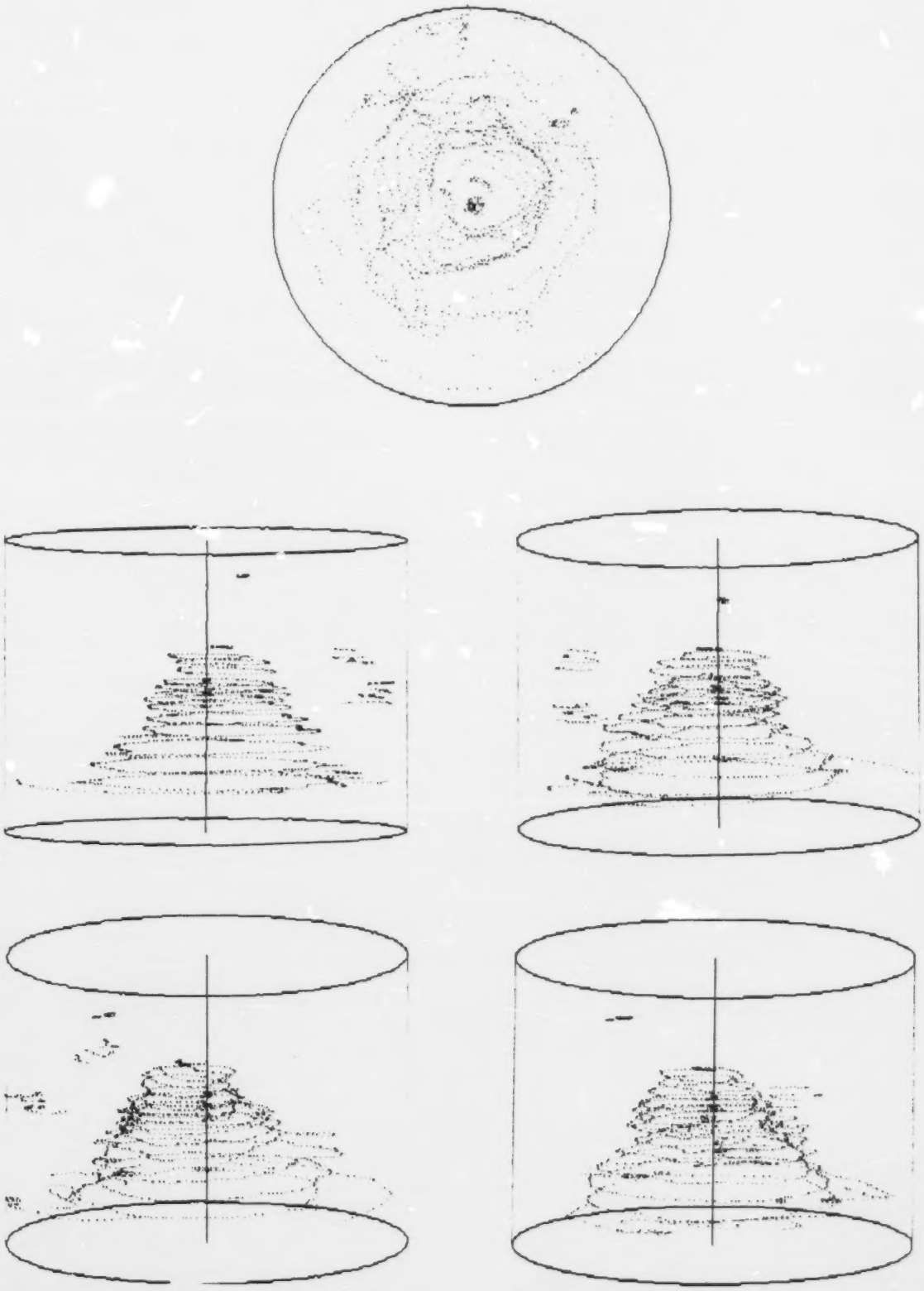

PROJECT No. 902-2013 DRAWN RR REVIEWED _____ DATE APR 91

Golder Associates

RESPONSE OF LVDT EXTENSOMETERS AND FLUID INJECTION RECORD - TEST 8

Figure 4.34

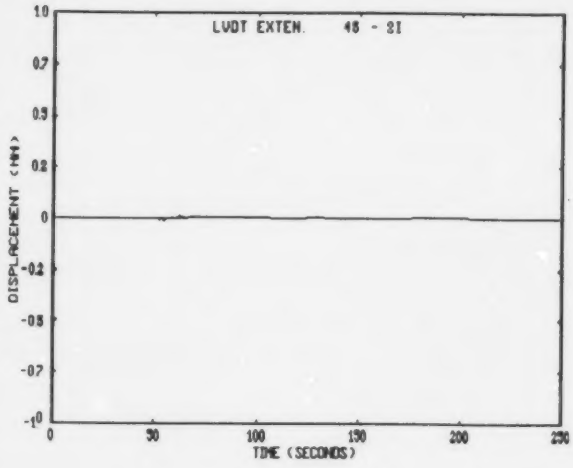

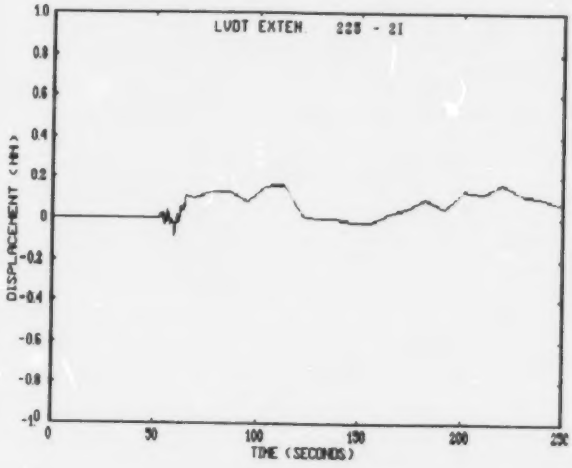

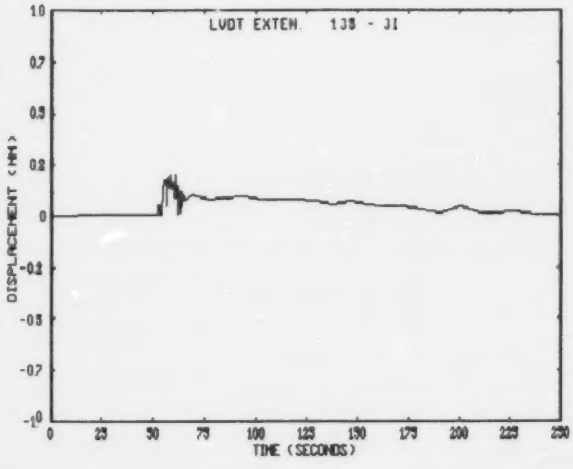

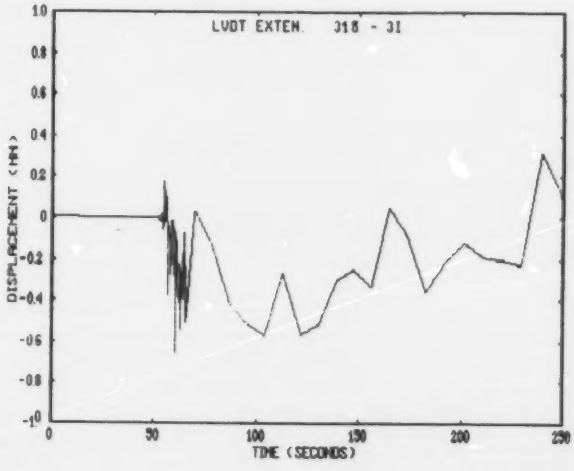

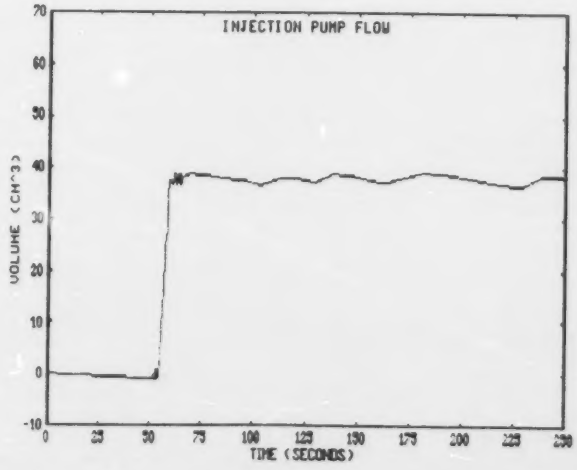

PROJECT No. 902-2013 DRAWN RR REVIEWED ____ DATE APR 91

RESPONSE OF PIEZOMETERS - TEST 8

Figure 4.35

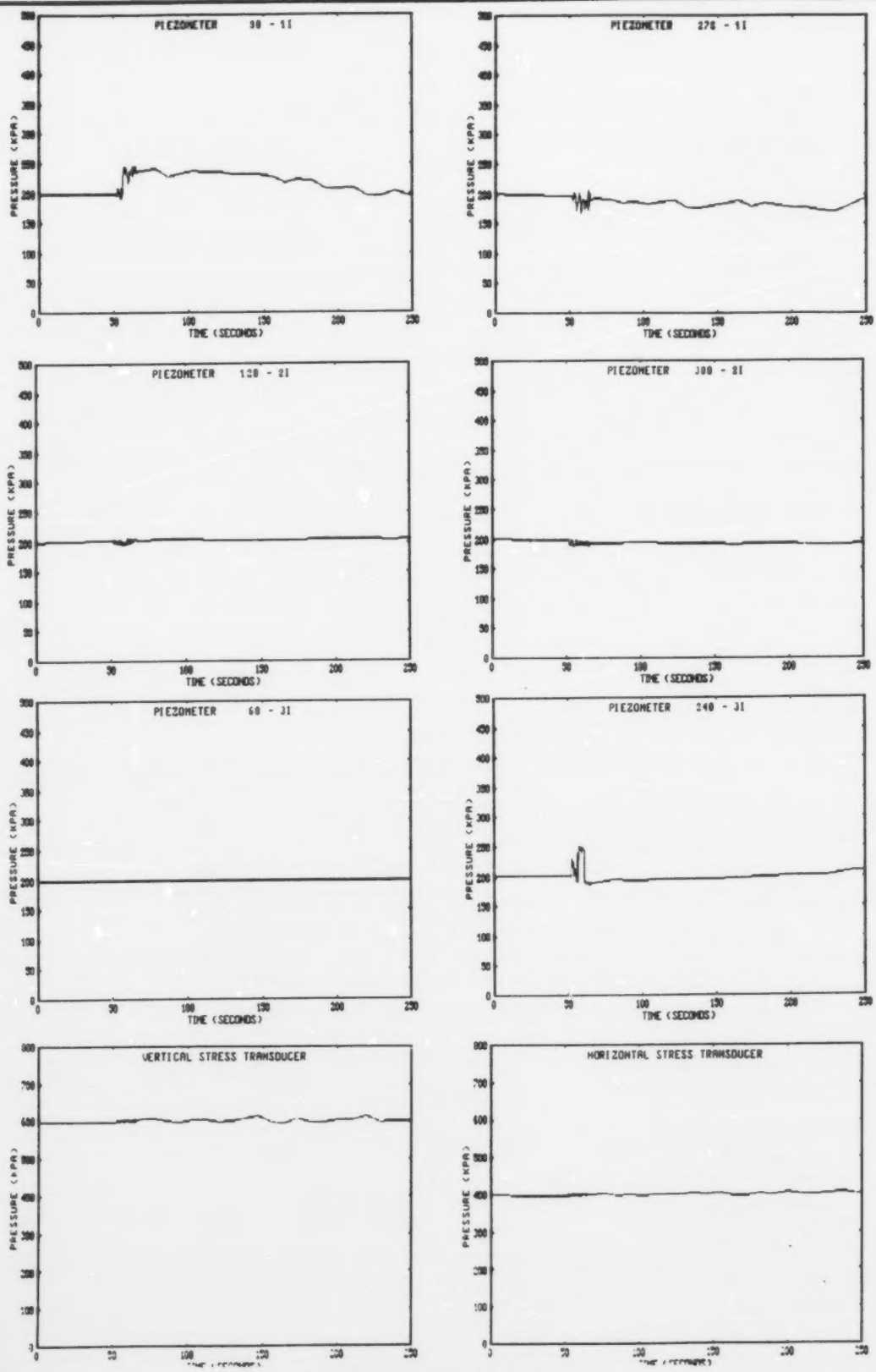

PROJECT No. 902-2013 DRAWN RR REVIEWED ____ DATE APR 91

INJECTION PRESSURE CURVES - TEST 8

Figure 4.36

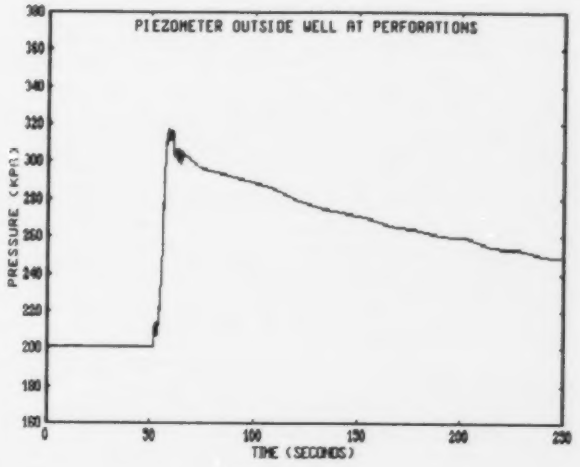

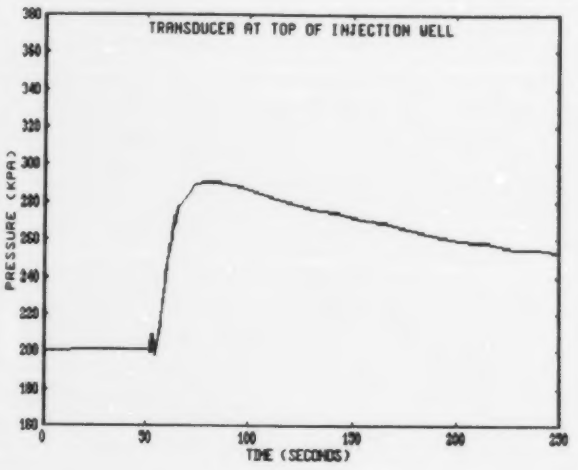

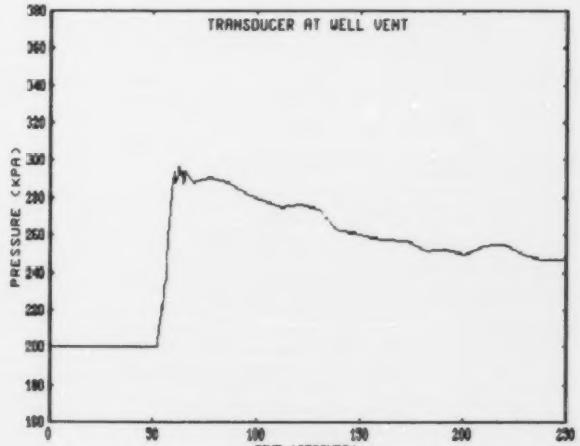

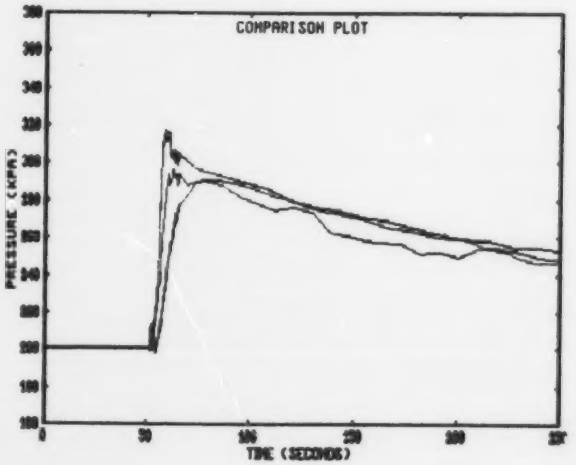

PROJECT No. 902-2013 DRAWN RR REVIEWED _____ DATE APR 91

SHEAR STRENGTH OF SAMPLES TAKEN FROM LARGE SCALE FRACTURE TESTS

Figure 5.1

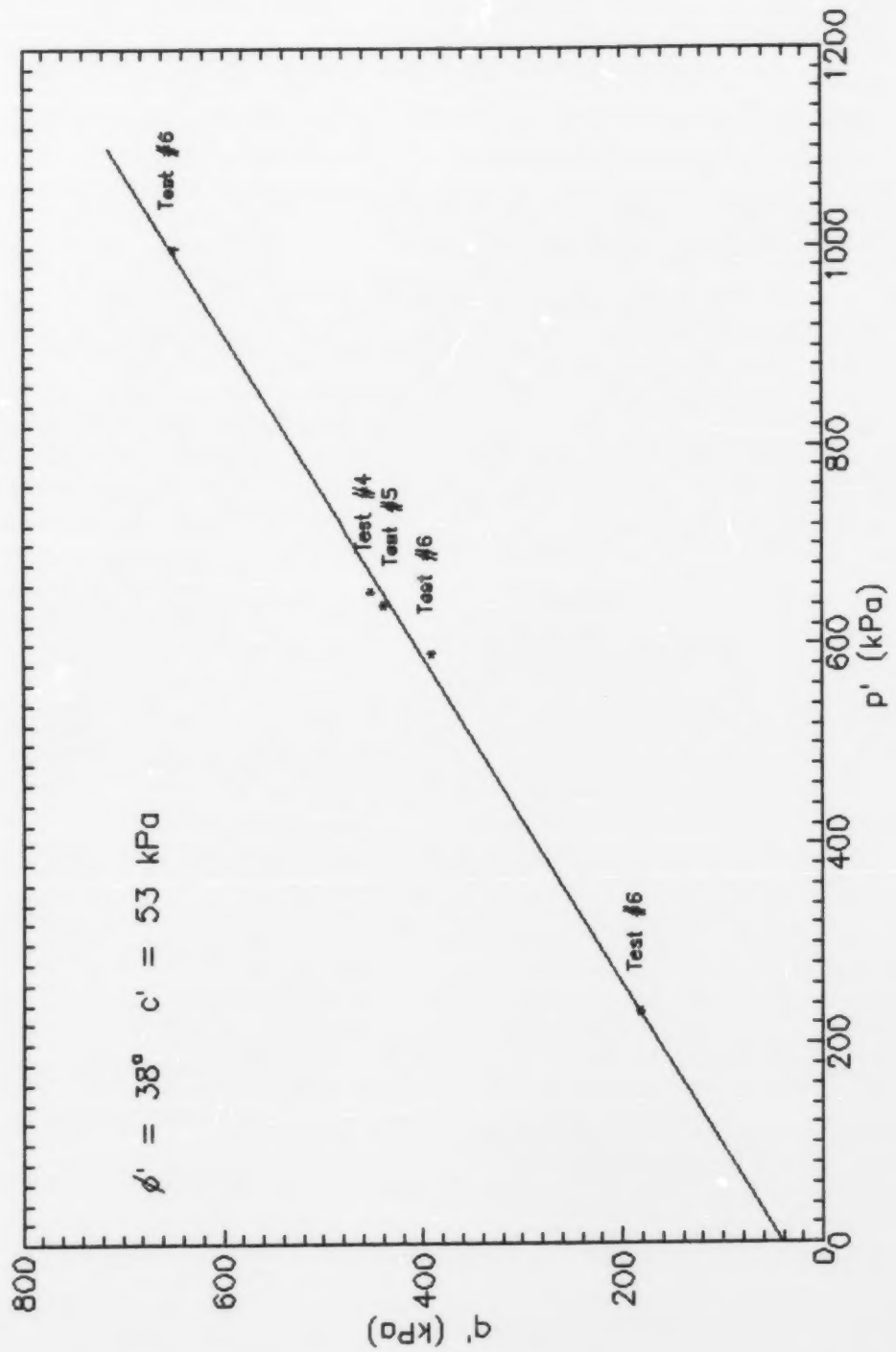

PROJECT No. 902-2013 DRAWN RR REVIEWED _____ DATE APR 91

BULK DENSITY OF SAMPLES TAKEN FROM LARGE SCALE FRACTURE TESTS

Figure 5.2

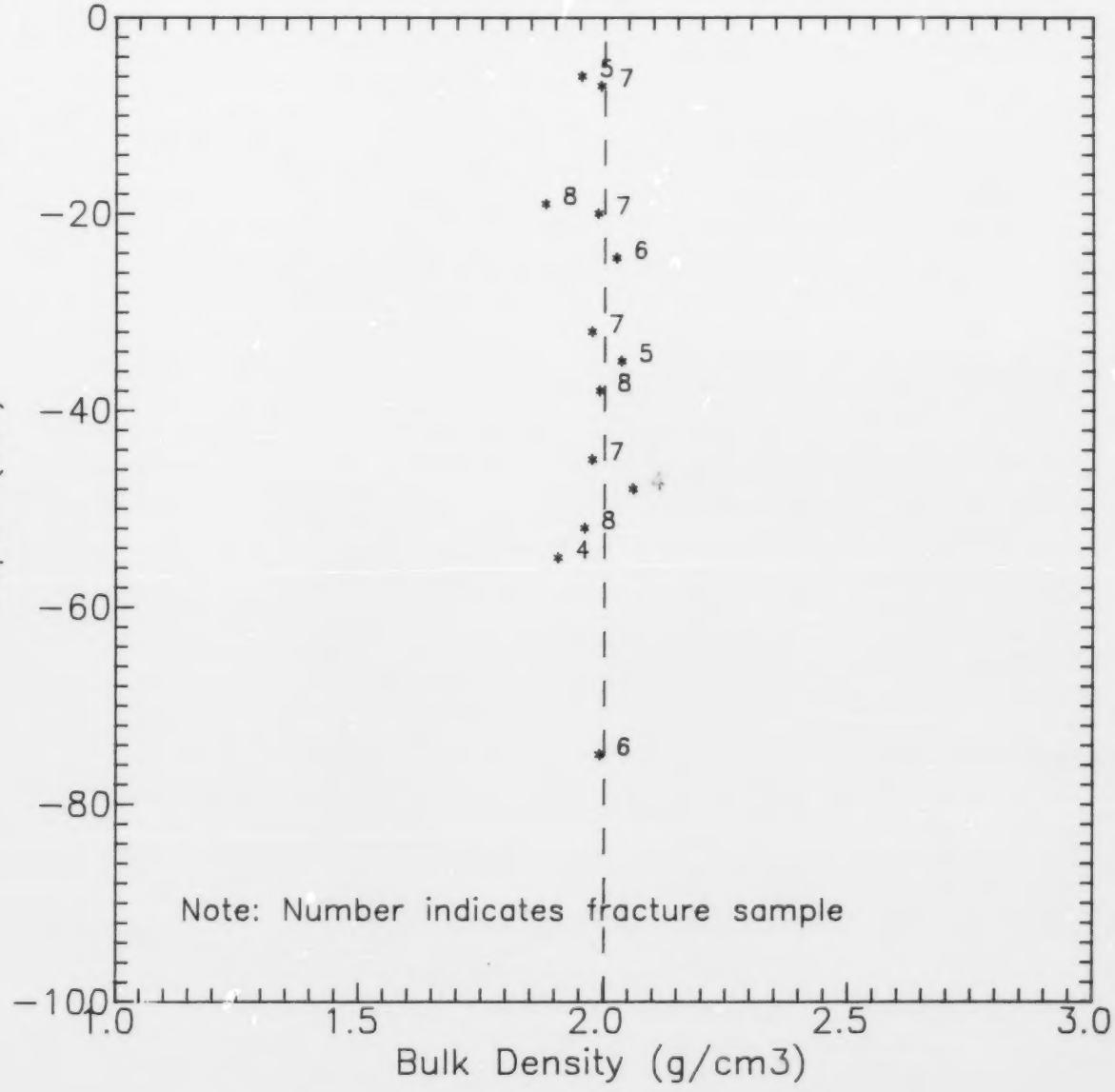

PROJECT No. 902-2013 DRAWN _____ REVIEWED _____ DATE JUL 91

Golder Associates

POROSITY OF SAMPLES TAKEN FROM LARGE SCALE FRACTURE TESTS

Figure 5.3

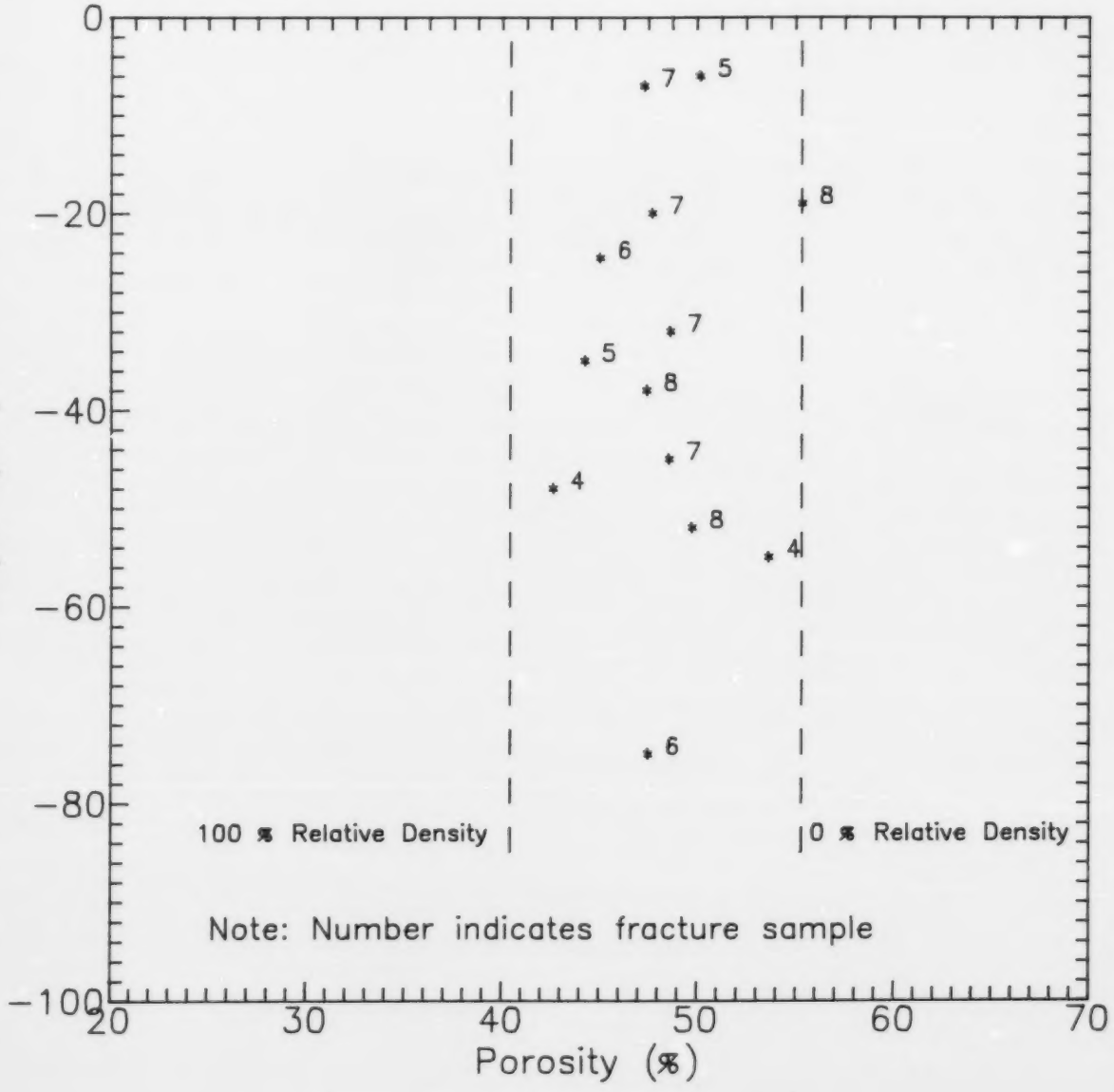

PROJECT No. 912-2013 DRAWN ____ REVIEWED ____ DATE JUL 91

Golder Associates

SUMMARY OF LARGE SCALE FRACTURE TESTS | **Figure 6.1**

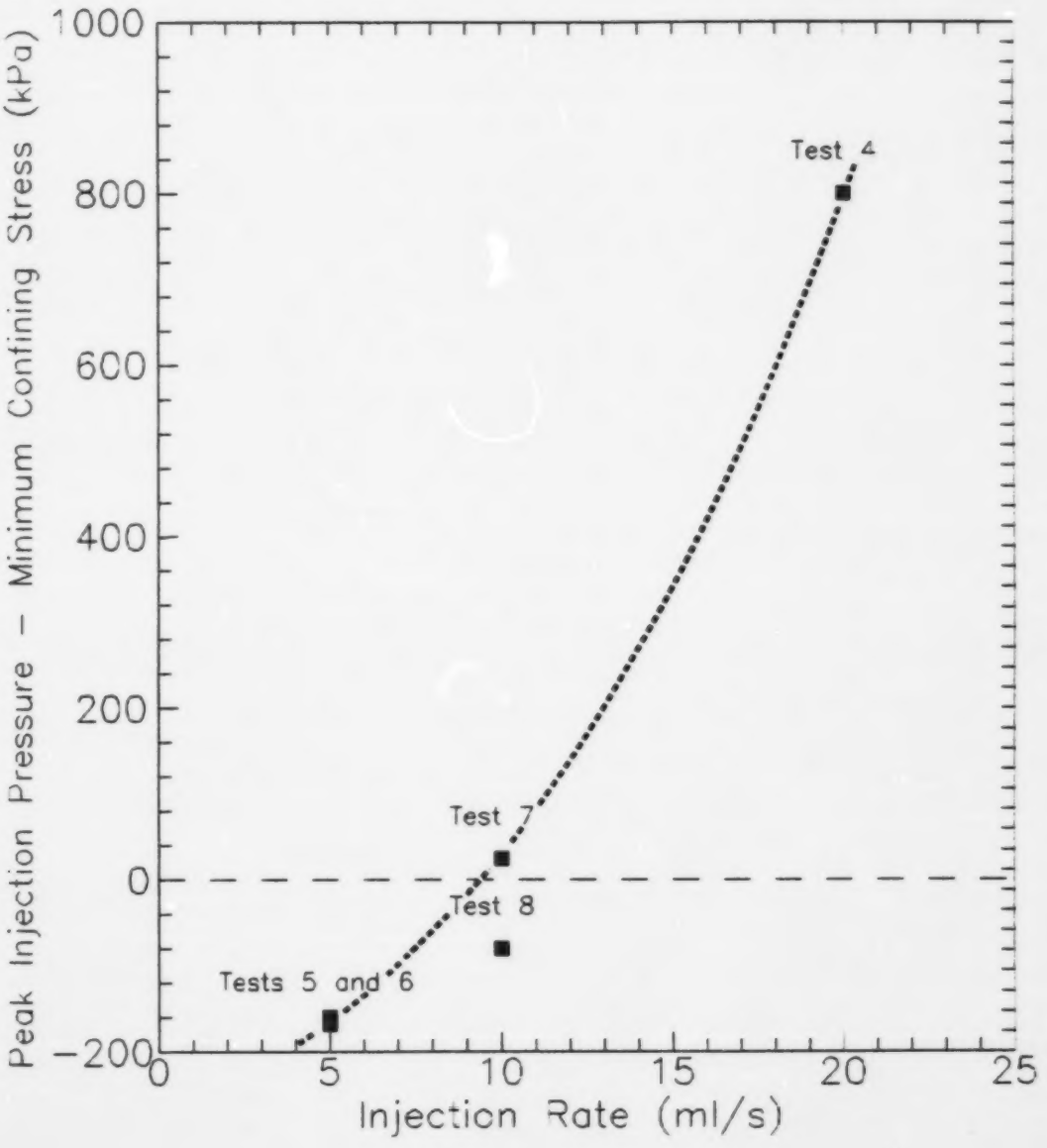

PROJECT No. 902-2013 DRAWN RR REVIEWED ____ DATE APR 91

SUMMARY OF INJECTION PRESSURE - TIME CURVES | **Figure 6.2**

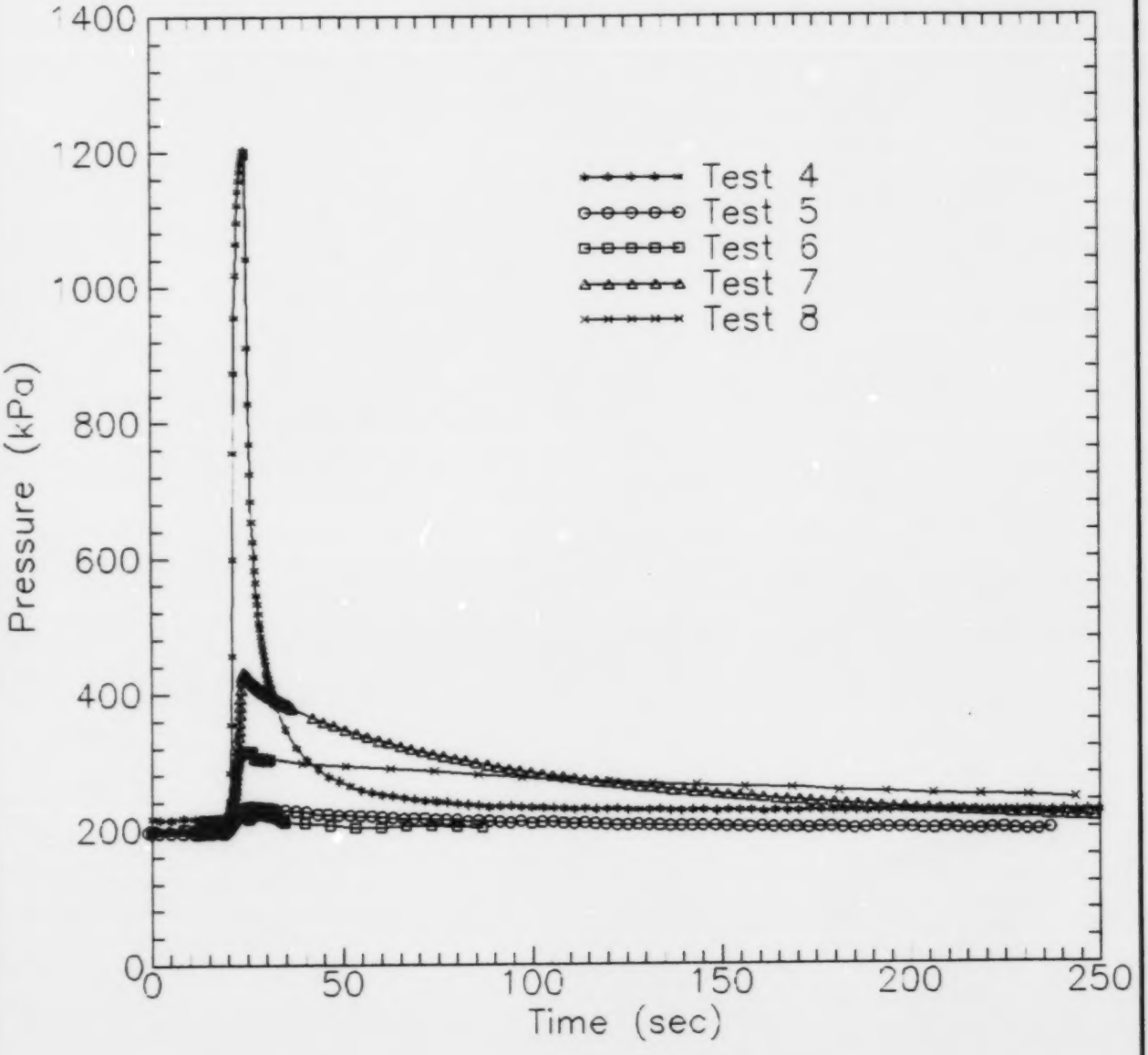

PROJECT No. 902-2013 DRAWN ____ REVIEWED ____ DATE JUL 91

Golder Associates

NOTES ON SCALING CONSIDERATIONS FOR RADIAL FRACTURES IN OIL SANDS

T.J. Boone, Esso Resources Canada Ltd., January 1990

1. CALCULATION OF THE RATE OF FRACTURE PROPAGATION FOR A CONSTANT INJECTION RATE

First, let us assume that (i) the volume of fluid stored in the fracture is small relative to the volume of fluid that has leaked-off into the formation, (ii) that the leak-off from the fracture can be represented by a standard 1D leak-off model, and (iii) that the fluid in the sands and injected into the fracture have the same Newtonian behaviour. Based on these assumptions Carter's approximation can be used to calculate the rate of fracture propagation [Howard and Fast, Gertsma and DeKlerk]. Their developments can be readily generalized to poroelastic materials [Rice and Cleary] as described subsequently.

If a unit pressure change is applied instantaneously to a fracture face, the flow rate normal to the fracture at the face, q_n, is given by:

$$q_n = \frac{\kappa \Delta P}{(\pi c t)^{1/2}} \tag{1}$$

where κ is the mobility ($\kappa = k/\mu$, where k is permeability (Darcies) and μ is the fluid viscosity), c is the diffusivity coefficient, t is time and ΔP is the pore pressure change at the wall which is assumed to occur at t=0. The poroelastic definition of the diffusivity coefficient is:

$$c = \frac{2GB^2\kappa\,(1-\nu)\,(1+\nu_u)^2}{9\,(\nu_u-\nu)\,(1-\nu_u)} \tag{2}$$

where G is the shear modulus, ν is the drained Poisson's ratio, ν_u is the undrained Poisson's ratio and B is Skempton's B coefficient. If it can be assumed that B = 1 and $\nu_u = 0.5$, Equation (2) reduces to:

$$c = \frac{2\kappa G(1-\nu)}{(1-2\nu)} \tag{3}$$

The constant rate of injection into the fracture, Q, is assumed to equal the rate of leak-off from the fracture so that:

$$Q = \int_0^A q_n \, dA \tag{4}$$

where both A and q_n are functions of time. Let τ be the time at which the fracture radius first reaches a given extent, R, so that $(t-\tau)$ represents the length of time that the surface at r=R has been exposed to the fluid. Equation 4 can then be written as:

$$Q = \frac{\kappa \Delta P}{(\pi c)^{1/2}} \int_0^t \frac{dA}{d\tau} \frac{d\tau}{(t-\tau)^{1/2}} \tag{5}$$

Performing the integration in (5) gives:

$$A = \frac{(\pi c)^{1/2}}{\kappa \Delta P} \frac{Q\, t^{1/2}}{\pi} \tag{6}$$

and substituting $2\pi r^2$ for A results in the variation of r with time (Gertsma and DeKlerk, Eq. 24):

$$r = \left\{ \frac{Q}{\pi^2 \kappa \Delta P} \right\}^{1/2} (\pi c t)^{1/4} \tag{7}$$

This approximation should be reasonably accurate for $ct/r^2 < 0.1$ and may be suitable for approximate scaling purposes for larger values of ct/r^2.

2. PRESSURE DROP ALONG THE FRACTURE.

In general for leak-off dominated fractures it is expected that the pressure drop along the fracture should be small. Generally, it is assumed that the pressure at the crack front is equal to the stress acting normal to the fracture, S_n. Gertsma and DeKlerk provide a formula for estimating the pressure at the well, p_w:

$$p_w = S_n - \frac{5}{4\pi} \frac{G w_w}{r} \ln\left\{ \frac{r_w}{r} \right\} \tag{8}$$

where r_w is the radius of the wellbore and w_w is the fracture width at the wellbore.

$$w_w = 2 \left\{ \frac{\mu Q r}{G} \right\}^{1/4} \tag{9}$$

3. DEVELOPMENT OF CONFINING STRESSES DUE TO FLUID LEAK-OFF.

Diffusion of pore pressure from the fracture causes volumetric expansion in the vicinity of the fracture and increases in the confining stress acting normal to the fracture. This effect can also be manifested as an increase in the injection pressure. For the elastic case, the maximum value of the fracture pressure increase, ΔP_c, can be found to be:

$$\Delta P_{c,max} = \frac{S_n - \eta P_o}{1-\eta} - S_n \qquad (10)$$

where P_o is the initial pore pressure and η is a poroelastic coefficient which is defined as follows:

$$\eta = \frac{3(\nu_u - \nu)}{2B(1-\nu)(1+\nu_u)} = \frac{\alpha(1-2\nu)}{2(1-\nu)} \quad , \quad \alpha = 1 - \frac{K}{K_s} \qquad (11)$$

where K and K_s are the bulk moduli of the soil skeleton and grains, respectively. Typically η varies from 0.3 to 0.4 for rock and sand.

Detournay *et al.* provide results for the case of a stationary, 2D Griffith crack which can be used to estimate the development of the confining stress. A significant fraction of this stress change will have developed by the time $t = 0.1\ ct/r^2$. For the 3D case and for cases where there is shear dilation the development of these stresses should occur more rapidly.

REFERENCES

Howard, G.C. and Fast, C.R.: "Optimum Fluid Characteristics for Fracture Extension," *Drill. and Prod. Prac.*, API (1957) 261.

Geertsma, J. and DeKlerk, F.: "A Rapid Method of Predicting Width and Extent of Hydraulically Induced Fractures," *JPT* (Dec. 1969) **21**, No. 12, 1571-1581.

Rice, J.R. and Cleary, M.P.: "Some Basic Stress Diffusion Solutions for Fluid-saturated Elastic Porous Media with Compressible Constituents," *Rev. Geophys. and Space Phys.* (1976) **14**, 227-241.

Detournay, E., Cheng, A., Roegiers, J.-C., and McClennan, J.: "Poroelastic Considerations in In-Situ Stress Determination by Hydraulic Fracturing," *Proc* , Second International Workshop on Hydraulic Fracturing Stress Measurements, Vol. 1, B.C. Haimson, J.-C. Roegiers, and M.D. Zoback (eds.), Minneapolis, MN (1988) 410-424.

GOLDER ASSOCIATES Drawn: GCR Checked: _____ Date: 22 MAR 91

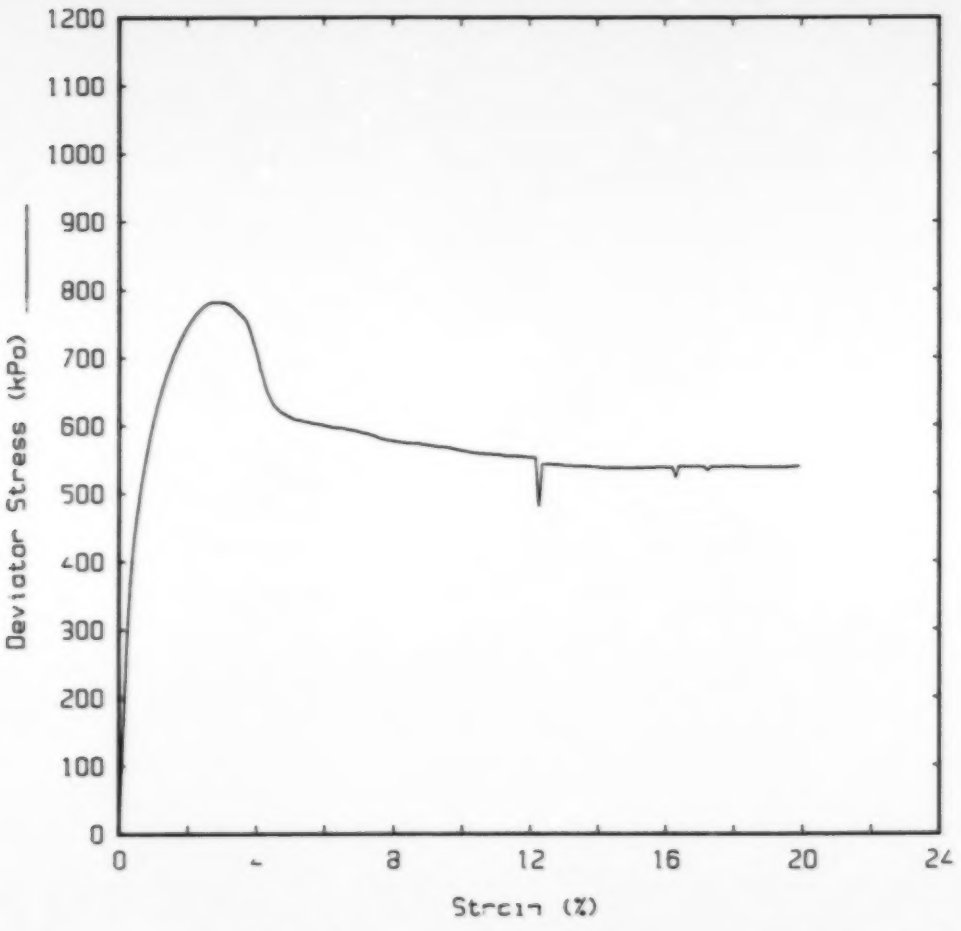

Isotropically Consolidated Drained Triaxial Test

Project Number : 902-2013	
Computer File : CID-6-3-22	
Test Description: STRAIN CONTROLLED DRAINED TEST	
Date of Test : 22 MAR 91	
Effective Consolidation Stress	= 200 kPa
Initial Back Pressure	= 1000 kPa
Pre Consolidation Void Ratio	= .449
Post Consolidation Void Ratio	= .434
Initial State Parameter	= -.486
Ø' max	= -1.4°
Strain Rate	= 8.8 %/hr.

COLDER ASSOCIATES Drawn: GCR Checked: _____ Date: 22 MAR 91

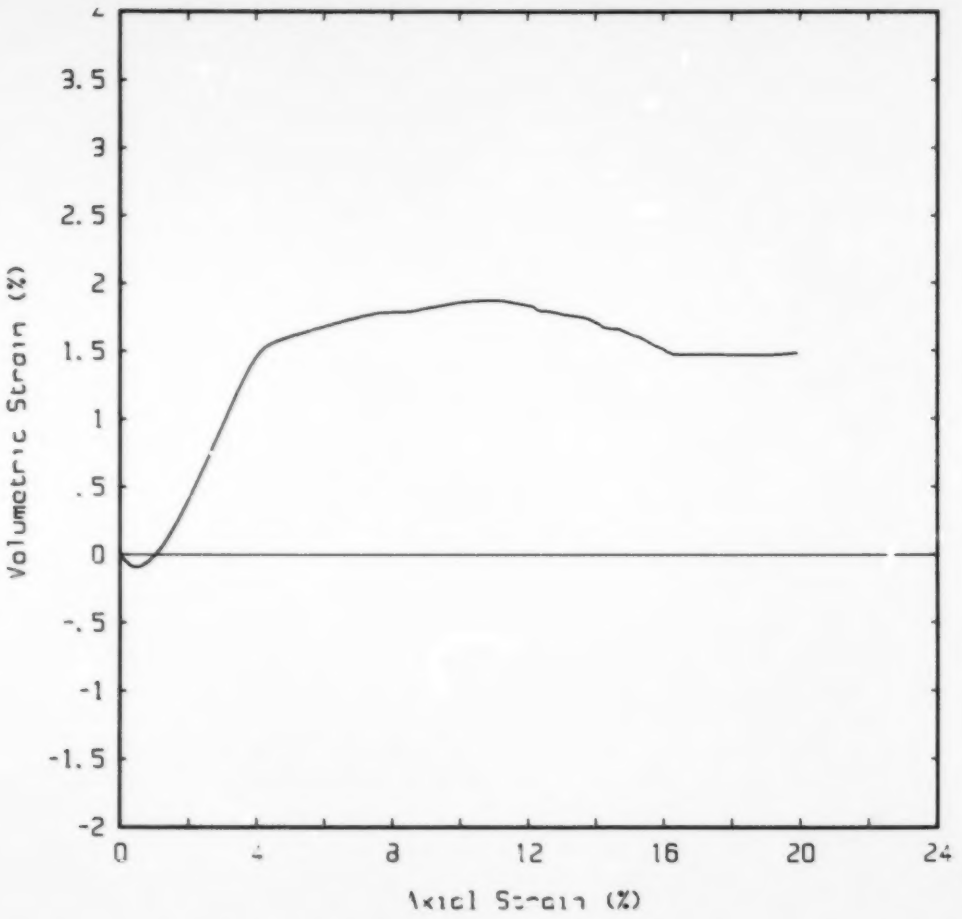

Isotropically Consolidated Drained Triaxial Test

Project Number	: 902-2013
Computer File	: CID-6-3-22
Test Description	: STRAIN CONTROLLED DRAINED TEST
Date of Test	: 22 MAR 91

Effective Consolidation Stress	= 200 kPa
Initial Back Pressure	= 1000 kPa
Pre Consolidation Void Ratio	= .449
Post Consolidation Void Ratio	= .434
Initial State Parameter	= -.486
ϕ'_{max}	= 41.4°
Strain Rate	= 8.8 %/hr.

GOLDER ASSOCIATES Drawn: GCR Checked: _____ Date: 25 MAR 91

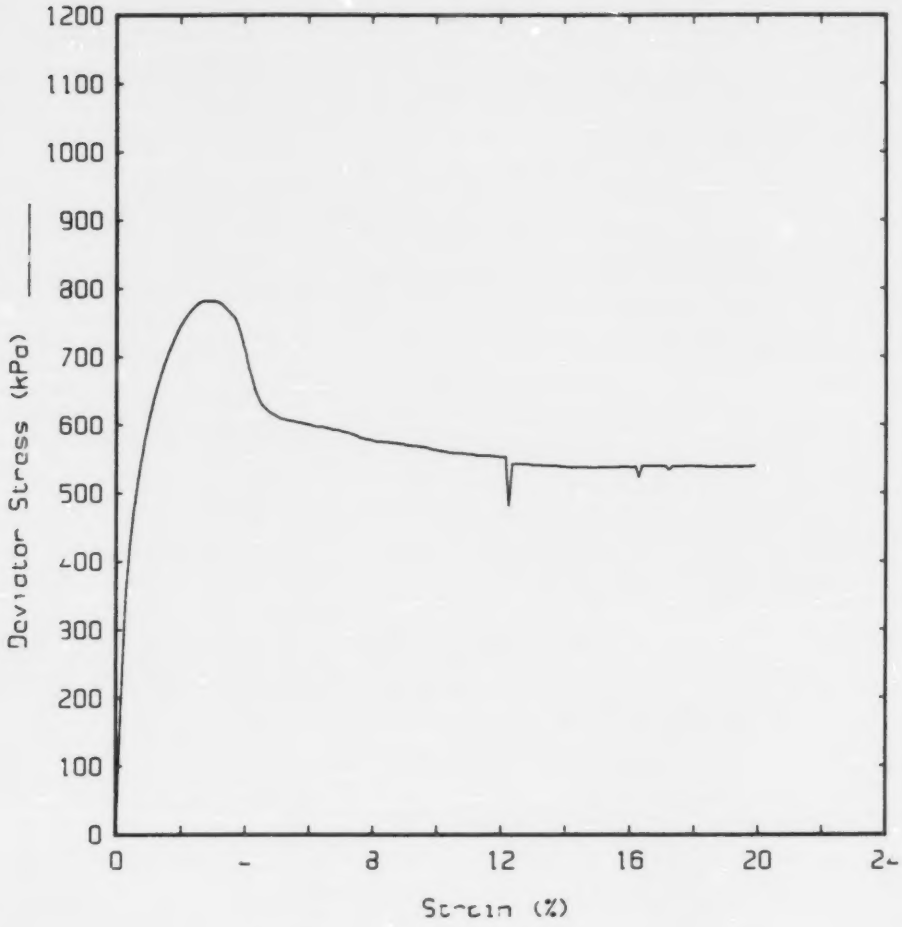

Isotropically Consolidated Drained Triaxial Test

Project Number : 902-2013	
Computer File : CID-6-3-22	
Test Description: STRAIN CONTROLLED DRAINED TEST	
Date of Test : 22 MAR 91	
Effective Consolidation Stress	= 200 kPa
Initial Back Pressure	= 1000 kPa
Pre Consolidation Void Ratio	= 1.261
Post Consolidation Void Ratio	= 1.238
Initial State Parameter	= .317
Ø max	= 41.9
Strain Rate	= 8.8 %/hr.

GOLDER ASSOCIATES Drawn: GCR Checked: _____ Date: 25 MAR 91

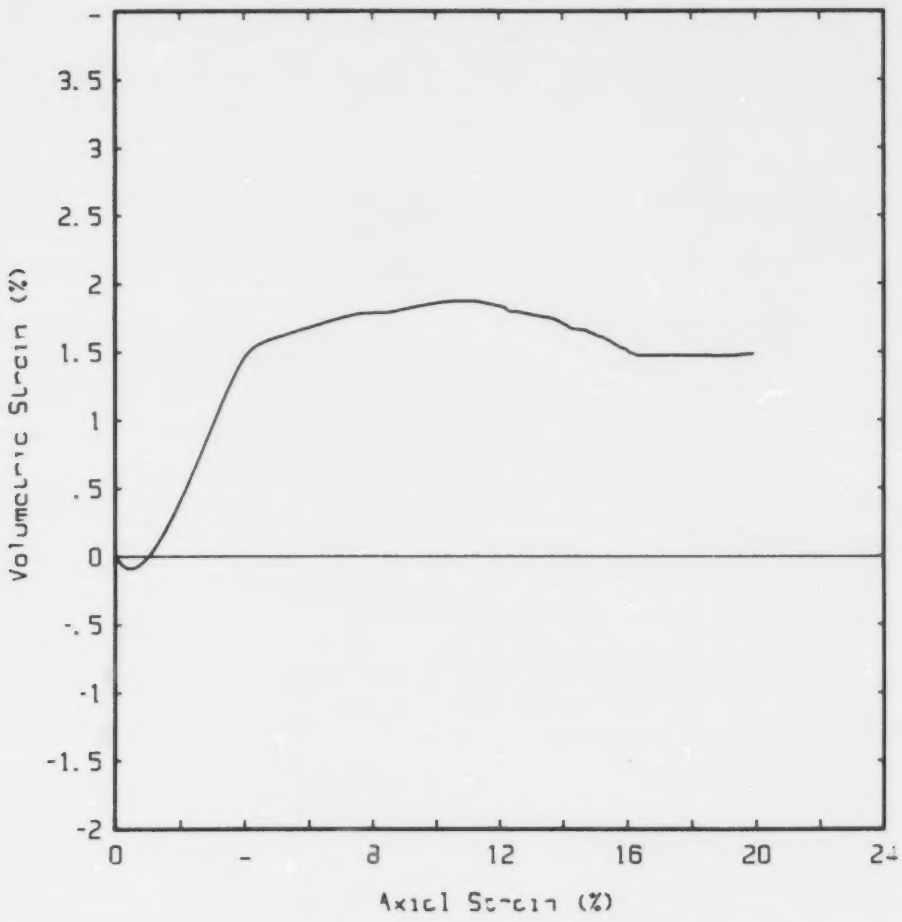

Isotropically Consolidated Drained Triaxial Test

Project Number	: 902-2013
Computer File	: CID-6-3-22
Test Description	: STRAIN CONTROLLED DRAINED TEST
Date of Test	: 22 MAR 91

Effective Consolidation Stress	= 200 kPa
Initial Back Pressure	= 1000 kPa
Pre Consolidation Void Ratio	= 1.261
Post Consolidation Void Ratio	= 1.238
Initial State Parameter	= .317
δ_{max}	= -1° -
Strain Rate	= 0.8 %/hr.

GOLDER ASSOCIATES Drawn: GCR Checked: _____ Date: 22 MAR 91

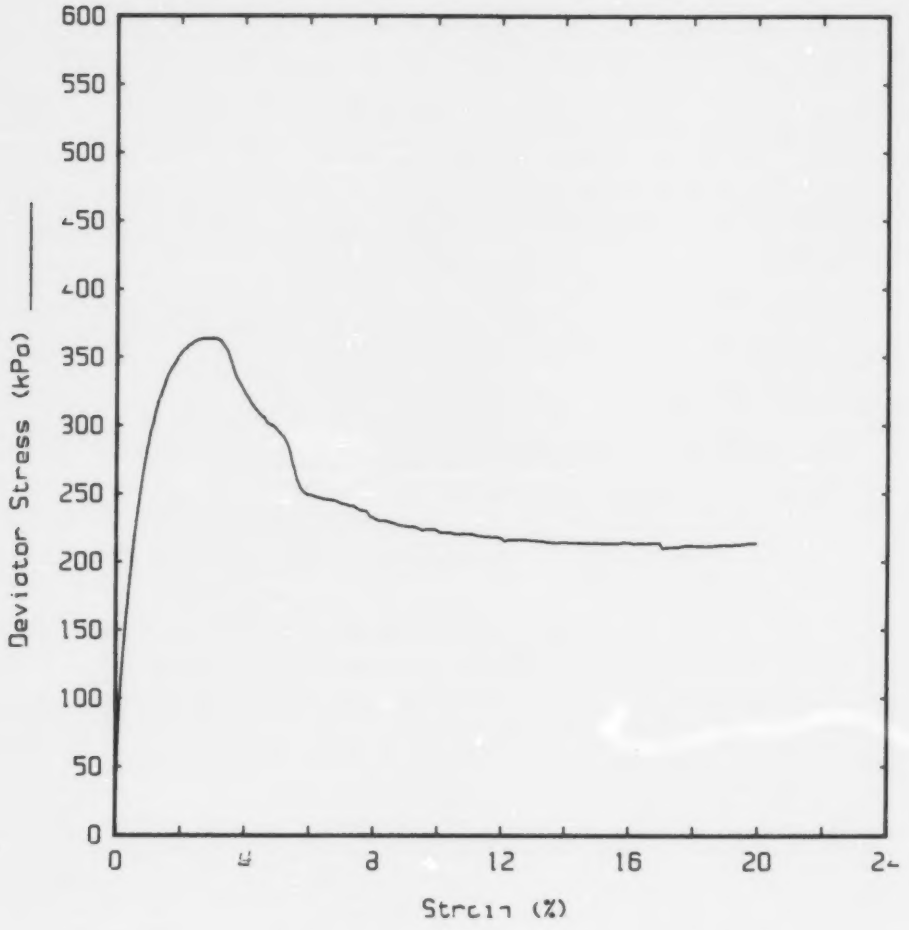

Isotropically Consolidated Drained Triaxial Test

Project Number : 902-2013	
Computer File : CID-6-1-42	
Test Description: STRAIN CONTROLLED DRAINED TEST	
Date of Test : 21 MAR 91	
Effective Consolidation Stress	= 50 kPa
Initial Back Pressure	= 1150 kPa
Pre Consolidation Void Ratio	= 1.059
Post Consolidation Void Ratio	= 1.014
Initial State Parameter	= .070
ϕ'_{max}	= 51°.7
Strain Rate	= 9.7 %/hr.

GOLDER ASSOCIATES Drawn: GCR Checked: _____ Date: 22 MAR 91

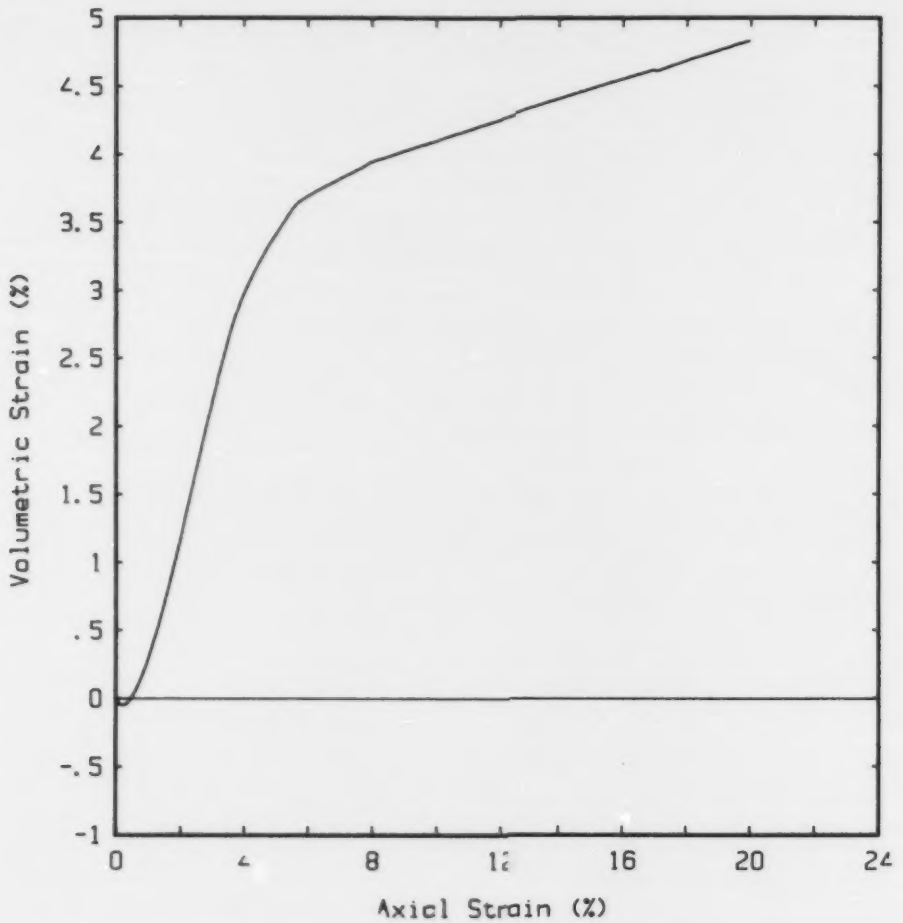

Isotropically Consolidated Drained Triaxial Test

Project Number : 902-2013	
Computer File : CID-3-1-42	
Test Description: STRAIN CONTROLLED DRAINED TEST	
Date of Test : 21 MAR 91	
Effective Consolidation Stress	= 50 kPa
Initial Back Pressure	= 1150 kPa
Pre Consolidation Void Ratio	= 1.059
Post Consolidation Void Ratio	= 1.014
Initial State Parameter	= .070
ϕ'_{max}	= 51°.7
Strain Rate	= 9.7 %/hr.

GOLDER ASSOCIATES Drawn: GCR Checked: _____ Date: 20 MAR 91

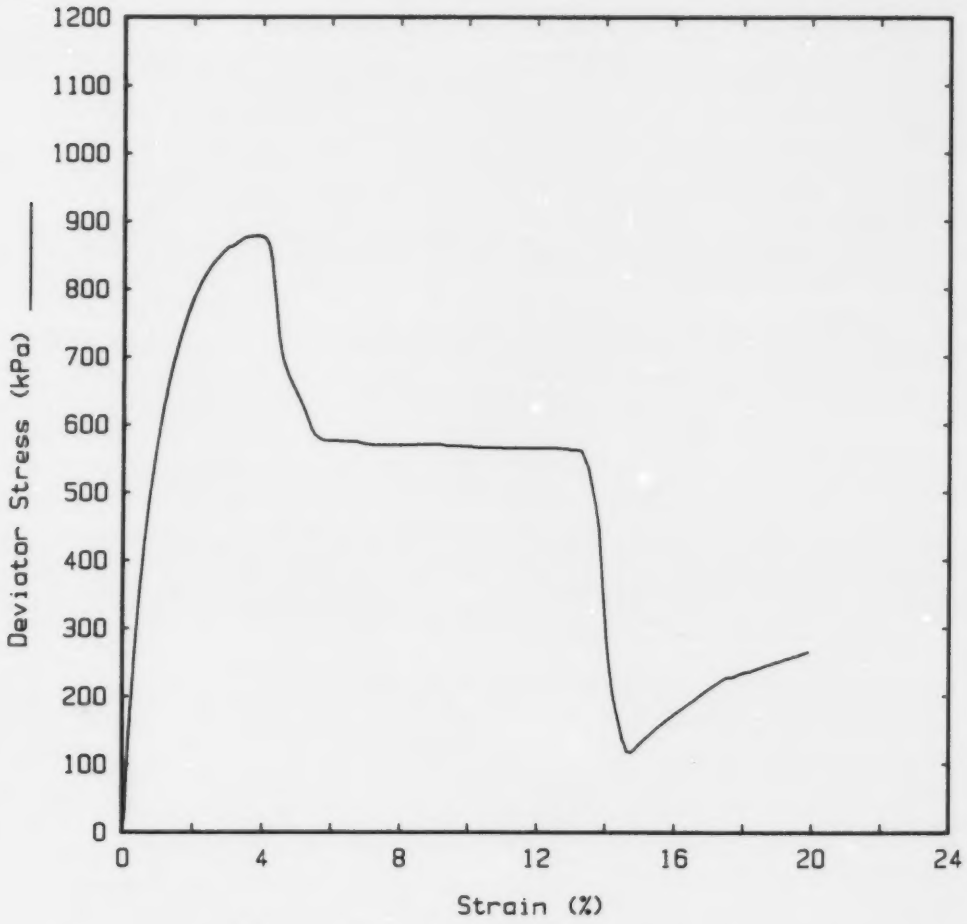

Isotropically Consolidated Drained Triaxial Test

Project Number	: 902-2013
Computer File	: CID-5-2
Test Description	: STRAIN CONTROLLED DRAINED TEST
Date of Test	: 19 MAR 91

Effective Consolidation Stress	= 200 kPa
Initial Back Pressure	= 1000 kPa
Pre Consolidation Void Ratio	= 1.088
Post Consolidation Void Ratio	= 1.075
Initial State Parameter	= .154
Ø'max	= 43.4 °
Strain Rate	= 8.7 %/hr.

GOLDER ASSOCIATES Drawn: GCR Checked: _____ Date: 20 MAR 91

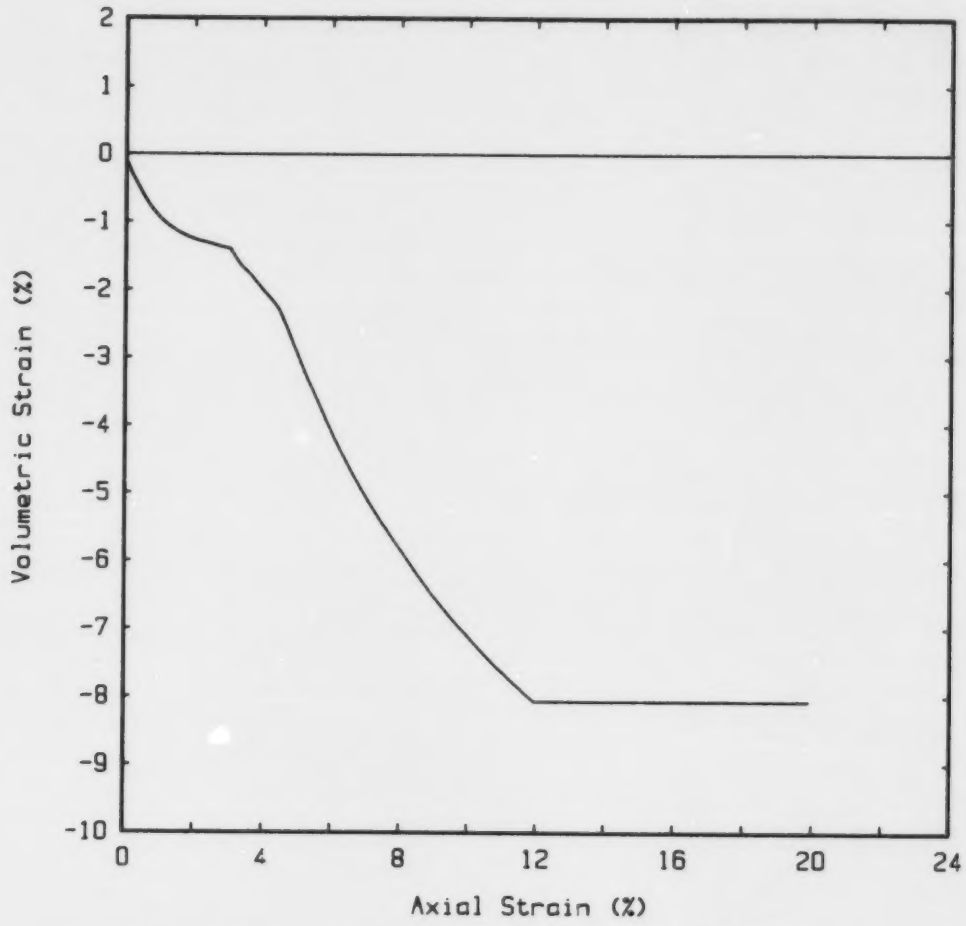

Isotropically Consolidated Drained Triaxial Test

Project Number : 902-2013	
Computer File : CID-5-2	
Test Description: STRAIN CONTROLLED DRAINED TEST	
Date of Test : 19 MAR 91	
Effective Consolidation Stress	= 200 kPa
Initial Back Pressure	= 1000 kPa
Pre Consolidation Void Ratio	= 1.088
Post Consolidation Void Ratio	= 1.075
Initial State Parameter	= .154
Ø'max	= 43.4 °
Strain Rate	= 8.7 %/hr.

GOLDER ASSOCIATES Drawn: GCR Checked: _____ Date: 19 MAR 91

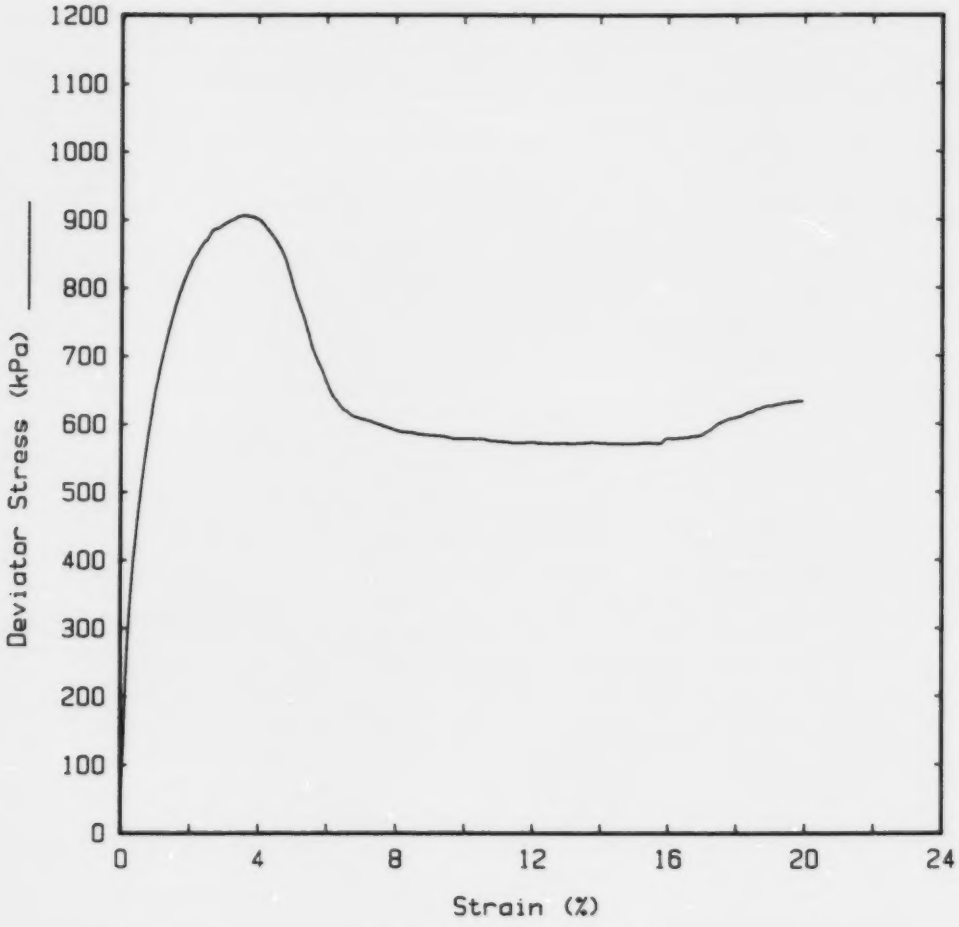

Isotropically Consolidated Drained Triaxial Test

Project Number : 902-2013	
Computer File : CID-4-2	
Test Description: STRAIN CONTROLLED DRAINED TEST	
Date of Test : 18 MAR 91	
Effective Consolidation Stress	= 200 kPa
Initial Back Pressure	= 1000 kPa
Pre Consolidation Void Ratio	= 1.121
Post Consolidation Void Ratio	= 1.099
Initial State Parameter	= .179
Ø'max	= 43.9°
Strain Rate	= 9.7 %/hr.

GOLDER ASSOCIATES Drawn: GCR Checked: _____ Date: 19 MAR 91

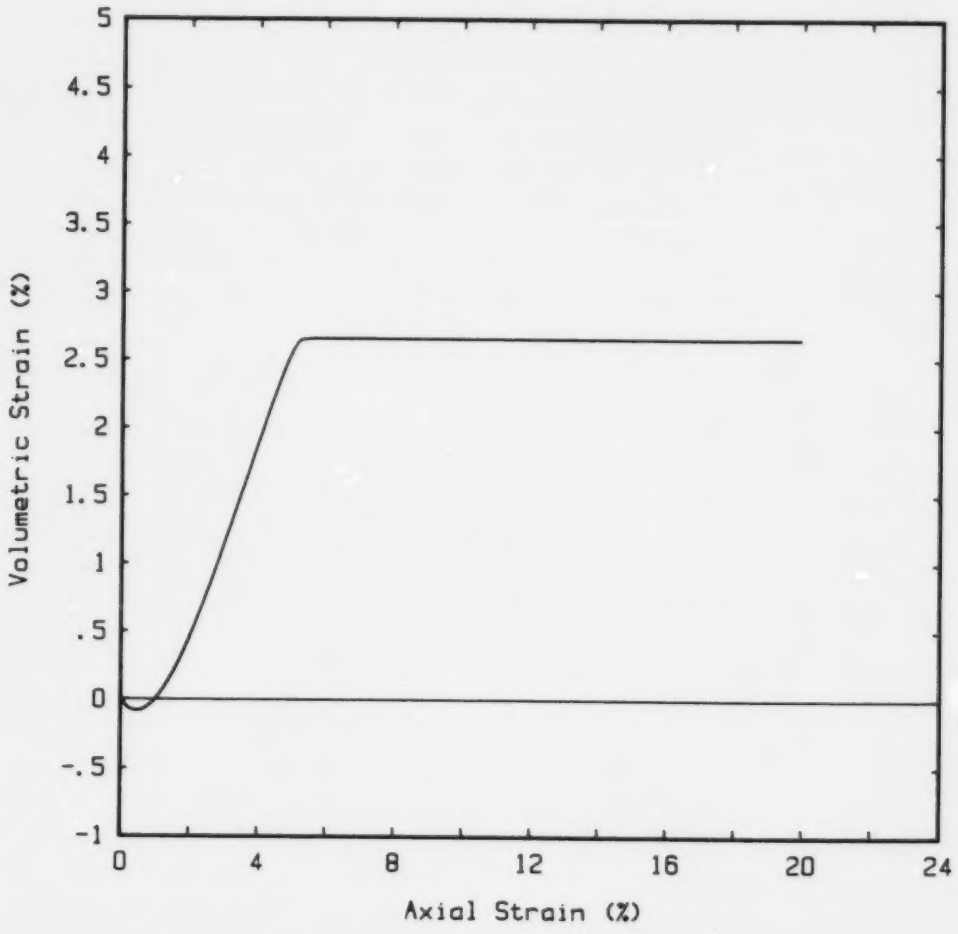

Isotropically Consolidated Drained Triaxial Test

Project Number : 902-2013	
Computer File : CID-4-2	
Test Description: STRAIN CONTROLLED DRAINED TEST	
Date of Test : 18 MAR 91	
Effective Consolidation Stress	= 200 kPa
Initial Back Pressure	= 1000 kPa
Pre Consolidation Void Ratio	= 1.121
Post Consolidation Void Ratio	= 1.099
Initial State Parameter	= .179
Ø'max	= 43.9°
Strain Rate	= 9.7 %/hr.

GOLDER ASSOCIATES Drawn: GCR Checked: _____ Date: 26 MAR 91

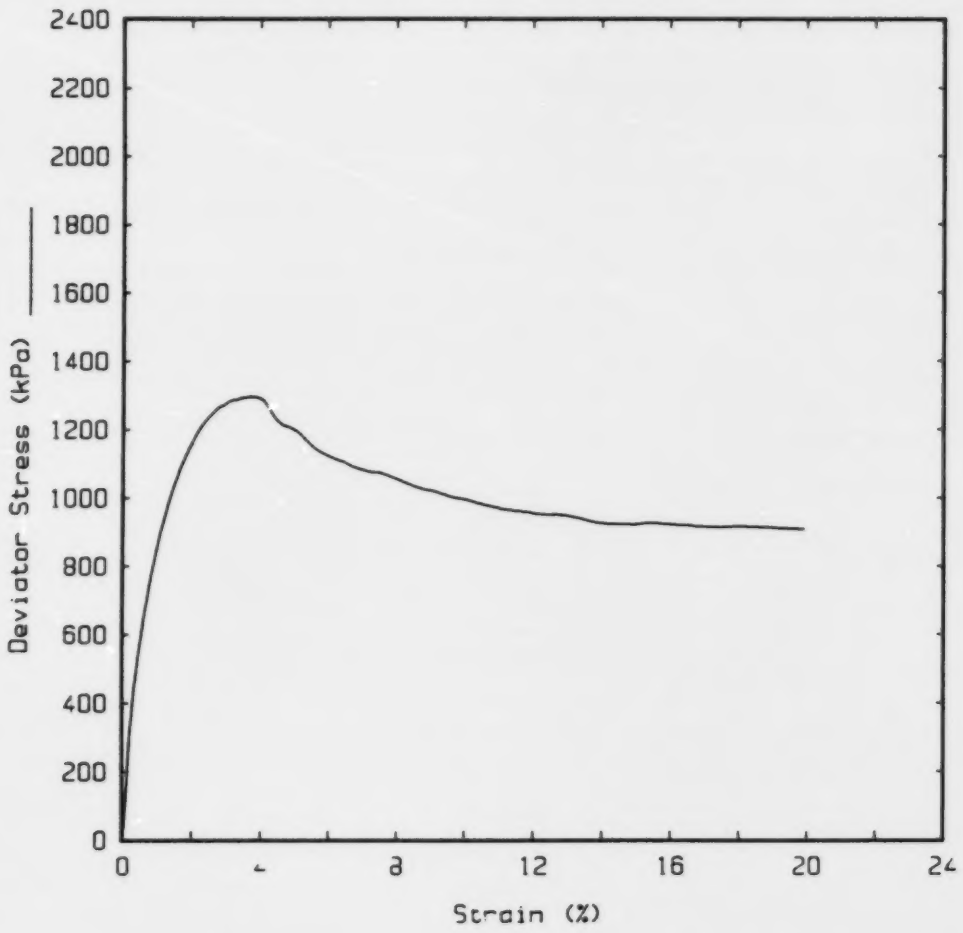

Isotropiccl1y Consolidated Drained Triaxial Test

Project Number : 902-2013	
Computer File : CID-6-4-27	
Test Description: STRAIN CONTROLLED DRAINED TEST	
Date of Test : 25 MAR 91	
Effective Consolidation Stress	= 350 kPa
Initial Back Pressure	= 850 kPa
Pre Consolidation Void Ratio	= 1.214
Post Consolidation Void Ratio	= 1.189
Initial State Parameter	= .277
ϕ'_{max}	= 40.5°
Strain Rate	= 10.4 %/hr.

GOLDER ASSOCIATES Drawn: GCR Checked: _____ Date: 26 MAR 91

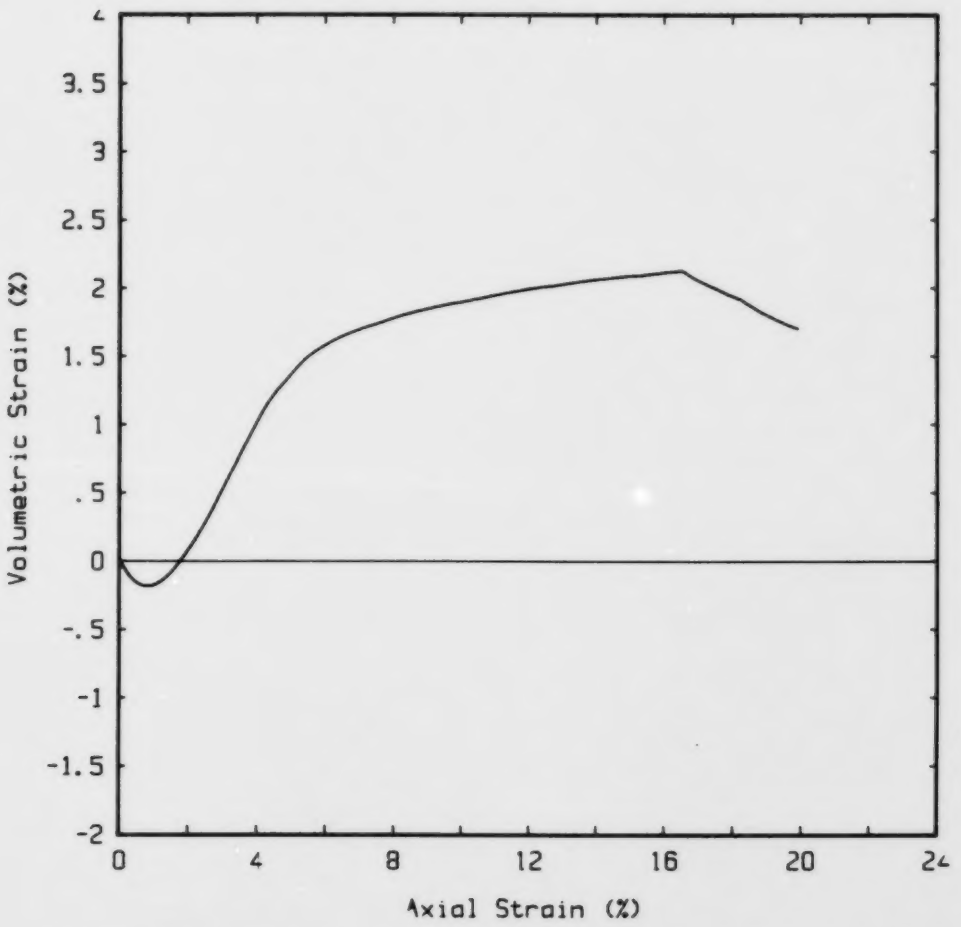

Isotropically Consolidated Drained Triaxial Test

Project Number	: 902-2013
Computer File	: CID-6-4-27
Test Description:	STRAIN CONTROLLED DRAINED TEST
Date of Test	: 25 MAR 91

Effective Consolidation Stress	= 350 kPa
Initial Back Pressure	= 850 kPa
Pre Consolidation Void Ratio	= 1.214
Post Consolidation Void Ratio	= 1.189
Initial State Parameter	= .277
ϕ'_{max}	= 40.5°
Strain Rate	= 10.4 %/hr.